SELECTIVE ACTIVATION OF TERBIUM(III) AND EUROPIUM(III) LUMINESCENCEWITH TRIARYLBORON-FUNCTIONNALIZED CARBOXYLATE LIGANDS.

AND

LUMINESCENT 8-HYDROXYQUINOLINE DIPICOLYLAMINE COMPLEXES AS SENSORS FOR ZINC(II).

by

Maria Varlan

A thesis submitted to the Department of Chemistry

In conformity with the requirements for

the degree of Master of Science

Queen's University

Kingston, Ontario, Canada

(September, 2012)

Abstract

The impact of a tri-substituted boron moiety on the chelate sensitization of Tb(III) and Eu(III) lanthanide luminescence and their resulting photophysical properties was investigated. Two triarylboron-functionalized carboxylate ligands **1** and **2** and their respective Tb(III) and Eu(III) complexes, **1Tb**, **2Tb**, **1Eu** and **2Eu** were synthesized and fully characterized. The photophysical properties of these compounds were studied and it was established that these three-coordinate boron ligands are highly effective in selective activation of Tb(III) and Eu(III) luminescence yielding high efficiency green and red luminescence, respectively. Potential applications of these triarylboron-functionalized chelate Tb(III) and Eu(III) complexes as luminescent sensors for dipicolinic acid (DPA), a biomarker for anthrax spores, as well as small anions such as F^- and CN^- in organic solution were examined by titration experiments using UV-Vis absorption and fluorescence emission measurements. Further studies were carried out into the application of the lanthanide complexes as solid substrate luminescent sensors for the same analytes.

Furthermore a novel zinc-binding compound, composed of both an 8-hydroxyquinoline fluorophore and a dipyridyl metal binding site, was designed for application as a luminescent sensor for Zn(II), due to the recent link between the metal ion and certain high-profile neurological conditions such as Alzheimer's and epilepsy. The target ligand compound **1-OH** was successfully synthesized and characterized using UV-Vis, Fluorescence and NMR spectroscopy. Further studies of the ligand are recorded by studying the effects of the addition of both four-coordinate boron and tris(8-hydroxyquinolinato)aluminum active sites to the **1-OH** molecule frame. The four compounds' abilities in luminescent Zn(II) detection in organic media were examined by titration experiments with Zn(II) using UV-Vis absorption and fluorescence emission measurements.

Acknowledgements

First and foremost, I would like to express huge thanks to my supervisor, Dr Suning Wang for her prized guidance, enthusiasm and never-ending patience. I am incredibly grateful for being given the opportunity to work in the Wang group with such lovely bright compounds that kept my work fun and exciting. Her excitement and enthusiasm for my project kept me motivated and I will take much valued knowledge and experience from my time spent working with her.

Many thanks to all the professors and staff at Queen's University that have helped and taught me throughout my university career. Special mentions to my supervisory committee members Dr. Jean-Michel Nunzi and Dr Anne Petitjean for taking time to consider my work and for their helpful suggestions during my annual meeting.

Hugs to my family! Thanks to my parents, to Muni and Ioana for the constant push to achieve more and not settle for less. Dear giant family of scientists; thank you for not indulging my self-pity and reminding me that I should stop sulking and get back to work. I may not have liked you very much then, but I'm very grateful for the push!

I would like to acknowledge the enormous influence had on me by Dr Yi Sun, Dr Barry Blight and Dr Youngjin Kang. You have taught me skills I will have with me forever and have supported and motivated me in times of discouragement. I could not have finished these projects without your guidance, thank you so very much! Gratitude to the members of the Wang lab I have had the pleasure to meet and get to know of the years. You guys have been lovely and have made my time here so very enjoyable! Special mention to Yingli Rao, you are the wisest young person I know. These two years without your advice would have been a hot mess.

Thanks to roommates present and past, special mentions to Megan French and Tamara DeWinter for witnessing, accepting and putting up with all the crazy. You guys made it fun!

Much gratitude to my "Thesis Officers" Vladimir Zlojutro and Graham Garrett for keeping the writing on track. Your aid and encouragement in its completion were priceless.

Table of Contents

List of Figures

List of Tables

List of Symbols and Abbreviations

A	absorbance
Å	angstrom
Al	aluminum
Anal	analysis
Alq_3	tris(8-hydroxyquinolato) aluminium
B3LYP	Becke 3-Parameter Exchange, Lee, Yang and Parr
°C	degrees Celsius
c	concentration
calcd	calculated
$CDCl_3$	deuterated chloroform
CD_2Cl_2	deuterated dichloromethane
CH_3CN	acetonitrile
CH_2Cl_2	dichloromethane
cm	centimetres
COSY	Correlation Spectroscopy
CV	cyclic voltammetry
d	doublet
DCM	dichloromethane
dd	doublet of doublets
DFT	density functional theory
DMF	dimethylformamide
DMSO	dimethylsulfoxide
ε	molar absorptivity
EDTA	ethylenediamine tetraacetic acid

EL	electroluminescence
eq.	equivalent
eV	electron volt
g	gram
HOMO	highest occupied molecular orbital
HRMS	high resolution mass spectrometry
Hz	hertz
ICT	Intramolecular charge transfer
ILCT	intra-ligand charge transfer
ISC	intersystem crossing
J	coupling constant
K	Kelvin
l	path length
L	liter
LC	ligand centered
LLCT	ligand to ligand charge transfer
LMCT	ligand to metal charge transfer
LUMO	lowest unoccupied molecular orbital
m	meter, multiplet
M	molar
MC	metal centred
mes	mesityl
mg	milligram
MHz	megahertz
mL	millilitre

MLCT	metal to ligand charge transfer
^{3}MLCT	triplet metal to ligand charge transfer
MMCT	metal to metal charge transfer
mmol	millimole
MO	molecular orbital
mol	mole
m. p.	melting point
nm	nanometers
NMR	nuclear magnetic resonance
OLED	organic light emitting diode
Ph	phenyl
ppm	parts per million
q	8-hydroxyquinoline
r.t	room temperature
s	seconds
S_0	singlet ground state
S_1	singlet excited state
T_1	1st level excited triplet state
T_2	2nd level excited triplet state
TBAF	tetra-n-butylammonium fluoride
TBACl	tetra-n-butylammonium chloride
TBACN	tetra-n-butylammonium cyanide
td	triplet of doublets
THF	tetrahydrofuran
TLC	thin layer chromatography

UV	ultraviolet
UV-Vis	ultraviolet-visible
δ	chemical shift
μs	microsecond
λ	wavelength
Φ	quantum yield
τ	lifetime

Chapter 1

Introduction

1.1 Luminescence

The word luminescence derives from the Latin term *lumen*, signifying light, and is presently defined as "a spontaneous emission of radiation from an electronically (or vibrationally) excited species not in thermal equilibrium with its environment".[1] Though first referred to and defined by its modern term *luminescenz* in 1888 by German scientist Eilhard Wiedemann,[2] scientific examination of luminescent materials can be dated back to 1603 when Bolognese cobbler Vincenzo Cascariolo observed distinct light emission irradiating from a chunk of charcoal-reduced barite mineral.[3] Nowadays, the field of study of luminescence has expanded considerably since its early beginnings and is comprised of many subcategories, one of which will be discussed in more detail below. Types of luminescence have been categorized by method of excitation of the emissive species and include but are not limited to: bioluminescence, chemiluminescence, electroluminescence, sonoluminescence, thermoluminescence and photoluminescence.[4] Out of the 6 examples stated above, only photoluminescence will be explored and described in this thesis.

1.2 Photoluminescence

Photoluminescence (PL) is defined as the emission of radiation from an excited electronic state following the photo-excitation of the emissive species. Light is a convenient external source of energy to promote excitation and also permits for versatile control of the excited level reached

by the emissive species by varying the wavelength of the light energy (or the energy of the photon). The Jablonski diagram (Figure 1.1) below illustrates the two pathways of photoluminescence: fluorescence and phosphorescence. Every energy level is comprised of several closely spaced vibrational states. Most molecules have a Singlet ground state populated by an even number of electrons of opposite spin (paired electrons).

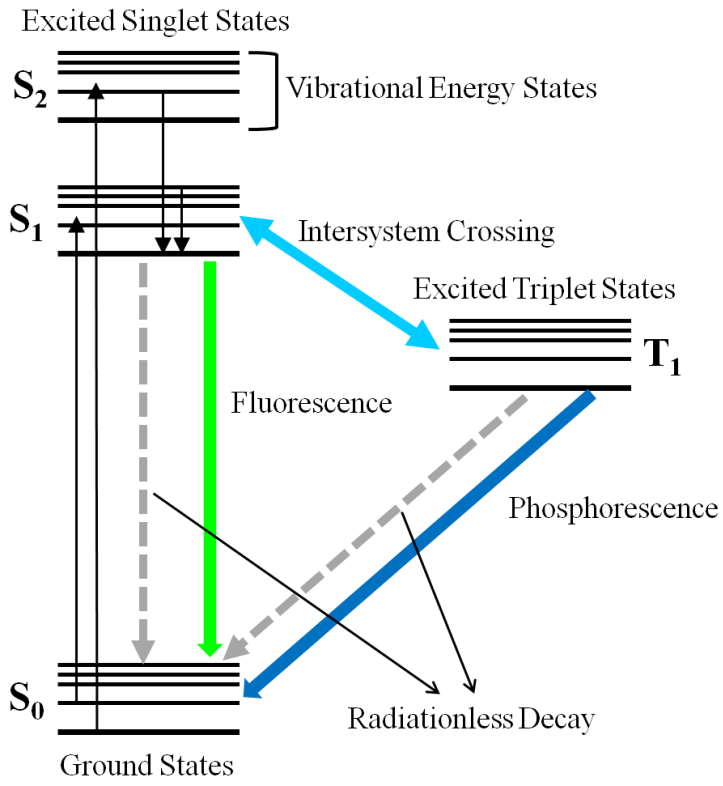

Figure 1.1. Jablonski Energy Diagram

Fluorescence consists of the emission caused by the transition from the singlet excited state to the ground state. Upon photo-irradiation, a molecular ground state electron (S_0) is promoted to an excited state (S_1, S_2, etc.), conserving its spin and maintaining its parity to the

electron that remained in the ground state. Relaxation of the electron back down to the ground state is consequently spin-allowed ($S_1 \rightarrow S_0$) and transpires quickly with simultaneous energy dissipation in the form of light.[5]

The phosphorescence pathway is comprised of a different mechanism than that of fluorescence. Upon photo-irradiation, a ground state electron is promoted to an excited state (S_1) and then endures intersystem crossing (ISC) to an excited triplet state (T_1) wherein the electron in the excited state orbital has the same spin as that of the remaining ground state electron.[5] The electron then undergoes relaxation to the singlet ground state (S_0) while emitting a photon. Transitions of an unpaired electron to the ground state are spin-forbidden because they occur between states with different spin quantum numbers ($T_1 \rightarrow S_0$), resulting in much longer emission lifetimes (10^{-6}s to s) and emission rates (10^3-10 s^{-1}) than those observed for spin-allowed fluorescence (10^{-9}s) with emission rates of (10^8 s^{-1}). [6] Though phosphorescence occurs quite rarely in organic materials due to the forbidden singlet-triplet transition, it is common in metal complexes due to spin-orbital coupling.[7]

The resulting emitted light for both fluorescence and phosphorescence has lower energy (longer wavelength) than that used to originally irradiate the species due to rapid decay of the excited electron to a lower vibrational energy level within the excited state (S_1) before returning to the ground state. As a result, the emission wavelength is constantly a little longer than the excitation wavelength resulting in two distinct peaks separated by a difference identified as the Stokes Shift. Fluorescence exhibits a smaller Stokes's shift as its absorption and emission bands are generally close to each other and may even overlap a bit. Phosphorescence, however, shows significantly larger Stokes's shifts due to the triplet energy level involved being lower than the singlet level involved in fluorescence.[8]

1.2.1 Characteristics of Fluorescence and Phosphorescence

The potential of a substance to exhibit luminescence has shown to be dependent on certain variables that include molecular structure and chemical environment. The importance and nature of these variables will be discussed herein as well as their effect on emission if luminescence does transpire.

Quantum yield, for both fluorescence and phosphorescence, is an important attribute to characterize the luminescence of a compound and is defined as the ratio between the number of photons emitted over the number of photons absorbed by an emissive sample. This is further discussed in Section **1.2.2**.

Fluorescence arises most frequently from a transition from the lowest vibrational level of the first excited state to a vibrational level of the electronic ground state and is typically attributed to $\pi \rightarrow \pi^*$ transitions within organic compounds. Therefore, compounds containing aromatic functional groups with low-lying $\pi \rightarrow \pi^*$ transitions are most commonly found to exhibit fluorescence. Highly conjugated double bond structures may also display fluorescent emission, but their numbers are far fewer than the aromatic systems.[5]

The quantum efficiency of fluorescent aromatic systems increases with the number of fused aromatic rings and heterocycles when compared to their singular components. Additions of various substituents on the skeleton of aromatic moieties induce shifts in both absorption maxima and emission wavelength and subsequently, quantum yield. Luminescence is particularly favored in molecules with high rigidity as they decrease the odds of radiationless decay. A significant increase in fluorescence is therefore observed in certain organic aromatic chelating agents when they are complexes with metal ions.[9] The structures of some commonly known fluorescent substrates are illustrated in Figure 1.2.

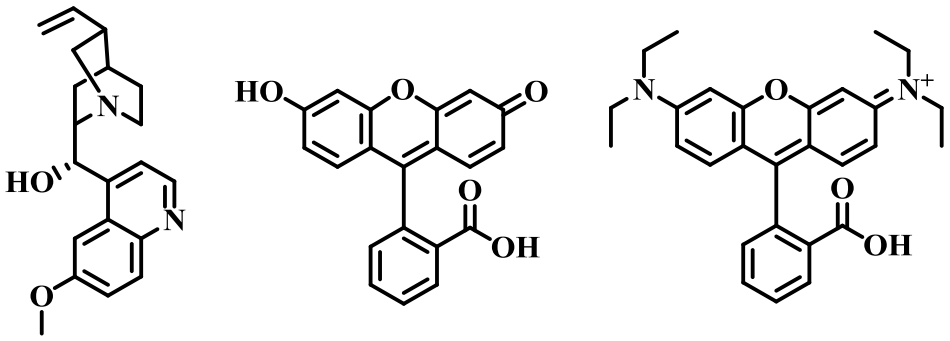

Quinine **Fluorescein** **Rhodamine B**

Figure 1.2. Examples of typical fluorescent molecules.[5]

The presence of heavy atoms either in molecules or in their surrounding solvent may lead to a decrease in fluorescence due to the "heavy atom effect". "The heavy atom effect" occurs in the presence of atoms such as halogens or metals and it induces spin-orbital coupling, therefore encouraging intersystem crossing into the triplet state and the subsequent electron spin state change, resulting in a decrease in fluorescence. As a result, compounds incorporating heavy atoms are often used when phosphorescence is desired.[9] Phosphorescence is most often not readily observed at ambient temperatures due to deactivation caused by oxygen as well as the presence of other quenching impurities.[5]

Photoluminescence lifetime, as discussed previously, is one of the main characteristics used to distinguish between a phosphorescent compound and a fluorescent compound, due to the phosphorescence having a lifetime of microseconds to seconds whereas fluorescence exhibits much shorter emission lifetimes of nanoseconds.

An important class of phosphorescent compounds are metal complexes that are comprised of a transition metal ion and one or more organic ligands. These compounds typically display mixed singlet-triplet states with emission lifetimes in the microseconds regime. The

combination of metal and ligands may lead to charge transfer transition between the two components, most commonly between π orbitals of the ligand and the d orbitals of the transition metal ion. Where fluorescence emission is found to be based on π→π* transitions, the introduction of the d orbitals by the transition metal induces transitions such as metal-to-ligand charge transfer (MLCT) or ligand-to-metal charge transfer (LMCT) in addition to the ligand centered π→π* transition.[5] The introduction of heavy transition metal centers such as Pt and Ir induces strong spin-orbital coupling, facilitating intersystem crossing into the triplet state and enhancing phosphorescent emission.[10]

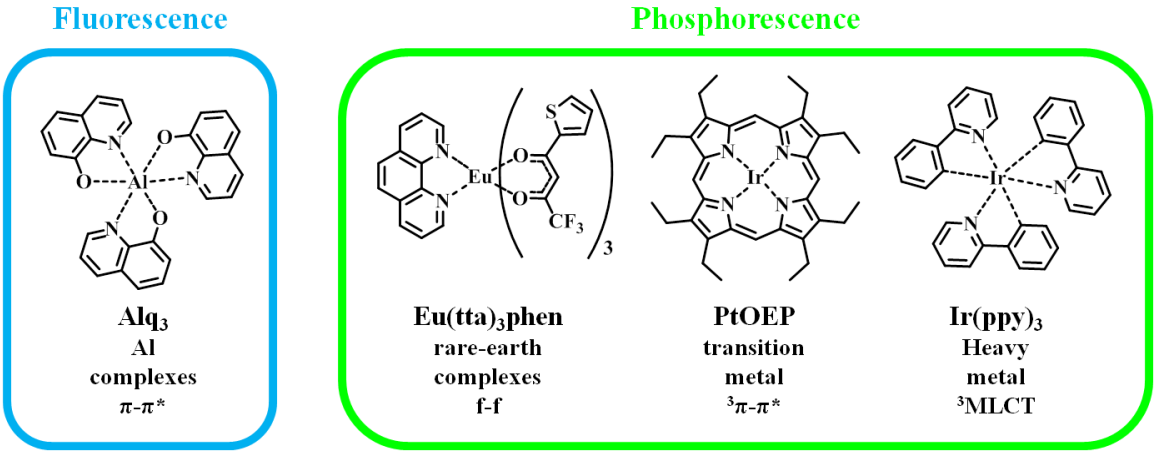

Figure 1.3. Examples of typical luminescent metal complexes Alq_3,[15] $Eu(tta)_3phen$,[11] PtOEP[12] and $Ir(ppy)_3$.[13,14]

The emission lifetimes of Pt(II) or Ir(III) compounds are significantly shorter (microseconds) than those of organic phosphorescent compounds due to heavy-metal atom spin orbital coupling increasing probability of the normally forbidden transition to the ground state.[5] Typical examples of fluorescent and phosphorescent metal compounds are shown in Figure 1.3, wherein the non-transition metal Al(III) complex exhibits fluorescence and heavy transition metals Ir and Pt display phosphorescence.

Lanthanide metal complexes often display phosphorescence as well, however, their emission mechanism differs greatly from that of transition metal complexes and is further discussed in section **1.4**.

1.2.2 Quantum Yield

Quantum yield is an important characteristic of the emissive species and is used to indicate the efficiency with which the subject converts the excitation energy absorbed into radiative relaxation back to the ground state. The optimum value for this feature is 1.0, however even the most efficient species will rarely reach unity due to Stokes shift. Determination of the quantum yield of an unknown compound can either be attained with a calibrated integrating sphere or with the use of an appropriate emissive standard of known quantum yield whose absorption and emission profile match the unknown such as 9, 10-diphenylanthracene or quinine sulfate.[15]

If using the latter procedure, the absorption profile for both the standard and the unknown must closely match due to the intersecting point between the two peaks being assigned as the excitation wavelength for the quantum yield measurements, a value that must be suitable for both emissive compounds. Following Beer's Law below (Equation 1.1), where A is the absorbance, ε is the molar absorptivity, c is concentration and l is the path length, there is a direct correlation between the concentration of a sample and the amount of photons it absorbs.

$$A = \varepsilon c l$$

Equation 1.1

The significance of the concentration absorption ratio is important in quantum yield calculations due to molecules reflecting light off each other if the concentration exceeds a certain

limit, which would yield inaccurate absorption readings. Probabilities of radiationless decay as a means of energy dissipation are also augmented within a sample that is too concentrated as an increase of molecular collisions is observed. Therefore, in order to confirm accurate absorbance values for both standard and unknown sample, the intersection point of their peaks must be at or below an absorption reading of 0.05.[16]

Once the excitation wavelength is accurately determined for both unknown and standard samples, the quantum yield can be calculated by using equation 1.2:

$$\phi_u = \phi_s \left[\left(\frac{A_s}{A_u} \right) \left(\frac{E_u}{E_s} \right) \left(\frac{n_u^2}{n_s^2} \right) \right]$$

Equation 1.2

Within the quantum yield equation, subscripts u and s symbolize the unknown and standard samples, respectively, A is absorbance, E denotes integrated area of the emission peak and n stands for the refractive index of the solvent utilized.[17]

1.3 Luminescent Aluminum Complexes

A multitude of chelated aluminum complexes have been reported in recent years due to their good luminescent and electron-transporting properties, their low production cost and, most notably, their application in organic light-emitting diodes (OLEDs). The vast majority of previously reported fluorescent aluminum complexes are based on N,O-chelating ligands due to the great success of Alq_3 (q=8-hydroxyquinolinato), a stable and bright emitter and a commonly used electron-transport material in OLEDs, which will be discussed in more detail in the following section.

1.3.1 Tris-(8-hydroxyquinolinato) Aluminum

Arguably one of the most important milestones in the development of a stable EL device, the discovery of tris(8-hydroxyquinolinato) aluminum (Alq_3) in 1987 by Tang and VanSlyke[18] has yielded prolific insight into luminescent Al(III) compounds and their applications. The Alq_3 molecule is comprised of a central Al(III) surrounded by three bidentate 8-hydroxyquinolinato ligands (q) in octahedral symmetry, thus creating a compound with fully filled coordination sites and a net charge of zero as shown in Figure 1.4. The Alq_3 molecule may assume either *fac*- (C_3 symmetry) or *mer*- (C_1 symmetry) isomer geometry with the latter being more thermodynamically stable (by 4 kcal/mol).[19]

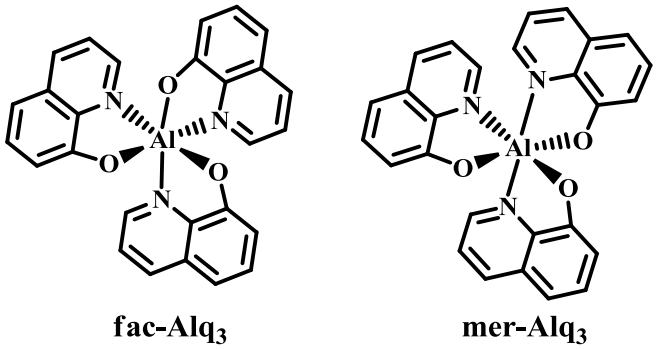

Figure 1.4. Molecular structures of Alq_3.

In DMF solution Alq_3 exhibits fluorescence emission band at 526 nm and photoluminescence quantum efficiency of 11%,[20] while in thin-film solid state PL quantum efficiency of 32% has been recorded.[21] In addition to its impressive quantum efficiency, Alq_3 is a remarkably stable compound and can be sublimed without any signs of decomposition at 350°C, making it an ideal luminophore for applications in EL devices.

Since its discovery, there have been extensive research efforts in improving the efficiency of the Alq_3 molecule as well as manipulating the compound's emission characteristics through the addition of varying functional groups.

1.3.2 Functional group-modified Alq_3

DFT calculations performed on the Alq_3 compound to establish the molecule's electronic properties indicated that both ground and excited state are localized on the 8-hydroxyquinoline ligand with the HOMO and LUMO being confined to the phenoxy and the pyridyl moiety, respectively.[22] The lowest electronic transition within the molecule is therefore deduced to be composed of $\pi \rightarrow \pi^*$ transitions in the quinolate units occurring by partial charge transfer from the phenoxy ring to the pyridyl ring. These results indicate that by introducing a variety of functional groups to the hydroxyquinoline units in the Alq_3 molecule, the HOMO or LUMO energies and their band-gap may be modified and subsequently, the emission properties of the compound may be manipulated.

Much work has been completed by Azenbacher and his associates with functionalized Alq_3 compounds in the efforts of elucidating our understanding of altered Alq_3 molecules and their subsequent electronic and photophysical attributes.[23]

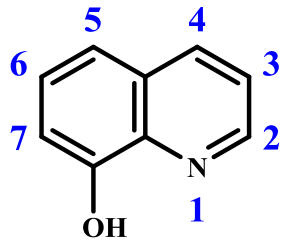

Figure 1.5. Numbering system for 8-hydroxyquinoline.

Their work involved the addition of a variety of functional groups, either electron-withdrawing or electron-donating to the C5 position on the quinoline moiety, either through an

ethynyl linker producing molecules 1a-1k (shown in Figure 1.6, Series 1) or through direct attachment to the ligand (Figure 1.7, Series 2) resulting in molecules 2a-2n. The C5 position is utilized for both these studies due to the HOMO being localized on the phenoxy oxygen and the C5 position para to the mentioned oxygen atom, a position that also reduces steric hindrance with the central Al(III) atom.[24] Emission patterns for both sets of molecules were shown to be similar to those of Alq_3 with emission energy shifts towards either end of the visible spectrum depending on the electronic nature of the functional group moiety.

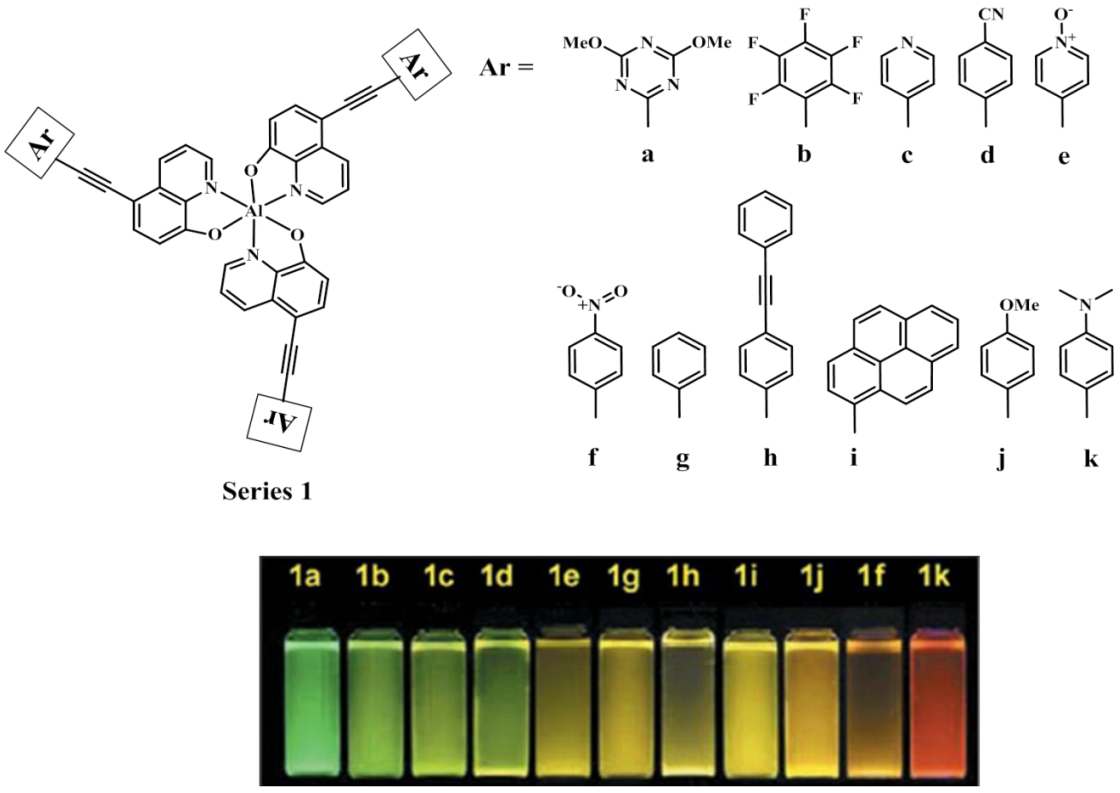

Figure 1.6. (Top) Molecular structures of complexes 1a to 1k and (bottom) photographs of molecules 1a-1k in solution under UV light irradiation.[23b]

Electron-withdrawing groups in Series 1 resulted in blue-shifted emission from the original 526 nm of Alq_3 up to 520 nm such as molecule 1a, along with a significant simultaneous

increase in fluorescence lifetime and quantum yield (from Φ=0.17 to Φ=0.31 for complex 1a). Electron-donating groups, as expected, resulted in red-shifted emission up to 600 nm by 1k along with decreases in both quantum yield (down to 0.009 for complex 1k) and lifetime. These observations are consistent with electron withdrawing groups lowering the HOMO and widening the band-gap resulting in an emission blue-shift, while electron donating substituents raise the HOMO resulting in emission red-shift.

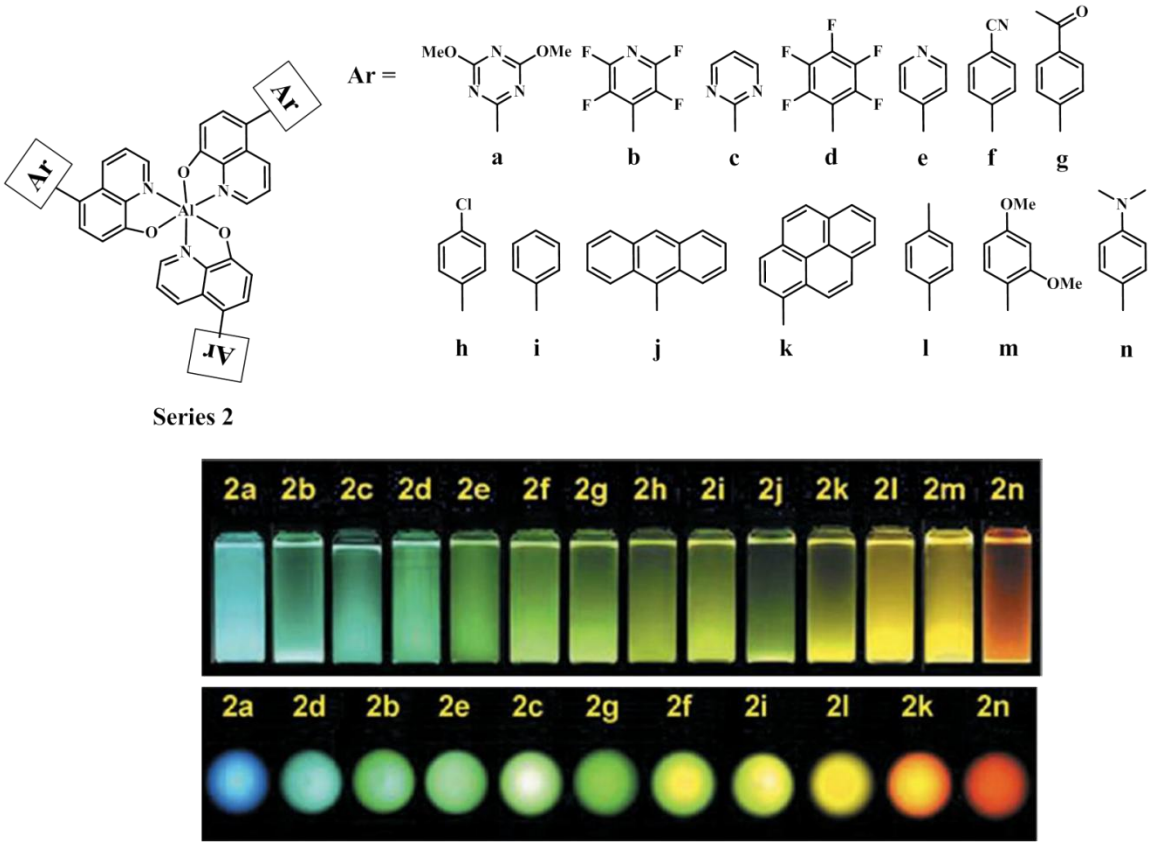

Figure 1.7. (Top) Molecular structures of complexes 2a- 2n, (middle) photographs of complexes 2a-2n in CH_2Cl_2 solution under UV light irradiation and (bottom) emission of OLEDs fabricated using the 2a-2n complexes.[23b]

Series 2 showed similar results but with a wider range of emission colors from 490 nm to 612 nm when compared to that of Series 1 from 520 nm to 600 nm. This phenomenon is attributed to the substituents being directly attached to the quinoline ligand in Series 2, without the extra acetylene linker presented in Series 1, resulting in a greater emission sensitivity to the functional group.

1.4 Lanthanide Luminescence

1.4.1 Introduction to Lanthanides

Lanthanides, derived from the Greek *lanthanein* meaning 'to lie unseen, to escape notice',[25] are comprised of the fifteen elements in the top row of the f-block of the periodic table. Lanthanides possess the electronic configuration [Xe] $4f^n5s^25p^6$ where n diverges from 0 to 14 and are most stable in the 3+ oxidation state under aqueous environment. The 3+ oxidation state is remarkably consistent throughout the rare earth metals due to the significant stabilization experienced by the 4f, 5d and 6s orbitals upon ionization of the neutral lanthanide metal.[26] The 4f energy level lies below the 5d and 6s levels, therefore, when the lanthanide is ionized, the 5d and 6s levels are foremost affected resulting in the Ln(III) ion possessing a [Xe] $4f^n$ configuration. The stability of the 3+ oxidation state for the rare earth metals is further reinforced by the high enthalpies for trivalent lanthanide hydration.[27]

The coordination chemistry of lanthanide metals can be described as very ionic in character due to their hard Lewis acid quality. Rare earth ions exhibit strong electrostatic nature in their bonding and are attributed with high charge density leading to a coordination preference for hard Lewis bases and high coordination numbers. This affinity for negatively charged or neutral donor groups with large ground state dipole moments makes carboxylic acids and amines,

that contain O and N as coordinating atoms and have high versatility in terms of increasing coordination number, ideal ligands for rare earth ions.[28] Multiple bonds between the lanthanide ion and its coordination atom within rare earth complexes are impossible as the 4f orbitals are shielded by both the 5s and 6p orbitals, forbidding them from directly participating in bonding and thus making π bonds between the metal and its ligand unattainable.

Owing to their high ionic character, lanthanide ions are inclined to form complexes with high coordination numbers, flexible coordination geometries and can easily undergo ligand exchange. The most commonly observed coordination number for lanthanide complexes are 8 and 9 for light-mid lanthanide ions (La(III)-Tb(III)) and heavy lanthanide ions (Dy(III)-Lu(III)) respectively. However, many exceptions to this rule exist, as coordination numbers have been shown to vary with ligand steric bulk[29-30] from 3 to 12.

The highly shielded 4f orbitals provide the lanthanide ion with a large variety of electronic levels (via Russell-Saunder Coupling[31]), depending on the number of f electrons. The total number of f-orbital energy levels (*f*) may be calculated with equation 1.3 where n is the number of f electrons, ranging from 0 to 14.

$$f = \frac{14!}{n!\,(14-n)!}$$

Equation 1.3

The significant shielding effect on f orbitals results in that the f-energy levels are well defined, stable and do not show much variation with the chemical environment of the lanthanide ion such as solvent or coordinating ligands.[32] Both spectroscopic and magnetic characteristics of the lanthanide ion are therefore mostly kept intact when complexed to a ligand. Further

discussion into the spectroscopic characteristics of lanthanide ions is divulged below in order to gain additional understanding into rare earth metal chemistry.

1.4.2 Lanthanide Ion Luminescence

Lanthanide ions possess particular spectroscopic properties due the shielding of their 4f orbitals by their populated 5s and 5p subshells and are characterized by electronic transitions within the 4f shell. This shielding effect causes the rare earth electrons to behave like inner electrons as opposed to valence electrons and their emission and absorption spectra consist of very sharp and narrow bands.[33] Furthermore, these narrow absorption bands have low molar absorption coefficients. Transitions between f orbitals of lanthanide ions are Laporte-forbidden yet spin-orbital coupling attenuates this occurrence.[34] The Laporte-forbidden nature of the f-f transitions give rise to very long emission lifetimes of micro-milliseconds. This long lifetime characteristic is unique to lanthanides as it occurs under ambient conditions while most organic compounds exhibiting phosphorescence do so at low temperatures or in the absence of oxygen.[35] The energy of f-f transitions is also largely independent of lanthanide's chemical environment such as solvent or chelated ligands and as such lanthanide emission remain mostly the same though peak splitting and relative intensity may vary.[24] The low extinction coefficients of lanthanides cause in general weak luminescence of lanthanide compounds. Lanthanide emission can, however, be enhanced by 'sensitizing' lanthanide luminescence through the introduction of a binding ligand.

1.4.3 Sensitized Lanthanide Luminescence

The concept of sensitized lanthanide luminescence, first demonstrated by El-Sayed and Bhaumik in 1963,[36] consists of by-passing the lanthanide ion's poor absorption features by using

a chelating ligand as an energy collector, permitting for efficient excitation of the rare earth metal, and thus resulting in significantly enhanced lanthanide emission. Intramolecular energy transfer from ligand to metal in rare earth complexes has been studied since 1941,[37] and had since been expanded on by Crosby and co-workers by varying the molecular level positions of ligand relative to rare earth metal in order to optimize energy transfer.[38]

Bhaumik and El-Sayed first showed the sensitization method to be effective by exciting a europium tris(hexafluoroacetylacetonate) compound ($Eu(HFA)_3$) with a benzophenone aromatic ligand and observing triplet to f orbital energy transfer from the benzophenone moiety to the rare earth metal ion. Experimental design paid particular attention to proximity of molecular energy levels as advised by previous work[39]: the triplet energy level of the $Eu(HFA)_3$ chelate is just below that of the benzophenone sensitizer ligand energy level. Once the benzophenone was excited at 380 nm, the two-compound mixture was observed to experience a ten-fold increase in luminescence intensity of the characteristic Eu(III) red emission bands. Their work proved to be one of the first insights into by-passing the problems that arise with directly exciting lanthanide ions, a concept that is now referred to as the absorption-energy transfer emission mechanism (AETE).

The AETE mechanism, illustrated in figure 1.8, begins with the excitation of the light-harvesting ligand, more commonly referred to as the 'antenna'.[40] The antenna usually consists of an anionic chelating molecule, or one with a strong dipole moment for effective chelation to the rare earth metal that is capable of effectively absorbing the excitation energy and transferring it to the lanthanide ion through nonradiative methods for sensitized emission.

The antenna molecule is firstly excited from the ground state (S_0) to its singlet excited state (S_1); if the chromophore has several singlet excited states (S_1, S_2, S_3 etc..), non-radiative

relaxation may occur through internal conversion back down to the lowest excited singlet state (S_1). Secondly, intersystem crossing from a singlet to the lowest triplet excited state (T_1) occurs within the ligand through intersystem crossing (ISC). This step is followed by energy transfer from the ligand triplet excited state to the f* energy level of the lanthanide ion due to the long lifetime of T_1, if the excited f* state is close to but lower than that of T_1. Subsequent f*-f relaxation consequentially produces lanthanide luminescence by emitting a photon. Studies describing direct energy transfer from ligand excited singlet levels (S_1) to the f* energy level resulting in lanthanide luminescence sensitization have also been reported.[41]

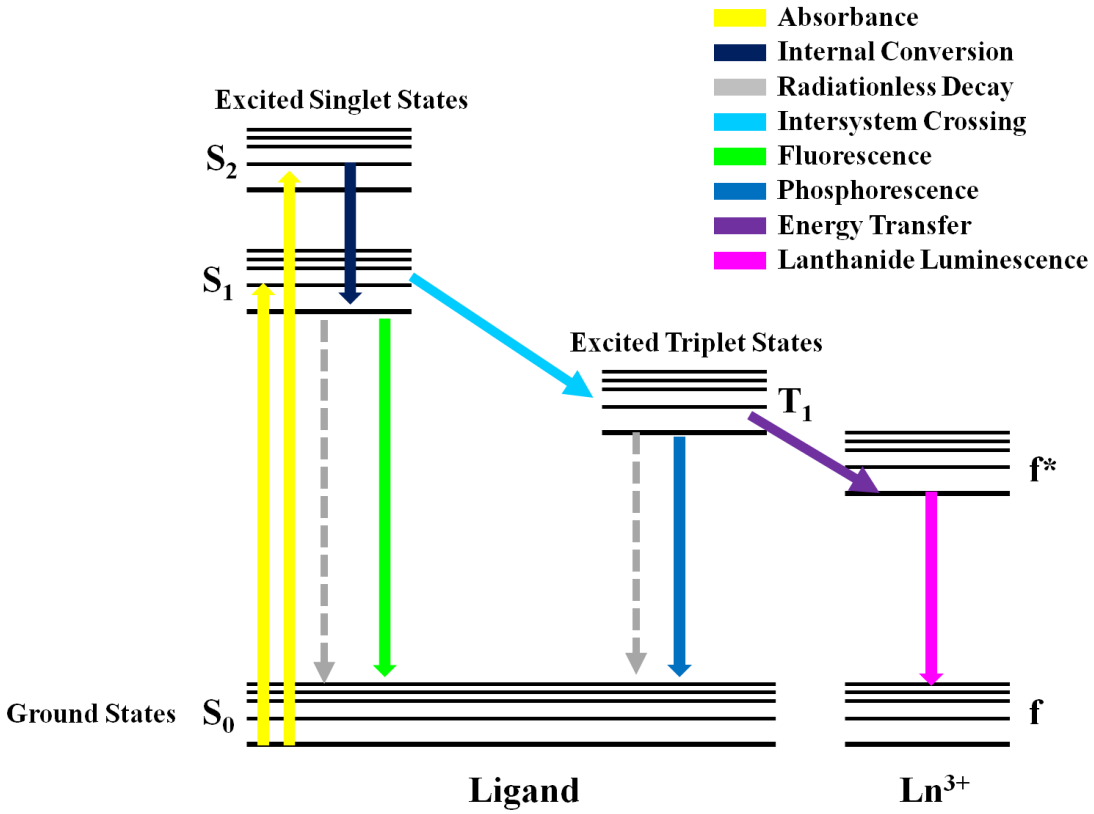

Figure 1.8. Jablonski Energy Diagram of Absorbance Energy Transfer Emission (AETE) mechanism for a Ln(III) complex **.**

The lanthanide sensitization mechanism is optimized if the above mechanism is at its most efficient. However, there are many alternative pathways by which its efficiency is compromised as can be observed in figure 1.8. Energy may be lost within the chromophore either by fluorescence from its lowest singlet excited state (S_1), phosphorescence from its lowest excited triplet state (T_1), or non-radiative decay from either position. Additionally, the energy transfer from the lowest excited triplet state of the ligand (T_1) to the f* state of the lanthanide is the most important step in the process and if faulty, can really cripple the efficiency of the sensitization mechanism. [42] If the f* energy level of the lanthanide is higher than the T_1 energy level of the ligand, the energy transfer from T_1 to f* cannot occur.

The most often used lanthanide ions in sensitization studies are Tb(III), Eu(III), Sm(III) and Dy(III) because they have excited states that lie just below in energy than most ligand triplet excited states and luminesce in the visible region. Characteristic emission spectra of the four lanthanides are shown in Figure 1.9, taken from a sensitization study by Bunzli et al., illustrating incredibly sharp peaks of their individual f-f transitions.

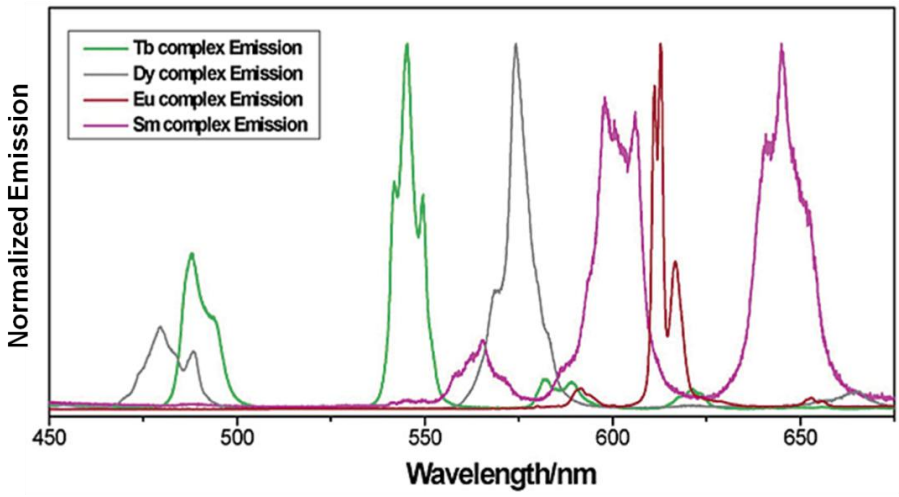

Figure 1.9. Characteristic lanthanide normalized emission peaks for Tb(III), Eu(III), Dy(III) and Sm(III) sensitized complexes.[43]

Amongst the other lanthanides, La(III) and Lu(III) have no f^n excited state, Gd(III) has an excited state above in energy to typical ligand triplet excited states and others have excited states that promote loss of energy via non-radiative pathways. Tb(III) and Eu(III) are the most popularly sensitized lanthanides of the series mentioned above due to their strong and pure luminescence colors of green due to emission band at λ_{em}=545 nm and red due to emission band at λ_{em}=615 nm, respectively, as shown in Figure 1.10. Tb(III) complexes emit characteristic peaks at λ_{em}=489 nm, 545 nm, 585 nm and 612 nm, corresponding to the $^5D_4 \rightarrow {}^7F_n$ transitions with n= 6, 5, 4 and 3 respectively while Eu(III) demonstrates emission bands at λ_{em}=579 nm, 590 nm and 617 nm from the $^5D_0 \rightarrow {}^7F_n$ transitions with n=0, 1 and 2.[44]

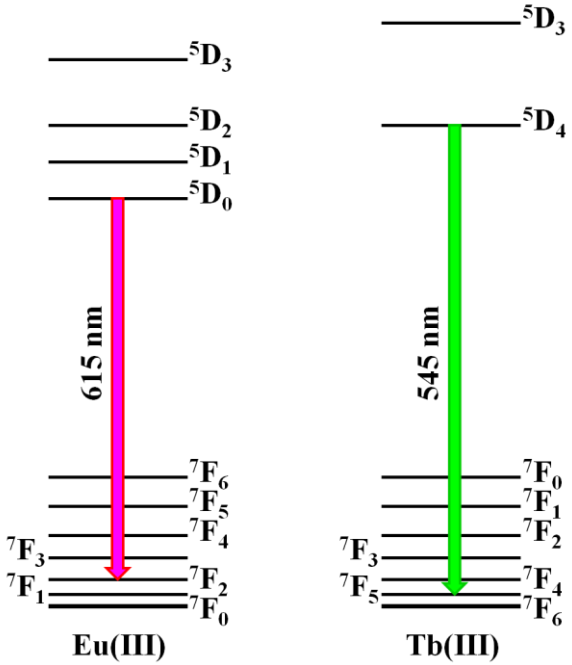

Figure 1.10. Energy diagram depicting lanthanide ion emission color for Eu(III) and Tb(III).

To conclude, the spectroscopic properties of lanthanide ions are remarkable and unique as they have the extraordinary quality of emitting strong sharp emission bands when compared to

the broader peaks observed for more standard organic compounds or luminescent polymers. However, in order to efficiently display those qualities, the addition of a light-harvesting antenna molecule is necessary to activate optimized lanthanide luminescence as their original emission is quite weak.

1.4.4 Luminescent Lanthanide Complexes as Sensors for the Anthrax Spore

The gram-positive positive bacterium *bacillus anthracis* was first linked to the cause of the anthrax disease by Prussian physician Robert Koch in 1876. Since Koch's Nobel-winning work in the field of microbiology linking common illnesses and the pathogens that cause them in the early 19th century,[45] scientific progress has led researchers to achieve not only the means of how to manufacture and isolate specific pathogens but also of how to apply this knowledge.

Evidence suggests that the first use of *bacillus anthracis* as a biological warfare agent was as an ambitious mission by the German forces in WWI to contaminate animal feed and livestock traded between neutral members of the Allies.[46] The more recent exploitation of the anthrax-causing bacteria occurred in 2001 as a means for bioterrorism when 22 people were infected by *bacillus anthracis* contaminated mail, resulting in 5 fatalities.[47] The occurrence has highlighted the need for an effective and sensitive detection method to prevent further biological attacks or outbreaks of the infection.

The *bacillus anthracis* bacterial spore has been employed as the delivery vehicle in anthrax attacks in the past due to its strong resistance to harsh environments[48] and is used as a microbial indicator for the presence of the *bacillus anthracis* bacteria. Contemporary means of endospore detection such as polymerase chain reaction and colony counting are labour heavy and require trained personnel to collect and analyze the test samples.[49] A convenient biomarker for the anthrax spore is dipicolinic acid (DPA), accounting for 5-15% of the dry mass of the spore and

has been shown to be present within the spore layers in concentrations of up to 1 M.[47] Current research into luminescent DPA sensors is based on the unique photophysical properties of high-affinity DPA chelation to lanthanide metals (Ln(III)). Upon sensitization by DPA, lanthanide metals trigger bright luminescence under UV excitation and convey longer emission lifetime than that of free Ln(III).[50]

Lester and Ponce developed a method by which DPA spores could be detected by simply using $TbCl_3$ as a luminescent sensor, exhibiting green emission upon activation with DPA.[51] However, issues such as non-selective binding of adjacent aromatic ligands to the Tb(III) ions can give rise to false positive signals[52] and anion binding to the sensing ion can additionally cause false negatives by blocking the sensor binding site.[53] In order to sides-step luminescent lanthanide sensing drawbacks such as false positives and negatives, water-induced emission quenching and weakly observable photophysical changes upon DPA binding, research into producing lanthanide 'platform' molecules for DPA sensing has flourished in recent years.

Such a platform was produced by Ponce et al. in the form of the macrocycle DO2A (1,4,7,10-tetraazacyclododecane-1,7-diacetate), shown in Figure 1.11, an intriguing compound that exhibits strong 1:1 binding to Tb(III), whilst keeping three adjacent coordinating sites open, permitting efficient Tb-DPA binding and eliminating water-induced emission quenching.[54]

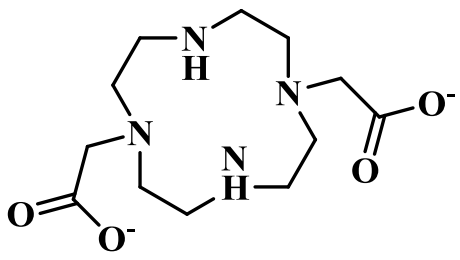

Figure 1.11. Molecular structure of Tb(III) platform DO2A.

The macrocycle cradles an atom of Tb(III) when exposed to a source of the lanthanide and forms a 1:1 complex with extremely weak green emission. Upon contact with DPA^{2-}, as shown in Figure 1.12, the $[Tb(DPA)]^{+}$ complex binds to the analyte in 1:1 ratio and forms the ternary $[Tb(DO2A)(DPA)]^{-}$ complex with higher affinity for DPA^{2-} ($K_{A=}$ $10^{10.7}$ M^{-1}) than that of simple Tb(III).[55] The $[Tb(DO2A)(DPA)]^{-}$ complex exhibits bright green emission of λ_{max} at 545 nm with a quantum yield of Φ_{em}= 0.10, much higher than that of Φ_{em}= 0.06 for the simple $[Tb(DPA)]^{+}$complex. The increased quantum yield marks for improved detection of the bacterial spore as the photophysical changes are observed more easily.

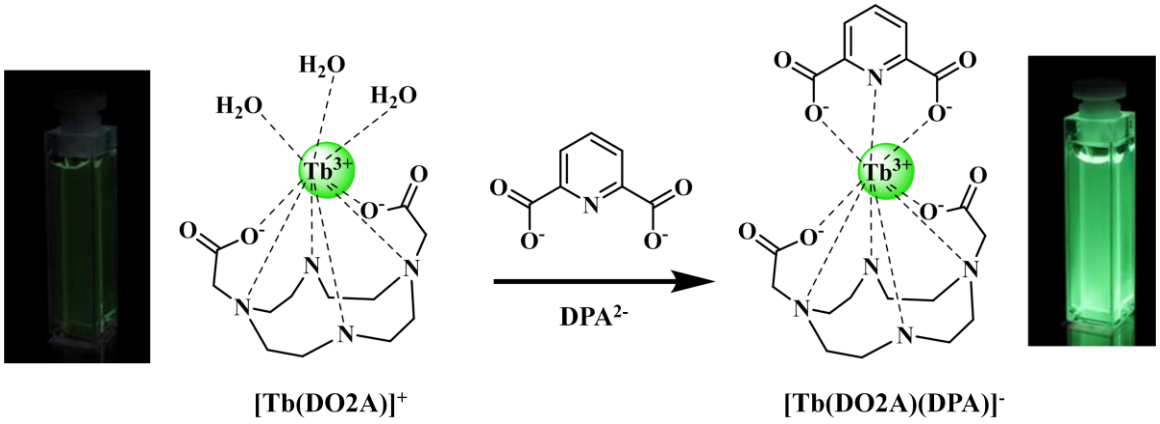

Figure 1.12. Molecular structure of complexes $[Tb(DO2A)]^{+}$ and $[Tb(DO2A)(DPA)]^{-}$ and photographs of their respective emission in solution under UV light.[54]

The first example of ratiometric DPA detection at a supramolecular monolayer surface was demonstrated by Huskens et al by building a sensing platform made up of a monolayer of β-cyclodextrin on a glass surface on which DPA-sensing building blocks are attached in a non-covalent manner.[56] The two building blocks are comprised of an ethylenediamine tetraacetic acid (EDTA) based ligand as well as a naphthalene based antenna, both attached to the β-cyclodextrin

monolayer by adamantyl groups and both designed for coordination to Eu(III) ions. After treatment with $EuCl_3$, a Eu(III)-platform complex is created with bright red emission shown in Figure 1.13 due to energy transfer from the europium-coordinated naphthalene moiety to the lanthanide center activating Eu(III) luminescence. Upon contact with DPA molecules, the DPA analyte displaces the naphthalene building block from the Eu(III) center resulting in a distinct blue emission due to the loss of energy transfer from the naphthalene moiety to the Eu(III). The system was shown to be remarkably sensitive with a detection limit of 25 nm of DPA, offering selective binding to the analyte with a response time of within 10 min.

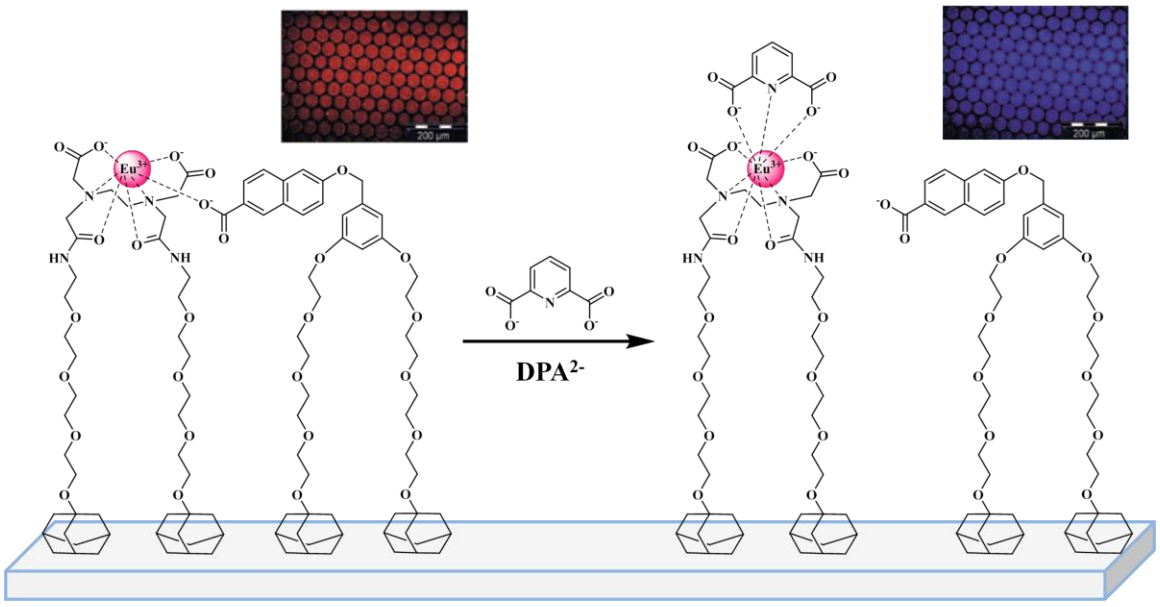

Figure 1.13. Molecular structure of ratiometric DPA detection system at a supramolecular monolayer surface with naphthalene and EDTA building blocks.[56]

These studies demonstrate the versatile application of sensitized lanthanide luminescence as highly efficient sensitive and selective sensor for DPA. Though simple molecules such as $EuCl_3$ and $TbCl_3$ can effectively detect DPA, the presence of 'platform' molecules aids in the selectivity and sensitivity of detection and by-pass several issued encountered by using lone lanthanide ions as sensing devices.

1.5 Organoboron Compounds

Organoboron chemistry has garnered remarkable attention within the last few decades due to its interesting photophysical properties and subsequent versatile applications; for instance, in OLEDs as emitters and electron- transport materials, as luminescent sensors for small anions and as photoresponsive materials. The wide research field of organoboron compounds is divided into two categories: three-coordinate boron (**1.5.1**) with trigonal planar geometry and four-coordinate boron (**1.5.2**) with tetrahedral geometry.

1.5.1 Three-Coordinate Boron Compounds

The trigonal planar three-coordinated organoboron compound, shown in Figure 1.14, exhibits sp^2 hybridization and possesses an empty p_π orbital perpendicular to the plane of the molecule, causing it to be electron deficient. This property not only gives the moiety remarkable photophysical properties due to its availability for charge transfer (**1.5.1.1**), but also leads it to be susceptible to attack by electron-donor groups such as oxygen, water or other Lewis bases. In order to synthesize air and moisture-stable three-corodinate boron compounds, the Wang lab has been the long-time user of sterically bulky substituents such as mesityl (2, 4, 6-trimethylbenzene) groups around the central boron atom to increase steric hindrance and prevent attack from electron donors. Though the added steric hindrance is able to block large electron donors such as

oxygen and water, small Lewis bases such as CN^- and F^- are still able to attack the central boron atom and triger a change in geomtetry and hybridization and subsequently an observable photophysical response, leading to applications as potential anion sensors (**1.5.1.2**).[57]

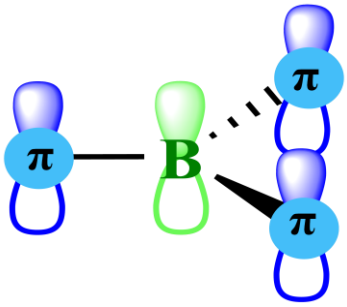

Figure 1.14. Molecular scheme of sp^2 hybridized three-coordinate boron.

1.5.1.1 Photophysical Properties of Three-Coordinate Boron Compounds

Three coordinate boron's unique empty p_π and the resulting electron deficiency, enables the moiety to participate in a charge transfer with an electron donating group that may lead to either fluorescence or overlap with an electron donating aromatic system, allowing it to act as an electron transport material.[58] Incorporating a three-coordinate boron moiety in a molecule with a donor group would therefore allow for intramolecular charge transfer (ICT) to occur, as shown in Figure 1.15, resulting significant emission from the molecule, with the HOMO level being positioned on the donor group and the LUMO localized on the boron moiety. The resulting excited state is highly polarized and can be stabilized by highly polar solvent, yielding observations of solvatochromism. Quantum efficiency of the compound is dependent on the nature of the donating group and emission can be manipulated by varying the π-conjugated system.

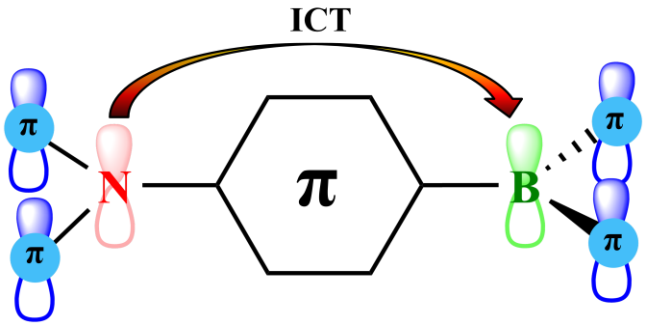

Figure 1.15. Intramolecular charge transfer in a three-coordinate boron compound.

Studies by Doi et al. indicate that distance between the donor group and the triarylboron moiety alters the efficiency of transfer significantly; increasing the distance yields both red-shifted emission of the compound as well as decreased quantum efficiency.[59]

Further work by Wang et al. classifies the triarylboron molecules into three categories: linear, U-shaped and V-shaped.[60] Linear molecules were found to have generally efficient through-bond charge transfer attributed to the conjugated aromatic linker with high quantum yields being observed. Both U and V-shaped molecules exhibited weak through-space charge transfer and overall decreased quantum yield values when compared to the linear molecules, with shorter molecule side-arms yielding larger quantum yield numbers than longer arms.

1.5.1.2 Three-Coordinate Boron Compounds as Anion Sensors

Inorganic anions such as fluoride, chloride and cyanide have widespread applications in industry and public domains as well as in a large array of chemical and biological processes. Numerous efforts have been dedicated to the production of a simple and sensitive mechanism of detection for these anions.[61] Special interest has been placed on developing fluorescent sensors for these anions due to the simplicity and high sensitivity of the process.

Fluoride anion detection methods are of particular interest due to its imperative usage in society such as in dental health, as an additive in drinking water and in osteoporosis prevention. Due to findings in the 1940s that communities with naturally occurring fluoride in their drinking water had overall better dental health than those without, community water fluoridation slowly became implemented worldwide.[62] Though extremely beneficial to society in small concentrations (0.7-1.2 ppm), excess fluoride can lead to several health problems such as bone disease, fluorosis and cancer due to fluoride's partiality to dental and bone tissue. The United States Environmental Protection Agency states that the maximum advised fluoride concentration in drinking water is 4 ppm, with strong recommendations that the concentration does not exceed 2 ppm.[63] Fluoride ions were also demonstrated to be side-products of the hydrolysis of phosphorofluoridate nerve agents, indicating that fluoride ions can be a convenient marker for nerve gases.[64] Due to their extended use in our society and its potentially harmful disadvantages, it is imperative to develop efficient, sensitive and easy to use sensors for fluoride ions.

Dimesityl-functionalized triarylboron compounds have proven to be excellent luminescent sensors for fluoride anions due to the central boron atom's empty p_π orbital, causing it to be electron deficient and a fine Lewis acid. The empty p_π orbital in triarylboron compounds is conjugated with the π system of the molecule and contributes to the compound's LUMO level.[65] A photophysical signal is observed upon binding of fluoride to the central boron atom due to that interaction modifying the conjugation of the system and altering the HOMO-LUMO band gap.[66] Though the bulky mesityl groups prevent large anionic species such as oxygen from attacking the boron center, small anions such as fluoride and cyanide can slip by the large steric presence to interact with the boron and cause photophysical signals. Furthermore, the triarylboron moiety is selective towards fluoride against some other common medium-sized anions such as

chloride, iodide and bromide due to their size, therefore accentuating the potential of the triarylboron unit as a luminescent sensor for fluoride.

Though luminescent three-coordinate boron fluoride sensors first surfaced in the late 1990's as boronic acids,[67] the first demonstration of the mesityl-functionalized boron sensor came from Yamaguchi et al. in 2001.[57] A series of boron-containing molecules, shown in Figure 1.16, were reported to exhibit a visible color change upon contact and binding with F^- anions in THF media, due to the disruption of the highly conjugated system by the boron-fluoride contact and subsequent sp^2 to sp^3 hybridization change.

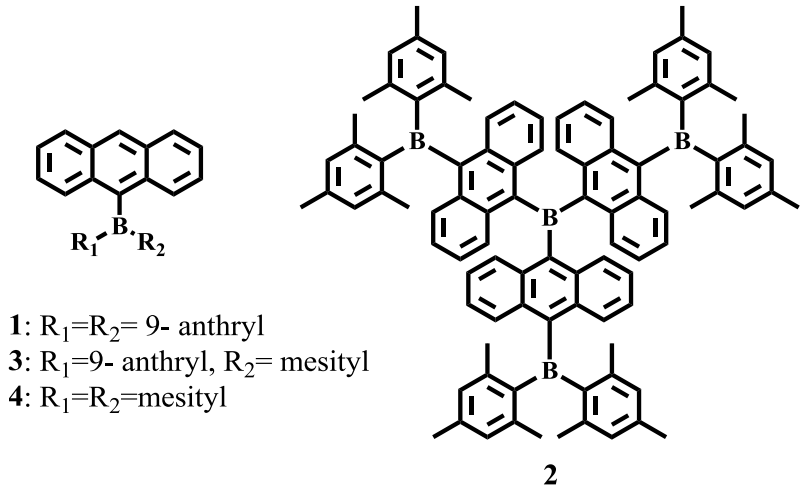

Figure 1.16. Molecular structure of Yamaguchi et al.'s triarylboron species as anion sensors.

Compounds 1, 3 and 4 displayed visible colorimetric photophysical changes from orange-shaded colors to colorless solutions upon excess addition of F- anions as monitored by UV-Vis absorption measurements, while compound 2 revealed a more complex binding pattern to the three outer boron atoms resulting in a more complicated absorbance spectrum. All four compounds exhibited strong interactions with fluoride ions with binding constants of Ka= 10^{-5}-10^{-6} M^{-1} in THF, with compound 1 demonstrating impressive selectivity towards F- anions,

showing weaker binding constants for AcO^- and OH^- and no complexation with Cl^-, Br^-, I^-, ClO_4^- and BF_4^-.

The interesting central boron hybridization change from sp^2 to sp^3 was further explored in the work towards developing fluoride detection methods, with specific attention paid to ratiometric fluorescent probes. Ratiometric fluorescent probes consist of molecules where the analyte binding site is covalently attached to two chromophores, and thus upon contact with the analyte, photophysical changes can be observed and monitored at two different wavelengths permitting for higher sensitivity, selectivity and correction for environmental effects.[68] Such sensors were reported by Tamao et al. through the synthesis of a triarylborane porphyrin conjugate displaying both colorimetric and ratiometric fluorescent responses to fluoride anions at three different wavelengths at 356 and 692 nm.[69]

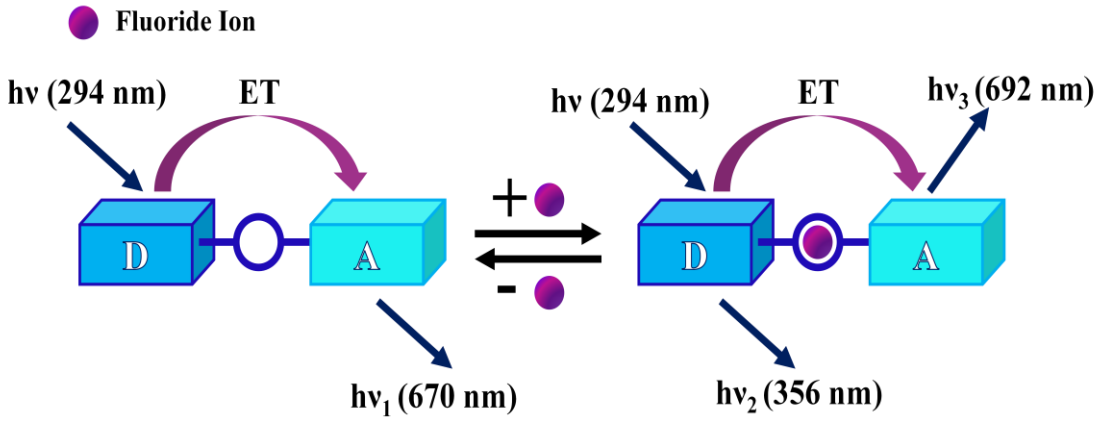

Figure 1.17. Scheme of emission radiation of a ratiometric sensor upon contact with fluoride anions.[69]

Within the molecule, the triarylboron (an energy donor, D) and the porphyrin moiety (energy acceptor, A) experience an internal charge transfer between the two once excited and produce a singular emission. Upon contact with fluoride and subsequent hybridization change at

the central boron atom, the electronic and dipolar interactions between the two moieties is disturbed resulting in both individual chromophores absorbing and emitting light differently as shown in Figure 1.17.

It was observed that energy transfer from the triarylborane moiety to the porphyrin group still occurs after complexation with fluoride, yet as fluoride is added, it is clear that the emission pattern of the sensor changes from a joint emission at 670 nm to two separate bands at 356 and 692 nm, shown in Figure 1.18, exhibiting ratiometric measurements of fluoride anion binding.

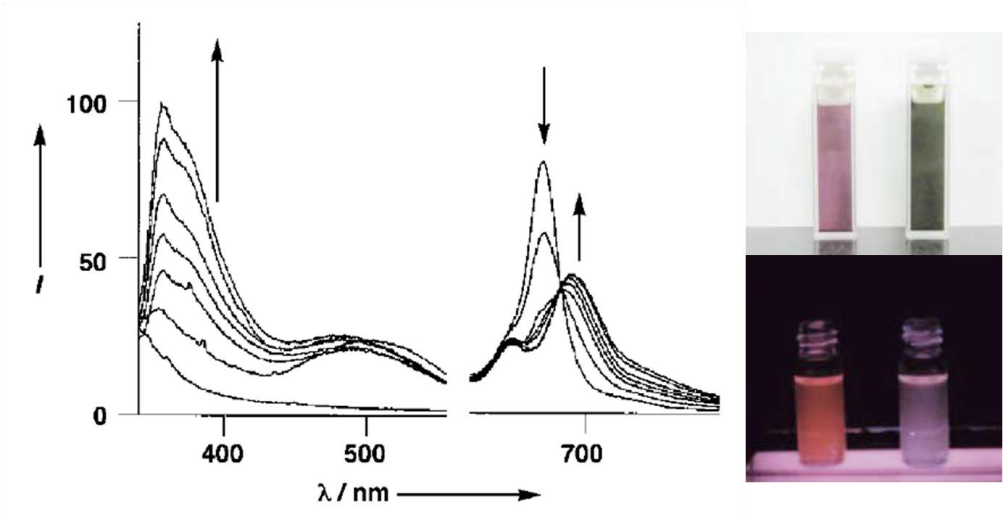

Figure 1.18. (Left) Fluorescence emission spectra of ratiometric sensor titration with TBAF in THF at rt. (Top Right) Photograph of ratiometric sensor in THF solution before (left) and after (right) addition of TBAF. (Bottom right) Same photograph under UV light radiation (294 nm).[69]

The sensor compound undergoes a colorimetric color change from purple to dark green as well as emission color change from red to blue as fluoride is added resulting in a complex with 1:1 stoichiometry in THF. High selectivity for fluoride was demonstrated as no spectral changes occurred when the sensing molecule was exposed to larger halides, acetates or hydroxides.

Though the above studies showed effective fluoride sensing abilities, they are carried out in organic solvents, and aqueous media are a lot more desirable and more practical in sensing studies. The main challenge in the development of an aqueous medium triarylboron luminescent sensor is the high hydration enthalpy encountered with these types of molecules ($\Delta H° = -504$ kJ/mol),[70] causing system dissociation in water. Gabbaï and his colleagues are leading researchers in the hunt for such a sensor by enhancing the Lewis acidity of the boron center by either introducing electron withdrawing groups within the π-conjugated skeleton of the sensing molecule, or adding secondary Lewis acidic boron to the compound. Most notably, some of their earlier work consists of the incorporation of both a rigid 1, 8- naphthalene backbone and two proximal Lewis acidic triarylboron binding sites for fluoride, shown in Figure 1.19. [71] .

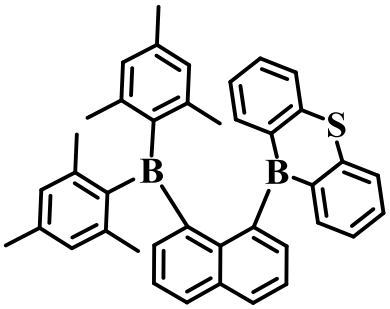

Figure 1.19. Molecular scheme of Gabbaï's aqueous medium fluoride anion sensor.

Initial observations of the sensor molecule under visible light are of an extremely bright yellow color that fades away as fluoride ions are added to the solution in THF. The sensor was shown to be stable in water and exhibit an association constant with fluoride of 5×10^{9} M^{-1}, higher than any value previously documented for a monofunctionnallized borane receptor, indicating the potential for triarylboron fluoride sensors in aqueous solutions.

1.5.2 Four-coordinate Boron Compounds

The four-coordinate boron is typically sp^3 hybridized with a tetrahedral geometry, shown in Figure 1.20, though recent studies have been reporting four-coordinated borons with planar geometry.[72]

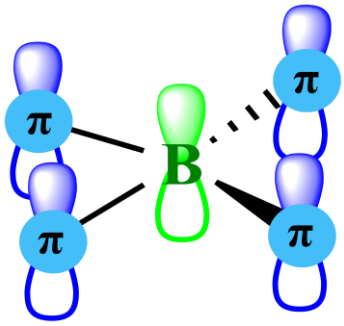

Figure 1.20. Molecular scheme of sp^3 hybridized four-coordinate boron.

Four coordinate boron compounds are classified based on the binding site nature of its chromophore chelate: N, N'-, C,C'-, N,C'-, O,O'-, C,O'- or N,O'-. Some examples of each of the before-mentioned binding modes are portrayed in Figure 1.21. Compound 1, an N,N'- chelate widely known as Bodipy, is the building block for a series of molecules popularly used as dyes.[73] Compound 2 is comprised of a N, C'- chelate backbone and displays unique thermally reversible photoisomerization from colorless to dark blue.[74] Compound 3 is a highly fluorescent O,O'-chelate diarylboron diketonate with a quantum yield in CH_2Cl_2 solution of Φ= 0.86.[75] Compound 4, comprised of a N,O'- chelate, exhibits blue fluorescence at 465 nm with a solution quantum yield of Φ= 0.406 in CH_2Cl_2 and was shown to produce high device performance in terms of luminance efficiency and power when incorporated as a hole block layer in an OLED device.[76]

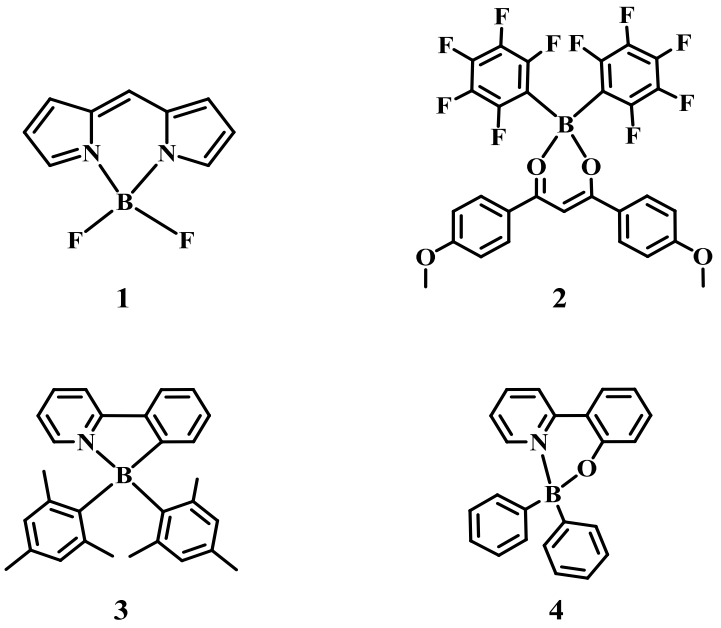

Figure 1.21. Molecular structure of model four-coordinate boron molecules.

Significant interest has arisen in 8-hydroxyquinoline-N,O'- chelated four-coordinate boron compounds due to their high potential as emitting materials as well as for other diverse applications in EL devices. Some examples are shown below in Figure 1.22.

Extensive work into this effort has been contributed by Wang et al., first demonstrating the synthesis and studies of 3 hydroxyquinoline-chelated boron atoms with varying aryl substituents on the central boron atom: $B(C_2H_5)_2q$, BPh_2q and $B(2\text{-Naph})_2q$.[77] All three compounds exhibit bright green-blue luminescence with excellent electron-transfer properties. It was additionally found that replacing aliphatic aryl substituents on the central boron atom with aromatic groups significantly increased the melting point of the compound due to solid state molecular interactions, indicating higher stability of the compound.

In order to further understand the electronic effect of substituents on the on the C5 position of the BPh_2q compound and their luminescent properties, Wang et al. synthesized BPh_2(2-methyl-q), BPh_2(5-(1-naphthyl)-q) and BPh_2(5-(2-benzothienyl)-q).[78] All three compounds exhibited emission in the green region of the spectrum with quantum yields of Φ= 0.34, 0.11 and 0.01, respectively, in CH_2Cl_2. It is noted that addition of electron-donating substituents at the C5 position results in a drastic decrease in quantum efficiency of the compound, a trend that has been previously observed with the $Al(5\text{-Me-q})_3$ compound.[79] The benzothienyl substituted-q compound demonstrates even lower quantum efficiency than that of the naphthyl-substituted compound, due to the 'heavy atom effect' of the sulfur atom quenching the emission of the compound.[5]

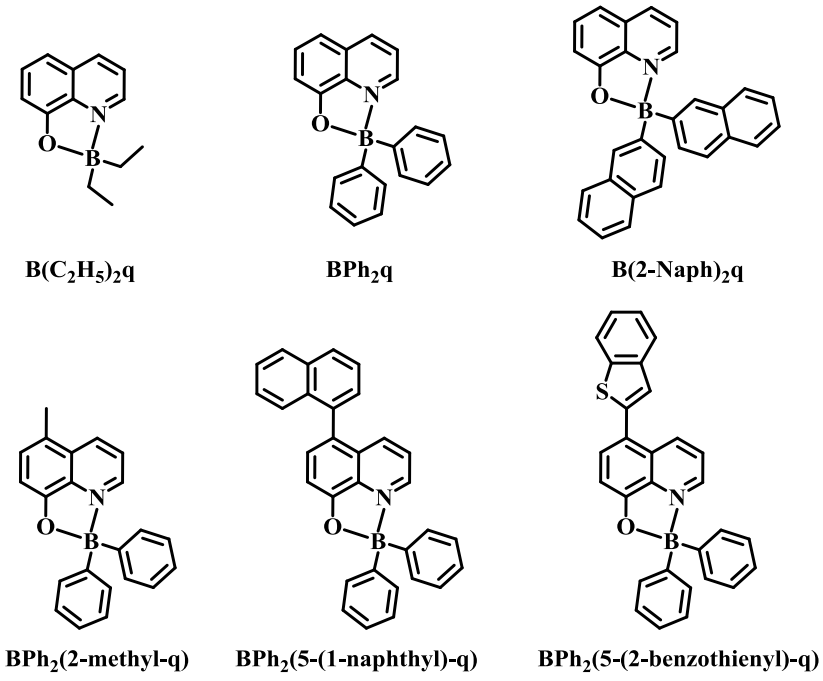

Figure 1.22. Molecular structures of substituted BPh_2q molecules by Wang et al.

These studies gave much insight into the luminescent and electronic properties of variously substituted BPh_2q compounds, and how their characteristics may be fine-tuned to accommodate desired applications.

1.6 Scope of the Thesis

The above discussion shows the versatile applications and uses of luminescent organoboron compounds and lanthanide compounds. Although much has been achieved in these research fields, the use of organoboron-based compounds for metal ions sensing especially Zn(II) ions has not yet been explored. Organoboron-functionalized lanthanide compounds are previously unknown. My research, therefore, focuses on the development of organoboron-functionalized lanthanide compounds and their applications. In addition, my research concerns the development of new organoboron-based compounds for potential use in Zn(II) ion sensing.

Chapter 2 will focus on the synthesis of Eu(III) and Tb(III) sensitizing triarylboron ligands and their respective lanthanide complexes. Full characterization of both ligands and complexes will be presented as well as preliminary data demonstrating their potential as luminescent sensors for DPA, F^- and CN^- anions in both solution and solid state.

Chapter 3 describes the synthesis, characterization and study of an assortment of organic luminescent sensor molecules for Zn(II). The ligands are comprised of two binding sites for the Zn(II) ion; both dipyridyl and hydroxyquinoline moieties were shown to successfully interact with the metal ion and trigger a certain photophysical response. Studies into the molecule's application as Zn(II) sensors will be reported therein.

1.7 References

[1] S. E. Braslavsky, *Pure Appl. Chem.* **2007**, 79, 293.

[2] E. Wiedemann, *Ann. Phys. Chem.*, **1888**, 34, 446.

[3] H. J. Queisser, *J. Lumin*., **1981**, 24, 3.

[4] B. Valeur and M. N. Berberan-Santos, *J. Chem. Educ.*, **2011**, 88, 731.

[5] J. R. Lakowicz, *Principles of Fluorescence Spectroscopy*, 2nd Ed., **1999**, Kluwer Academic/Plenum Publishers, New York.

[6] L. B. McGown and K. Nithipatikom, *Appl. Spectrosc. Rev.*, **2000,** 35, 353.

[7] H. Yersin, *Highly Efficient OLEDs with Phosphorescent Materials*, **2008**, Whiley-VCH Verlag GmbH & Co. KGaA, Weinheim, Germany.

[8] M. H. F. Wilkinson and F, Schut, *Digital Analysis of Microbes: Imaging, Morphometry, Fluorometry and Motility Techniques and Applications*, **1998**, John Wiley and Sons, New York.

[9] D. A. Skoog, F. J. Holler and T. A. Nieman, *Principles of Instrumental Analysis, 6th Ed.* Saunders Publishing Group, USA, **2007**.

[10] M. A. Baldo, M. E. Thompson and S. R. Forrest, *Nature*, **2000**, 403, 750.

[11] L.R. Melby, N.J. Rose, E. Abramson and J.C Caris, *J. Am. Chem. Soc.*, **1964**, 86, 5117.

[12] A. K. Bansall, W. Holzer, A. Penzkofer and T. Tsuboi, *Chem. Phys.*, **2006**, 330, 118.

[13] J. H. Seo, N. S. Han, H. S. Shim, J. H. Kwon and J. K. Song, *Bull.Korean Chem. Soc.*, **2011**, 31, 1415.

[14] W. M. Yen, S. Shionoya and H. Yamamoto, *Phosphor Handbook, 2nd Ed.*, CRC Press Taylor& Francis Group, USA, **2007**.

[15] (a) D. L. Pavia, G. M. Lampman and G. S. Kriz, *Introduction To Spectroscopy*; Brooks/Cole: Washington, **2001**.

[16] D. F. Eaton, *Pure & Appl. Chem.*, **1988**, 60, 1107.

[17] A. T. R. Williams, S. A. Winfield and J. N. Miller, *Analyst*, **1983**, 108, 1067.

[18] (a) C. W. Tang and S. A. VanSlyke, *Appl. Phys. Lett.*, **1987**, 51, 913. (b) C. W. Tang, S. A. VanSlyke and C. H. Chen, *J. Appl. Phys.*, **1989**, 65, 3611.

[19] A. Curioni and W. Andreoni, *J. Am. Chem. Soc.*, **1999**, 121, 8216.

[20] F. E. Lytle, D. R. Storey and M. E. Juricich: *Spectrochem. Acta*., **1973**, 29, 1357.

[21] D. Z. Garbuzov, V. Bulovic, P. E. Burrows and S. R. Forrest,. *Chem. Phys. Lett.*, **1996**, 249, 433.

[22] M. D. Hall and H. B. Schlegel, *Chem. Mater*., **2001**, 13, 2632.

[23] (a) C. Pérez-Bolívar, V. A. Montes and P. Anzenbacher Jr., *Inorg. Chem.*, **2006**, 45, 9610.; (b) V. A. Montes, R. Pohl, J. Shinar and P. Anzenbacher Jr., *Chem. Eur. J.*, **2006**, 12, 4523.; (c) V. A. Montes, G. Li, R. Pohl, J. Shinar and P. Anzenbacher Jr., *Adv. Mater.*, **2004**, 16, 2001.; (d) R. Pohl, V. A. Montes, J. Shinar and P. Anzenbacher Jr., *J. Org. Chem.*, **2004**, 69, 1723.

[24] C. H. Chen and J. Shi, *Coord. Chem. Rev.*, **2001**, 215, 79.

[25] E. Buxbaum, *Biophysical Chemistry of Proteins: An Introduction to Laboratory Methods*, Springer, New York, **2011**.

[26] J-C. G. Bünzli and C. Piguet, *Chem. Soc. Rev.*, **2005**, 34, 1048.

[27] M. L. Cable, **2010**, *Life in Extreme Environments: Lanthanide-based Detection of Bacterial Spores and Other Sensor Design Pursuits*, Ph.D. Thesis, California Institute of Technology, California, United States of America.

[28]R. Wang and Z. Zheng, "Rare Earth Complexes with Carboxylic Acids, Polyaminopolycarboxylic Acids and Amino Acids" *Rare Earth Coordination Chemistry*. Ed. C. Huang, John Wiley & Sons, Inc., **2010**.

[29] M. F. Lappert, A. Singh, R. G. Smith, H. A. Stecher and A. Sen, "Hydrocarbon-Soluble Homoleptic Bulky Aryl Oxides of the Lanthanide Metals: [Ln(OAr^R)$_3$)]" *Inorganic Syntheses*, Vol 27, Ed. A. P. Ginsberg, John Wiley & Sons, Inc., **2007**.

[30] Y-Y. Zhang and S-X. Liu, *Acta. Cryst.*, **2009**, C65, 269.

[31] N. Kaltsoyannis and P. Scott, *The f elements*, Oxford University Press Inc., New York, **1999**.

[32] S. V. Eliseeva and J-C. G. Bünzli, *Chem. Soc. Rev.*, **2010**, 39, 189.

[33] A. Vogler and H. Kunkely, *Inorg. Chim. Acta*, **2006**, 359, 4130.

[34] J-C. G. Bünzli and C. Piguet, *Chem. Soc. Rev.*, **2005**, 34, 1048.

[35] D. Parker and J. A. G. Williams, *Metal Ions in Biological Systems: The Lanthanides and Their Interrelations with Biosystems*, Marcel Dekker, Inc., New York, **2003**.

[36] (a) M. A. El-Sayed and M. L. Bhaumik, *J. Phys. Chem.*, **1965**, 69, 275; (b) M. A. El-Sayed and M. L. Bhaumik, *J. Chem. Phys.*, **1963**, 39, 2391.

[37] S. I. Weissman, *J. Chem. Phys.*, **1942**, 10, 214.

[38] G. A. Crosby and R. E. Whan, *J. Chem. Phys*., **1962**, 36, 863

[39] (a) S. I. Weissman, *J. Chem. Phys.*, **1942**, 10, 214.; (b) G. A. Crosby and R. E. Whan, *J. Chem. Phys*., **1962**, 36, 863.

[40] J-M. Lehn, *Angew. Chem. Int. Ed.*, **1990**, 29, 1304.

[41] K.R.Z.R. Grabowski and W. Rettig, *Chem. Rev.*, **2003**, 103, 3899.

[42] I. Hemmila and V. Laitala, V. *Journal Of Fluorescence.*, **2005**, 15, 529.

[43] S. Petoud, S. M. Cohen, J-C. G. Bunzli and K. N. Raymond, *J. Am. Chem. Soc.*, **2003**, 125, 13324.

[44] S. Cotton, *Lanthanide and Actinide Chemistry*, John Wiley & Sons, Inc., England, **2006**.

[45] D. Rifkind and G. L. Freeman, *The Nobel Prize Winning Discoveries in Infectious Diseases*, Elsevier Academic Press, London UK, **2005**.

[46] G. W. Christopher, T. J. Cieslak, J. A. Pavlin and E. M. Eitzen, *J. Am. Med. Assoc.*, **1997**, 278, 412.

[47] E. Gursky, T. V. Inglesby and T. O'Toole, *Biosec. Bioterr.*, **2003**, 1, 97.

[48] G. Gould and A. Hurst. *The Bacterial Spore* (1969) New York: Academic. **1969**.

[49] E. D. Lester and A. Ponce, *IEEE Eng. Med. Biol.*, **2002**, 21, 38.

[50] M. D. Yilmaz, S-H. Hsu, D. N. Reinhoudt, A. H. Velders and J. Huskens, *Angew. Chem.*, **2010**, 49, 5938.

[51] E. D. Lester and A. Ponce, *IEEE Eng. Med. Biol.*, **2002**, 21, 38.

[52] T. Gunnlaugsson, A. J. Harte, J. P. Leonard and M. Nieuwenhuyzen, *Chem. Commun.*, **2002**, 2134.

[53] R. D. Peacock, J. J. B. Perry, S. Aime and M. Botta, *J. Am. Chem. Soc.*, **2000**, 122, 9674.

[54] M. L. Cable, J. P. Kirby, K. Sorasaenee, H. B. Gray and A. Ponce, *J. Am. Chem. Soc*., **2007**, 129, 1474.

[55] I. Grenthe, *J. Am. Chem. Soc*., **1961**, 83, 360.

[56] M. D. Yilmaz, S-H. Hsu, D. N. Reinhoudt, A. H. Velders and J. Huskens, *Angew. Chem.*, **2010**, 49, 5938.

[57] S. Yamaguchi, S. Akiyama and K. Tamao, *J. Am. Chem. Soc*.,**2001**, 123, 11372.

[58] T. Noda and Y. Shirota, *J. Am. Chem. Soc*., **1998**, 120, 9714.

[59] H. Doi, M. Kinoshita, K. Okumoto and Y. Shirota, *Chem. Mater*., **2003**, 15, 1080.

[60] D. R. Bai, X-Y. Liu and S. Wang, *Chem. Eur. J.*, **2007**, 13, 5713.

[61] R. Martinez-Manez and F. Sancenon, *Chem. Rev.*, **2003**, 103, 4419.

[62] Centers for Disease Control and Prevention., *J.A.M.A.*, **1991,** 266, 1061.

[63] United States Environmental Protection Agency, *Basic Information about Fluoride in Drinking Water* http://water.epa.gov/drink/contaminants/basicinformation/fluoride.cfm/ (accessed: July 18. 2012)

[64] T. W. Hudnall, C.-W. Chiu and F. P. Gabbaï, *Acc. Chem. Res.*, **2009**, 42, 388.

[65] (a) S. Yamaguchi, S. Akiyama and K. Tamao, *J. Am. Chem. Soc.*, **2000**, 122, 6335. (b)S. Yamaguchi, T. Shirasaka and K. Tamao, *Org. Lett.* **2000**, 2, 4129.

[66] E. Galbraith and T. D. James, *Chem. Soc. Rev.*, **2010**, 39, 3831.

[67] C. R. Cooper, *Chem. Commun.*, **1998**, 1365.

[68] J. Raker and T. E. Glass, *J. Org. Chem*., **2002**, 67, 6113.

[69] Y. Kubo, M. Yamamoto, M. Ikeda, M. Takeuchi, S. Shinkai, S. Yamaguchi and K. Tamao, *Angew. Chem. Int. Ed.*, **2003**, 42, 2036.

[70] T. W. Hudnall, C.-W. Chiu and F. P. Gabbaï, *Acc. Chem. Res.*, **2009**, 42, 388.

[71] S. Sole and F. P. Gabbaï, *Chem. Commun*., **2004**, 1284.

[72] H. Braunshweig, R. D. Dewhurst, K. Kraft, S. Ostreicher and K. Radacki, *Angew. Chem. Int. Ed.*, **2012**, 51, 2183.

[73] A. Schmitt, B. Hinkeldey, M. Wild and G. Jung, *J. Fluoresc.*, **2009**, 19, 755.

[74] Y-L. Rao, H. Amarne and S. Wang, *Coord. Chem. Rev*., **2012**, 256, 759.

[75] A. Nagai, K. Kokado, Y. Nagata, M. Arita and Y. Chujo, *J. Org. Chem.*, **2008**, 73, 8605.

[76] N. G. Kim, C. H. Shin, M. H. Lee and Y. Do, *J. Organomet. Chem.*, **2009**, 694, 1922.

[77] Q. Wu, M. Esteghamatian, N-X. Hu, Z. Popovic, G. Enright, Y. Tao, M. D'Iorio and S. Wang, *Chem. Mater*., **2000**, 12, 79.

[78] Y. Cui, Q-D. Liu, D- R. Bai, W-L. Jia, Y. Tao and S. Wang, *Inorg. Chem.*, **2005**, 44, 601.

[79] L. S. Sapochak, A. Padmaperuma, N. Washton, F. Endrino, G.T. Schmett, J. Marshall,D. Fogarty, P.E. Burrows and S. R. Forrest, *J. Am. Chem. Soc.*, **2001**, 123, 6300.

Chapter 2

Selective activation of Terbium(III) and Europium(III) luminescence with Triarylboron-functionalized carboxylate ligands

2.1 Introduction

Lanthanide ions usually display weak luminescence due to non-radiative deactivation caused by poor molar absorptivity and can only be efficiently excited by laser beams.[1] Lanthanide emission can, however, be enhanced by 'sensitizing' lanthanide luminescence through the introduction of a chelating ligand.[2] Sensitization of the rare earth ion is achieved through the absorption-energy transfer-emission (AETE) mechanism that occurs within the lanthanide complex whereas the chelating ligand acts as an energy 'antenna' or light harvester for the metal ion, subsequently promoting an increase in lanthanide emission intensity by three orders of magnitude or more.[3] Suitable lanthanide chelates not only stimulate lanthanide luminescence but also assist the lanthanide to generate narrow emission bands, long luminescence lifetimes as well large Stokes shifts.[4] In some cases, such as terbium(III) benzoate and europium(III) benzoate, the quantum efficiency can be as high as 100% and 20% respectively at 254 nm excitation.[5] Consequently, rare earth chelates have found use in a wide array of fields such as electroluminescent devices,[6] luminescent sensors,[7] and cellular imaging.[8]

Triarylboron moieties within emissive materials have been extensively studied due to their low-lying p_π orbitals on the boron center providing them with excellent electron accepting abilities. This characteristic of the central boron atom makes these functional groups ideal promoters of strong charge-transfer luminescence within an emissive material due to their unique

influence on the compound's chromophore.[9] Triarylboron compounds can also be utilized as efficient selective luminescent sensors for CN^- and F^- anions due to the sterically protected central boron's empty p_π orbital atom being susceptible to attack from small nucleophiles and subsequently undergoing some change in either the absorption or emission spectrum of the molecule.[10]

The research reported in this chapter concerns the synthesis, characterization and photophysical properties of new triarylboron-functionalized carboxylic acid ligands and their use in achieving highly luminescent lanthanide complexes. Ligands **1** and **2** were designed and synthesized. These two ligands contain a sterically bulky duryl and a biphenyl linker, respectively, between the boron and the lanthanide-coupling carboxylate moieties, as shown in Figure 2.1a. The structures of their Tb(III) and Eu(III) compounds are shown in Figure 2.1b.

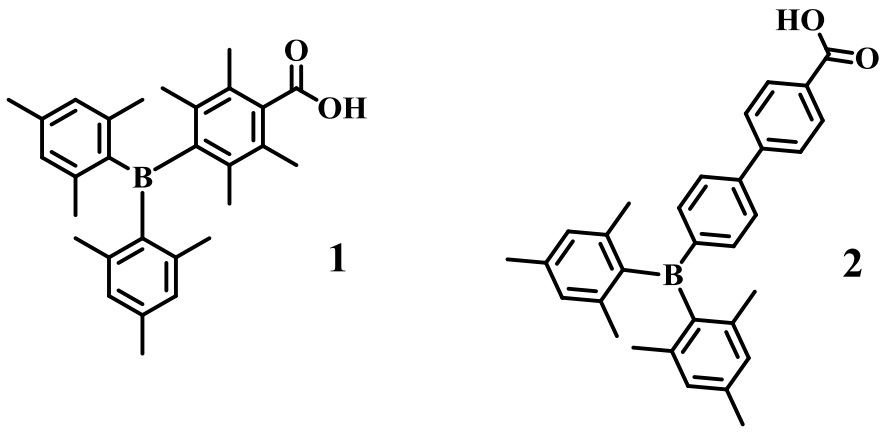

Figure 2.1a. The molecular structures of the two synthesized ligands **1** and **2**.

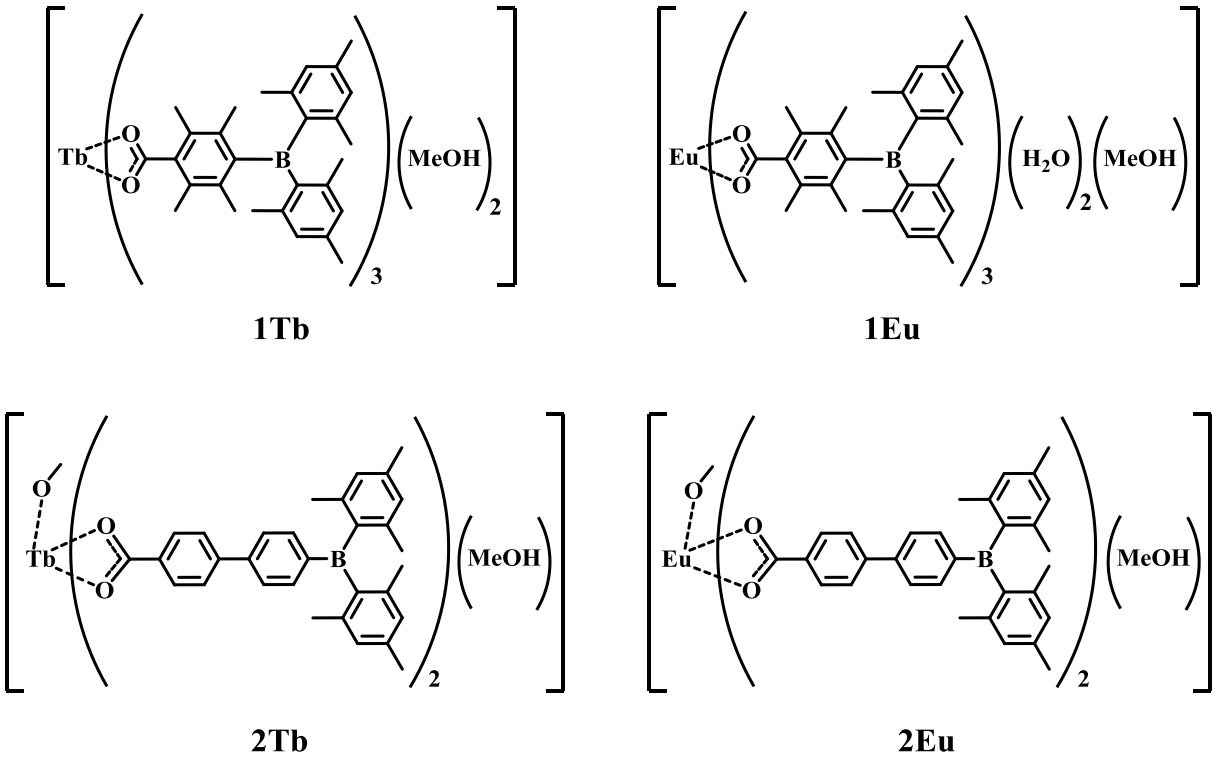

Figure 2.1b. The proposed molecular structures of the lanthanide complexes **1Tb**, **2Tb**, **1Eu** and **2Eu**.

2.2 Experimental Section

Ligand synthesis procedures were performed under N_2 using standard Schlenck line techniques. Complex synthesis was undergone under air at room temperature. Starting materials were purchased from Aldrich Chemical Co. and were utilized without further purification. Solvents were acquired from Fisher Scientific Co. and purified using the solvent purification system (Innovation Technologies Co.). Column chromatography was carried out on silica. Deuterated solvents $CDCl_3$ and CD_3OD were purchased from Cambridge Isotopes and used as acquired without additional purification or drying. NMR spectra were acquired on a Bruker Advance 400 MHz Spectrometer. All samples were measured at around 5 mg, with a deuterated

solution sample height of about 5 cm. UV-Vis data was recorded on a Varian Cary 50 Bio spectrometer. Fluorescence emission spectra were acquired using a PTI Time Master Pro spectrometer. Solid-state emission data was detected using a PTI LabSphere integration sphere simultaneously with the fluorescence spectrometer. Elemental analyses were performed at the Elemental Analysis Laboratory at the University of Montreal, Montreal, Quebec. IR Spectra were acquired using the diffuse reflectance infrared Fourier transform (DRIFT) method on a Varian 640 FTIR spectrometer.

Synthesis of 4-(dimesitylboryl)-2,3,5,6-tetramethylbenzoic acid (1)

The intermediate (4-bromo-2,3,5,6-tetramethylphenyl)dimesitylborane was synthesized as previously reported[11] by lithiating 1.2 g (4.1 mmol) of precursor 1,4-dibromo-2,3,5,6-tetramethylbenzene[12] at 195 K with n-BuLi (4.8 mmol) in dry nitrogenated THF and subsequently reacting it with dimesitylboron fluoride (1.1 g, 4.1 mmol) by using air and water sensitive schlenck line methods. The reaction was stirred overnight, worked up using water and CH_2Cl_2 and the product was purified using column chromatography and eluted with hexanes. The final product was created by stirring (4-bromo-2,3,5,6-tetramethylphenyl)dimesitylborane (1.50 g, 3.26 mmol) in dry degassed THF at 195 K under air and water sensitive schlenck line conditions and adding n-BuLi (3.6 mmol) drop wise to the reaction flask. The mixture was stirred at 195 K for 60 min after which CO_2 gas was bubbled into the reaction for an additional hour. Aqueous 1 M HCl solution was added to the reaction mixture to acidify the compound and the mixture was subsequently worked up using $CHCl_3$ and water. Column chromatography was used to purify the components of the reaction with the final product (**1**) being eluted with (5: 95) MeOH: CH_2Cl_2 as a white solid in 67% yield. ^{1}H NMR (400 MHz, 2% CD_3OD in $CDCl_3$): δ 6.66 (4H, s), 2.14 (12H, d, J=40Hz), 1.92 (6H, s), 1.88 (12H, s) ppm; ^{13}C NMR (100 MHz, $CDCl_3$): δ 175.4, 143.1, 139.9,

139.7, 138.5, 134.8, 133.5, 128.0, 127.8, 22.0, 20.2, 18.7, 16.0 ppm; ^{11}B NMR (400 MHz, 2% CD_3OD in $CDCl_3$): δ 77.95 ppm; IR (cm^{-1}): $_{asy}(CO_2^-)$1696, $_{sy}(CO_2^-)$1416 ; LRMS, m/z: [M^+] = 426.27; [M^+-mesityl] = 306.15. Anal Calcd for $C_{29}H_{35}BO_2$: C, 81.69; H, 8.27. Found: C, 81.17; H, 8.33.

Synthesis of 4'-(dimesitylboryl)biphenyl-4-carboxylic acid (2)

Compound **2** was synthesized, using a previously reported method[13], by dissolving (4'-bromobiphenyl-4-yl)dimesitylborane (1.1 g, 2.3 mmol) in dry and degassed THF and cooled to 195 K under N_2. Once cooled, n-BuLi (2.5 mmol in hexane) was slowly added dropwise to the flask and the mixture was left to stir for 60 min. CO_2 gas was bubbled into the reaction flask for an additional hour followed by the addition of 1 M aqueous HCl to acidify the mixture. The reaction was worked up using water and $CHCl_3$ and purified using column chromatography with (0.5: 99.5) MeOH: CH_2Cl_2 as the eluent. Final product (**2**) is a white powder in 54% yield.

Synthesis of the potassium salts of 1 and 2 (1-OK & 2-OK)

4-(Dimesitylboryl)-2,3,5,6-tetramethylbenzoic acid and 4'-(dimesitylboryl)biphenyl-4-carboxylic acid were modified into their respective potassium salts by individually dissolving the compounds in dry THF at 273 K under nitrogen and stirring them for 10 min under schlenck line conditions. One molar equivalent amount of potassium t-butoxide was added then to the reaction flask and the reaction mixtures were left to stir at 273 K for 60 min. Solvent was removed by vacuum, and the corresponding potassium salts were produced in quantitative yields.

Synthesis of 1Tb

To a solution of potassium 4-(dimesitylboryl)-2,3,5,6-tetramethylbenzoate (45 mg, 0.096 mmol) in 10 mL of THF, a mixture of $Tb(NO_3)_3 \cdot 6H_2O$ (14 mg, 0.033 mmol) in 5 mL THF was added dropwise and left to stir at 298 K for 1 h. The product was rinsed with MeOH 4 times and was collected as a white solid in 78% yield. IR (cm^{-1}): $_{asy}(CO_2^-)$1543, $_{sy}(CO_2^-)$1419 ; LRMS-MALDI, M^+ m/z (amu) = 1435.12. Anal Calcd for $C_{87}H_{102}B_3O_6Tb \cdot 2MeOH$: C, 71.35; H, 7.33. Found: C, 71.24; H, 7.28. Anal Calcd for $C_{87}H_{102}B_3O_6Tb$ (vacuum-pumped at 353 K): C, 72.81; H, 7.16. Found: C, 72.75; H, 7.11.

Synthesis of 2Tb

This compound was prepared as a white solid using the same procedure as described for $(B1)_3Tb$ except by using potassium 4'-(dimesitylboryl)biphenyl-4-carboxylate (28 mg, 0.058 mmol) and $Tb(NO_3)_3 \cdot 6H_2O$ (8.3 mg, 0.019 mmol) . The product was rinsed with MeOH 4 times and was collected in 60% yield. IR (cm^{-1}): $_{asy}(CO_2^-)$ 1549, $_{sy}(CO_2^-)$ 1420; Anal Calcd for $C_{64}H_{66}B_2O_4Tb \cdot (MeO)(MeOH)$: C, 69.08; H, 6.07. Found: C, 68.15; H, 5.74.

Synthesis of 1Eu

4-(Dimesitylboryl)-2,3,5,6-tetramethylbenzoate (45 mg, 0.096mmol) was dissolved in 10 mL of THF and a solution of $Eu(NO_3)_3 \cdot 6H_2O$ (14 mg, 0.033 mmol) in 5 mL THF was added dropwise and left to stir at 298 K for 1 h. The product was rinsed with MeOH 4 times and was collected as a white solid in 89% yield. IR (cm^{-1}): $_{asy}(CO_2^-)$ 1541, $_{sy}(CO_2^-)$ 1420 ; LRMS-MALDI, M^+ m/z (amu) = 1478.03. Anal Calcd for $C_{87}H_{102}B_3O_6Eu \cdot (MeO) \cdot 2(H_2O)$: C, 70.69; H, 7.35. Found: C, 69.24; H, 7.02.

Synthesis of 2Eu

This compound was prepared as a white solid using the same procedure as described for **1Eu** except by using potassium 4'-(dimesitylboryl)biphenyl-4-carboxylate (50 mg, 0.103 mmol) and $Eu(NO_3)_3 \cdot 6H_2O$ (15.3 mg, 0.034 mmol) . The product was rinsed with MeOH 4 times and was collected in 84% yield. IR (cm^{-1}): $_{asy}(CO_2^-)$1550, $_{sy}(CO_2^-)$1420 ; LRMS-MALDI, M^+ m/z (amu) = 1078.98. Anal Calcd for $C_{64}H_{66}B_2O_4Eu \cdot (MeO)(MeOH)$: C, 69.51; H, 6.11. Found: C, 70.02; H, 5.99.

2.3 Results and Discussion

2.3.1 Synthesis

The syntheses of the two triarylboron ligands and their respective lanthanide complexes were carried out using procedures described below. Elemental and MS analyses established that for ligand **1**, the lanthanide complex has the general formula of $Ln(\mathbf{1})_3(H_2O)_x(MeOH)_y$ (x = 0, y = 2 for **1Tb**, x =2, y = 1 for **1Eu**), while for ligand **2** the lanthanide complex has the general formula of $Ln(\mathbf{2})_2(OMe)(MeOH)$ **(2Tb** and **2Eu**). According to MS data, the lanthanide compounds are most likely oligomeric in solution and the solid state via either bridging carboxylate or methoxy ligands, as shown in Figure 2.2, which are commonly observed for carboxylate-chelated lanthanide compounds.[14] Efforts to obtain single crystals for the complexes were unsuccessful.

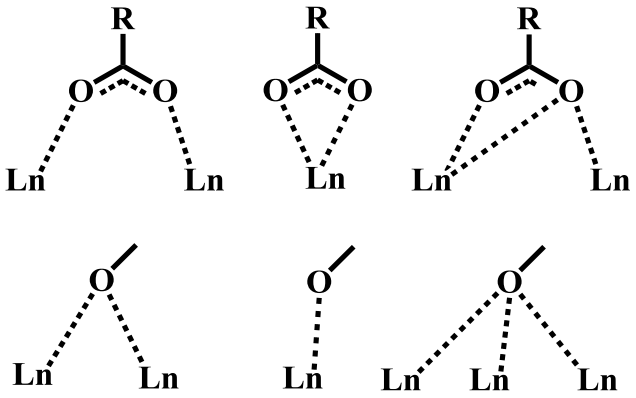

Figure 2.2. Suggested oligomeric binding models for the lanthanide complexes.

2.3.1.1 Synthesis of ligand **1**

The multi-step synthetic scheme for ligand **1** is illustrated in Scheme 2.1. Synthesis of the intermediate (4-bromo-2,3,5,6-tetramethylphenyl)dimesitylborane was attained by using previously published methods and was followed by a lithiation step performed at 195 K after which the reaction mixture was bubbled with CO_2 gas overnight. Final product was collected as a colorless odorous powder and purified using column chromatography. Full characterization was achieved using NMR spectrometry, UV-Vis absorption spectroscopy, fluorescence emission spectroscopy and IR spectroscopy.

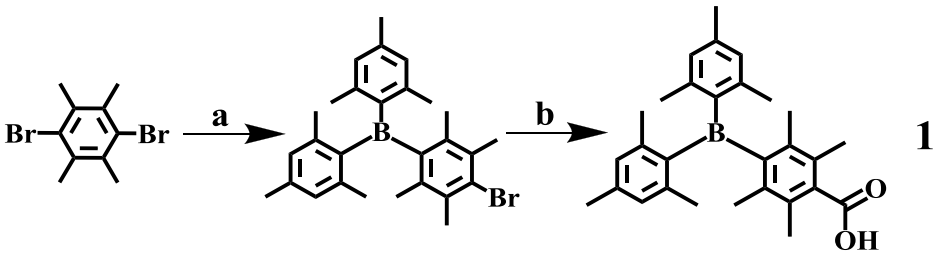

Reagents and conditions: a) (i) n-BuLi, 195 K, THF, 1 h; (ii) $(Mes)_2BF$, RT, 12 h; b) (i) n-BuLi, 195 K, THF, 1 h; (ii) CO_2, RT, 12 h; (iii) HCl aq.

Scheme 2.1. Synthetic scheme for ligand **1**.

2.3.1.2 Synthesis of ligand **2**

Ligand **2** was synthesized using a previously known multi-step process by Blight et al. (2012) shown in Scheme 2.2, with no additional change made to the existing method. Following a two-step lithiating process, the product was purified using column chromatography and confirmed by ^{1}H NMR, ^{13}C NMR and elemental analysis.

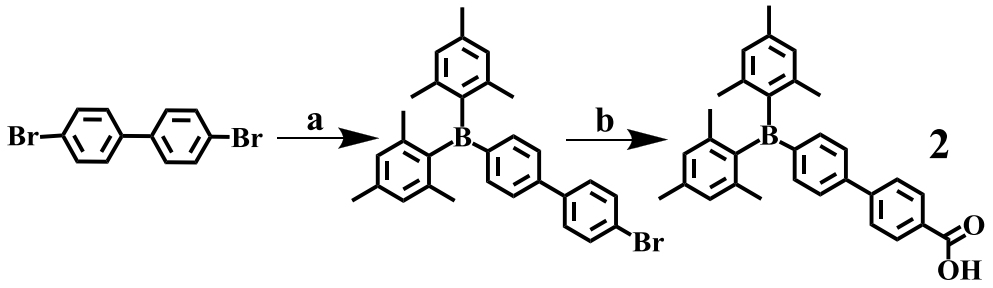

Reagents and conditions: a) (i) n-BuLi, 195 K, THF, 1 h; (ii) $(Mes)_2BF$, RT, 12 h; b) (i) n-BuLi, 195 K, THF, 1 h; (ii) CO_2, RT, 12 h; (iii) HCl aq.

Scheme 2.2. Synthetic scheme for ligand **2**.

2.3.1.3 Synthesis of potassium salts **1-OK** and **2-OK**

Due to the identical and simple procedure of the synthesis of the potassium salt of the two ligands, the procedure will be described briefly. The synthetic schemes are illustrated in Scheme 2.3. Using tBuOK as a source of base, the ligand is reacted with 1 equivalent of the potassium salt reagent under nitrogen at 273 K for an hour. Excess THF solvent was removed using the Schlenck line techniques as well as the t-butanol side-product of the reaction in order to isolate the potassium salt product. Previous attempts at creating ligand salts included reacting both compounds with an aqueous solution of NaOH under heat to convert the ligands to their

respective sodium salts. The sodium salts would be filtered out of the NaOH solution and washed with water. Low yields were obtained for these procedures due to the filter paper not collecting the entire mass of the product perhaps due to partial solubility in the solvent or to filter paper pore size. The alternate potassium salt procedure yielded much better results by utilizing an organic solvent instead.

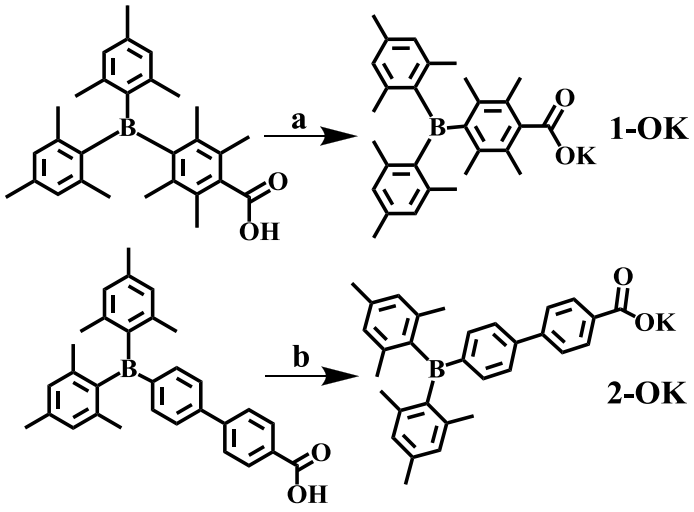

Reagents and conditions: a) (i) tBuOK., 273 K, 60 min, N_2; b) (i) tBuOK., 273 K, 60 min, N_2.

Scheme 2.3. Synthetic scheme for the potassium salt intermediates **1-OK** and **2-OK**.

2.3.1.4 Synthesis of **1Tb** and **2Tb**

Both complexes **1Tb** and **2Tb** were synthesized using an identical reaction procedure (shown in Scheme 2.4) and $Tb(NO_3)_3(H_2O)_5$ as a source of the Tb(III) ion using ligands **1** and **2** respectively. The reaction was performed at 298 K, and immediate precipitation of a white solid for both reactions was observed. Due to the poor solubility of the complex in MeOH, both complexes were isolated and purified via repeated centrifugation in MeOH.

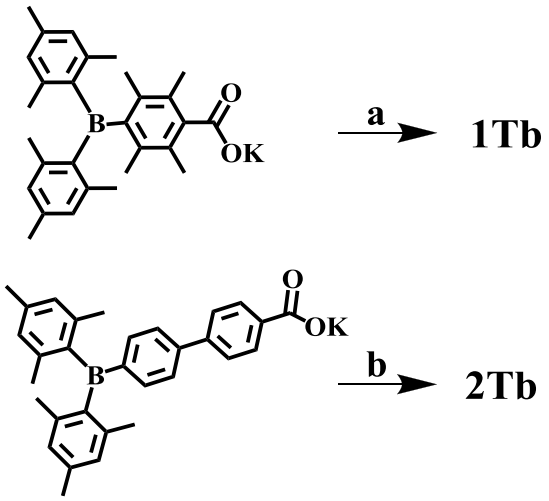

Reagents and conditions: (a) $Tb(NO_3)_3(H_2O)_5$, MeOH, 298 K, 1 h.; (b) $Tb(NO_3)_3(H_2O)_5$, MeOH, 298 K, 1 h.

Scheme 2.4. Synthetic scheme for the complexes **1Tb** and **2Tb.**

2.3.1.5 Synthesis of **1Eu** and **2Eu**

Complexes **1Eu** and **2Eu** were synthesized and purified using the same methodology as seen above for **1Tb** and **2Tb** except by using $Eu(NO_3)_3(H_2O)_6$ as a lanthanide source. The reaction scheme is portrayed in Scheme 2.5. Purification and isolation was also achieved by centrifugation in MeOH as the former procedure dictates to collect the white precipitate formed during the reaction.

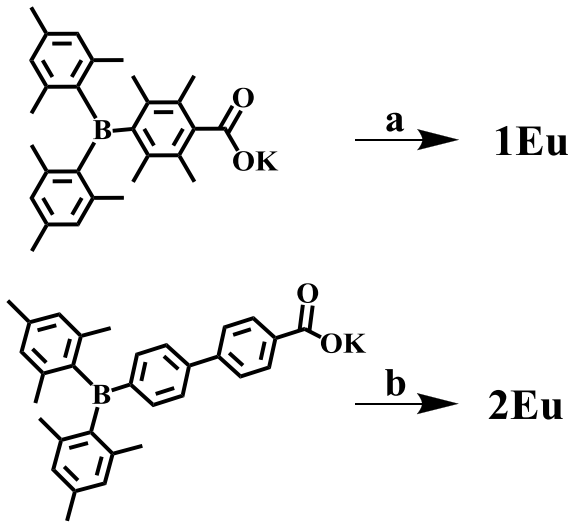

Reagents and conditions: (a) $Eu(NO_3)_3$, MeOH, 298 K, 1 h.; (b) $Eu(NO_3)_3$, MeOH, 298 K, 1 h.

Scheme 2.5. Synthetic scheme for the complexes **1Eu** and **2Eu.**

2.3.2 X-Ray crystallographic analysis

Single crystals of ligand **1** were acquired by slow evaporation at room temperature under air from a CH_2Cl_2 solution. X-ray crystallographic data was acquired and analyzed by Jiasheng Lu. A crystal was collected and mounted on glass fibers for analysis using a Bruker Apex II single-crystal X-ray diffractometer operating at 50 kV and 30 mA at 180 K with graphite monochromated Mo Kα radiation. The data collected was processed using the Bruker SHEXTL software. The crystal structure for ligand **1** is illustrated in Figure 2.3, while the crystal data is given in Table 2.1. Atomic coordinates for ligand **1** crystallographic data are noted in Table 2.2. Bond angles and lengths for ligand **1** are listed in Table 2.3. X-ray data for ligand **2** has been previously reported in literature.[13] No usable crystals for x-ray analysis were obtained for the lanthanide complexes.

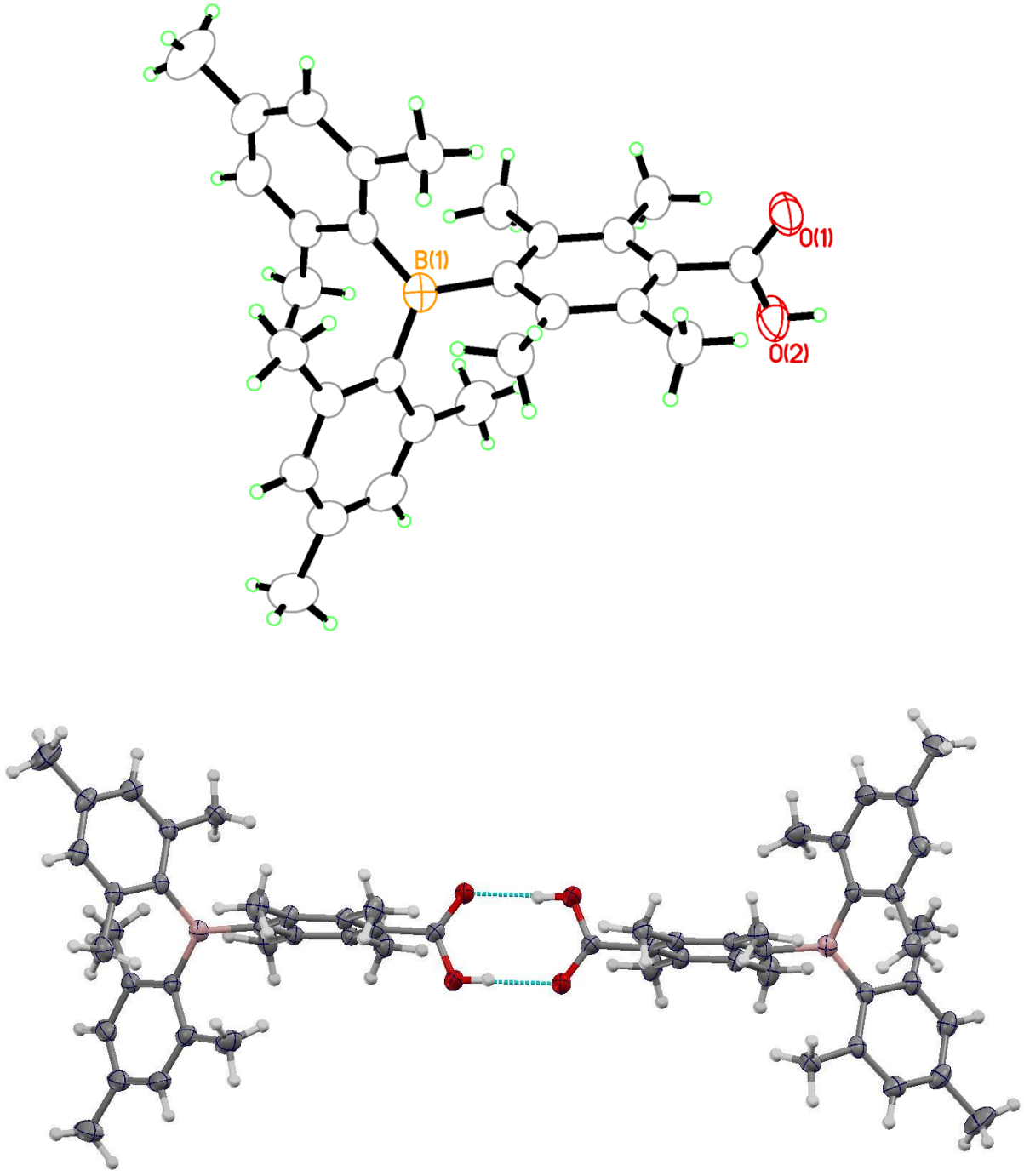

Figure 2.3. (Top) Crystal structure of ligand **1**. (Bottom) Crystal structure of ligand **1** as a dimer hydrogen bonded at the carboxylate moiety.

Table 2.1. X-Ray crystallography data for ligand **1**.

Compound	**1**	
Empirical formula	C19.33 H23.33 B0.67 O1.33	
Formula weight	284.25	
Temperature	180(2) K	
Wavelength	0.71073 Å	
Crystal system	Monoclinic	
Space group	P2(1)/c	
Unit cell dimensions	a = 9.7500(8) Å	□= 90°.
	b = 13.942(1) Å	□= 95.586(1)°.
	c = 19.171(2) Å	□ = 90°.
Volume	2593.5(4) $Å^3$	
Z	6	
Density (calculated)	1.092 Mg/m^3	
Absorption coefficient	0.066 mm^{-1}	
F(000)	920	
Crystal size	0.05 x 0.05 x 0.05 mm^3	
Theta range for data collection	1.81 to 26.00°.	

Index ranges	-12<=h<=12, -17<=k<=17, -23<=l<=23	
Reflections collected	25398	
Independent reflections	5081 [R(int) = 0.0482]	
Completeness to theta = 26.00°	99.9 %	
Absorption correction	Multi-scan	
Max. and min. transmission	0.9967 and 0.9967	
Refinement method	Full-matrix least-squares on F^2	
Data / restraints / parameters	5081 / 0 / 300	
Goodness-of-fit on F^2	1.010	
Final R indices [I>2sigma(I)]	R1 = 0.0475, wR2 = 0.1119	
R indices (all data)	R1 = 0.0860, wR2 = 0.1324	
Largest diff. peak and hole	0.172 and -0.159 e.$Å^{-3}$	

Table 2.2. Atomic coordinates (x 104) and equivalent isotropic displacement parameters (Å2x 103) for ligand 1. U(eq) is defined as one third of the trace of the orthogonalized Uij tensor.

	x	y	z	U(eq)
O(1)	1348(2)	4753(1)	9571(1)	62(1)
O(2)	579(2)	6194(1)	9817(1)	69(1)
C(1)	9047(3)	6737(2)	6011(1)	83(1)
C(2)	8206(2)	6989(2)	6606(1)	52(1)
C(3)	7990(2)	6322(2)	7121(1)	47(1)
C(4)	7223(2)	6533(1)	7678(1)	38(1)
C(5)	6652(2)	7461(1)	7737(1)	36(1)
C(6)	4734(2)	7106(1)	8681(1)	36(1)
C(7)	3523(2)	6865(1)	8253(1)	39(1)
C(8)	2446(2)	6381(1)	8536(1)	41(1)
C(9)	2606(2)	6122(1)	9243(1)	38(1)
C(10)	1456(2)	5626(1)	9554(1)	43(1)
C(11)	1123(2)	6148(2)	8087(1)	58(1)
C(12)	3329(2)	7148(2)	7486(1)	57(1)
C(13)	4875(2)	6812(1)	9388(1)	36(1)
C(14)	6185(2)	7004(1)	9855(1)	45(1)
C(15)	3813(2)	6309(1)	9673(1)	38(1)
C(16)	3973(2)	5995(2)	10432(1)	50(1)
C(17)	7099(2)	5764(1)	8226(1)	50(1)

C(18)	7626(2)	7886(2)	6658(1)	50(1)
C(19)	6864(2)	8137(1)	7204(1)	42(1)
C(20)	6254(2)	9139(2)	7196(1)	58(1)
C(21)	6301(2)	8738(1)	8766(1)	38(1)
C(22)	5296(2)	9427(1)	8901(1)	47(1)
C(23)	5698(3)	10317(2)	9177(1)	59(1)
C(24)	7060(3)	10557(2)	9355(1)	58(1)
C(25)	7464(3)	11539(2)	9639(2)	86(1)
C(26)	8044(2)	9868(2)	9251(1)	52(1)
C(27)	7707(2)	8981(1)	8949(1)	41(1)
C(28)	8881(2)	8308(2)	8843(1)	54(1)
C(29)	3775(2)	9264(2)	8704(1)	65(1)
B(1)	5893(2)	7758(2)	8390(1)	37(1)

Table 2.3. Bond lengths (Å) and angles (°) for ligand 1.

O(1)-C(10)	1.223(2)
O(2)-C(10)	1.301(2)
C(1)-C(2)	1.510(3)
C(2)-C(18)	1.380(3)
C(2)-C(3)	1.386(3)
C(3)-C(4)	1.394(3)
C(4)-C(5)	1.417(3)
C(4)-C(17)	1.514(3)
C(5)-C(19)	1.420(2)
C(5)-B(1)	1.571(3)
C(6)-C(13)	1.410(2)
C(6)-C(7)	1.411(2)
C(6)-B(1)	1.592(3)
C(7)-C(8)	1.401(3)
C(7)-C(12)	1.517(3)
C(8)-C(9)	1.396(3)
C(8)-C(11)	1.515(3)
C(9)-C(15)	1.394(3)
C(9)-C(10)	1.491(2)
C(13)-C(15)	1.405(2)
C(13)-C(14)	1.511(3)
C(15)-C(16)	1.512(3)
C(18)-C(19)	1.387(3)
C(19)-C(20)	1.518(3)
C(21)-C(22)	1.413(3)
C(21)-C(27)	1.422(3)
C(21)-B(1)	1.578(3)
C(22)-C(23)	1.391(3)
C(22)-C(29)	1.511(3)
C(23)-C(24)	1.380(3)
C(24)-C(26)	1.386(3)

C(24)-C(25)	1.511(3)
C(26)-C(27)	1.392(3)
C(27)-C(28)	1.510(3)
C(18)-C(2)-C(3)	117.74(19)
C(18)-C(2)-C(1)	121.4(2)
C(3)-C(2)-C(1)	120.8(2)
C(2)-C(3)-C(4)	122.23(19)
C(3)-C(4)-C(5)	119.91(17)
C(3)-C(4)-C(17)	117.87(18)
C(5)-C(4)-C(17)	122.13(17)
C(4)-C(5)-C(19)	117.53(17)
C(4)-C(5)-B(1)	121.59(16)
C(19)-C(5)-B(1)	120.77(16)
C(13)-C(6)-C(7)	119.15(16)
C(13)-C(6)-B(1)	119.74(16)
C(7)-C(6)-B(1)	120.99(15)
C(8)-C(7)-C(6)	120.40(17)
C(8)-C(7)-C(12)	118.23(16)
C(6)-C(7)-C(12)	121.34(16)
C(9)-C(8)-C(7)	118.90(17)
C(9)-C(8)-C(11)	120.27(17)
C(7)-C(8)-C(11)	120.83(18)
C(15)-C(9)-C(8)	122.30(16)
C(15)-C(9)-C(10)	118.25(17)
C(8)-C(9)-C(10)	119.45(17)
O(1)-C(10)-O(2)	122.29(17)
O(1)-C(10)-C(9)	122.86(17)
O(2)-C(10)-C(9)	114.85(17)
C(15)-C(13)-C(6)	120.86(16)
C(15)-C(13)-C(14)	118.06(16)
C(6)-C(13)-C(14)	121.05(16)
C(9)-C(15)-C(13)	118.29(16)

C(9)-C(15)-C(16)	121.18(17)
C(13)-C(15)-C(16)	120.52(17)
C(2)-C(18)-C(19)	122.40(19)
C(18)-C(19)-C(5)	120.17(18)
C(18)-C(19)-C(20)	117.53(17)
C(5)-C(19)-C(20)	122.29(17)
C(22)-C(21)-C(27)	117.54(18)
C(22)-C(21)-B(1)	121.54(17)
C(27)-C(21)-B(1)	120.84(16)
C(23)-C(22)-C(21)	120.1(2)
C(23)-C(22)-C(29)	117.53(19)
C(21)-C(22)-C(29)	122.23(19)
C(24)-C(23)-C(22)	122.6(2)
C(23)-C(24)-C(26)	117.4(2)
C(23)-C(24)-C(25)	121.3(2)
C(26)-C(24)-C(25)	121.3(2)
C(24)-C(26)-C(27)	122.5(2)
C(26)-C(27)-C(21)	119.81(18)
C(26)-C(27)-C(28)	117.19(18)
C(21)-C(27)-C(28)	122.99(17)
C(5)-B(1)-C(21)	118.38(16)
C(5)-B(1)-C(6)	122.26(17)
C(21)-B(1)-C(6)	119.37(16)

2.3.3. UV-Vis Absorption Spectra

UV-Vis absorption spectra for both the ligands **1** and **2** as well as their respective Tb(III) and Eu(III) complexes were recorded to better understand the electronic properties of the compounds. The absorption spectra of the free ligands are plotted in Figure 2.4, exhibiting a similar absorption band at ≈330 nm, likely caused by $\pi - p_\pi$ or π-π^*involving the triarylboron center. The absorption of ligand **2** is greater than that of ligand **1** due to the higher degree of conjugation present in the π-system.

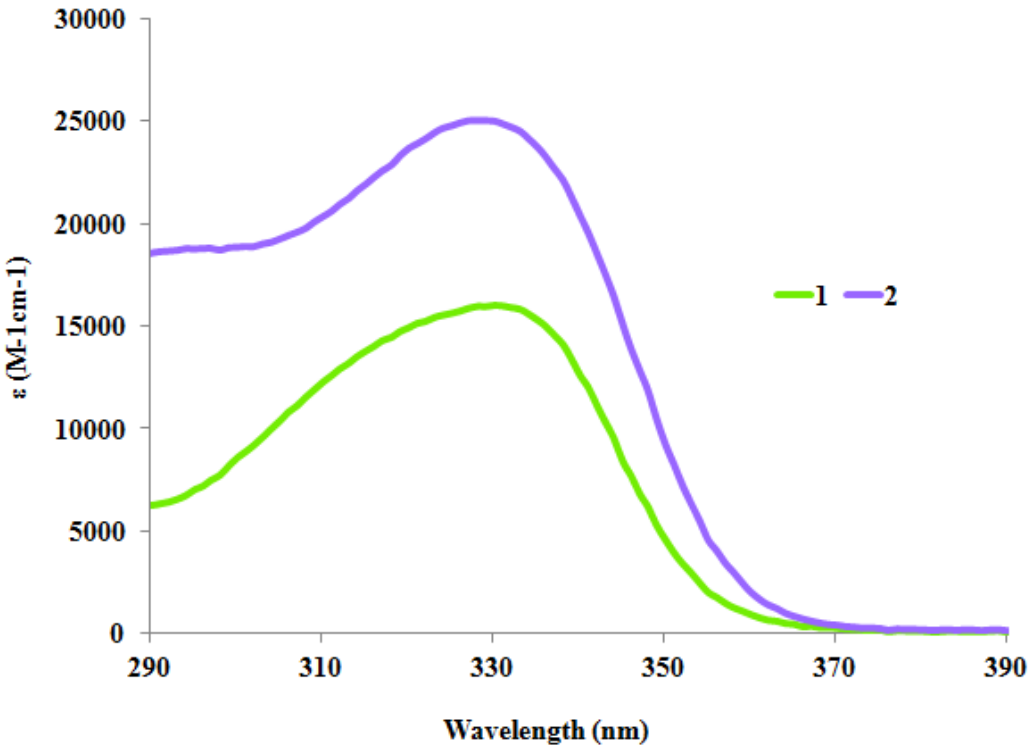

Figure 2.4. UV-Vis absorption spectra of ligands **1** and **2** recorded in THF at 298 K.

The UV-Vis absorption spectra for lanthanide complexes **1Tb**, **2Tb**, **1Eu** and **2Eu** are plotted in Figure 2.5. It is observed that the lanthanide complexes exhibit a similar absorption band wavelength as their respective free ligands at ≈330 nm, indicating $\pi - p_{\pi}$ or π-π^*transitions involving the triarylboron center. It is noted that all lanthanide compounds have greater molar absorptivity than the free ligand (approximately twice of that of the free ligand for complexes of ligand **2** and three times of the free ligand for complexes of ligand **1**), which can be attributed to the fact that the complexes contain more than one ligand and is consistent with the compositions established by CHN analysis.

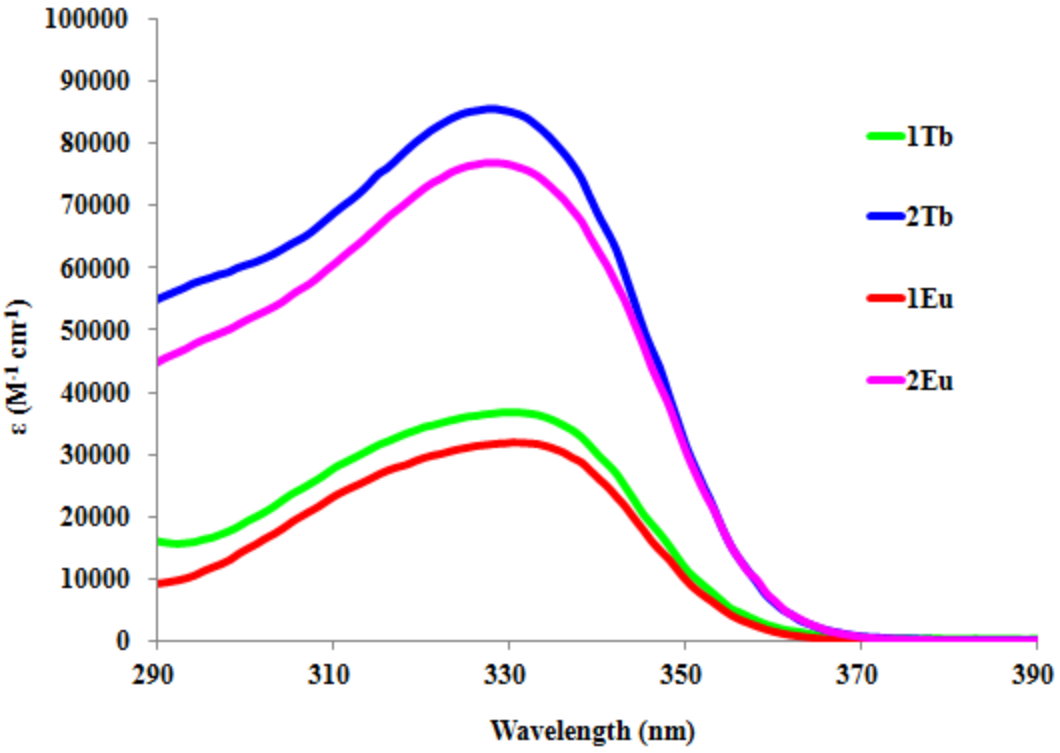

Figure 2.5. UV-Vis absorption spectra for the 4 lanthanide complexes **1Tb**, **2Tb**, **1Eu** and **2Eu** in THF at 298 K.

2.3.4 Luminescence

The luminescence properties of the ligands and their respective lanthanide complexes were examined by fluorescence and phosphorescence spectroscopies in both solid and solution state. Photophysical data acquired for all 6 compounds are summarized in Table 2.4.

Table 2.4. Photophysical properties of ligands **1** and **2** and their respective Tb(III) and Eu(III) complexes.

Compound	UV-Vis, nm (ε, M^{-1} cm^{-1})	λ_{ex}, nm THF, 298 K	λ_{em}[a], nm/τ, ms THF, 298 K	Φ^{b}_{sol}, THF	Φ_{ss}[c], total emission/Lanthanide Emission
1	330 (16,000)		384	0.05	-
2	328 (25,000)		406	0.14	-
1Tb	331 (43,000)	330	384, 489, 545, 585, 615/1.22(2)	-	0.70/0.56
2Tb	328 (60,100)	335	406	-	0.41/0.03
1Eu	331 (46,500)	345	384, 579, 590, 617/0.63(1)	-	0.14/0.04
2Eu	328 (65,800)	350	406, 579, 590, 617/0.54(1)	-	0.48/0.10

[a] In THF at 1×10^{-5}M. [b] Relative to 9, 10-diphenylanthracene = 0.95 in CH_2Cl_2. [c] Measured in the solid state in 10wt% doped PMMA polymer films using an integration sphere.

Both free ligands display weak blue fluorescence under UV radiation in THF solution (λ_{max} = 384 nm for **1** and 406 nm for **2**) as is demonstrated by their emission spectra in Figure 2.6, with quantum yields of 0.05 and 0.14 respectively in CH_2Cl_2. The higher quantum yield value calculated for ligand **2** can be attributed to the higher degree of rigidity caused by the additional conjugation present in the compound skeleton. Ligand **2** is slightly red-shifted from ligand **1** due

to the greater π conjugation and the conjugation length imparted by the biphenyl moiety compared to the duryl moiety for ligand **1**. This distance has been shown to alter the efficiency of the ICT in the triarylboron compound, causing a red-shift in emission as it is increased in a molecule.[15]

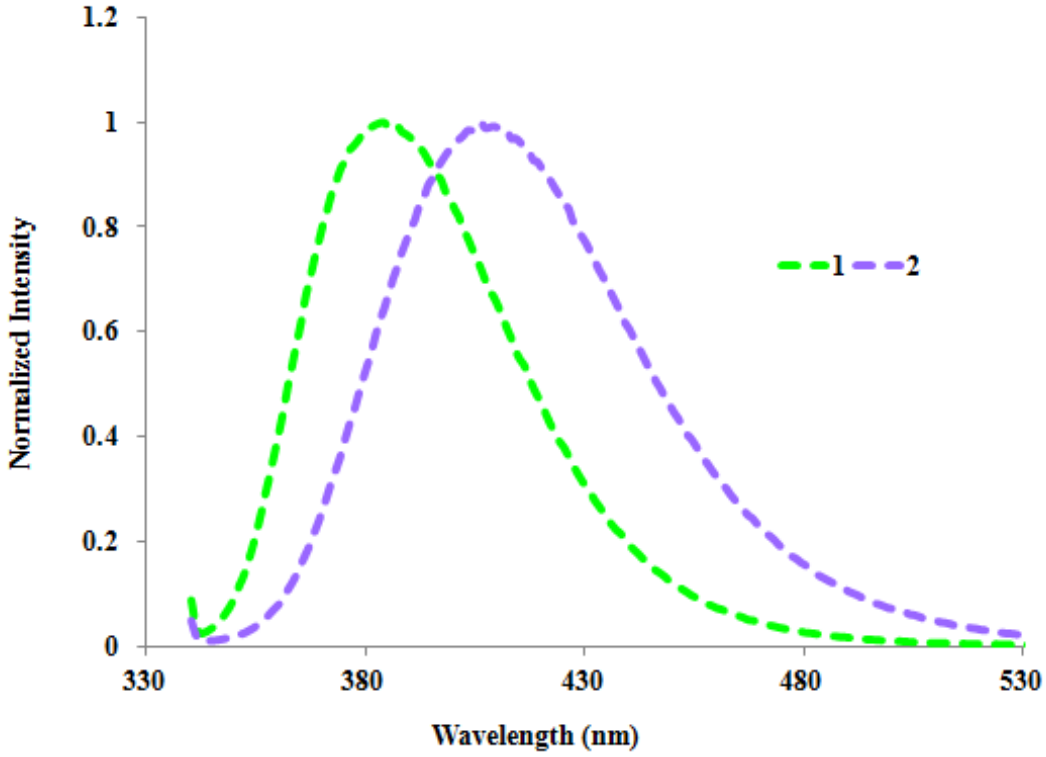

Figure 2.6. Normalized Emission spectra of ligands **1** and **2** in THF at 298 K.

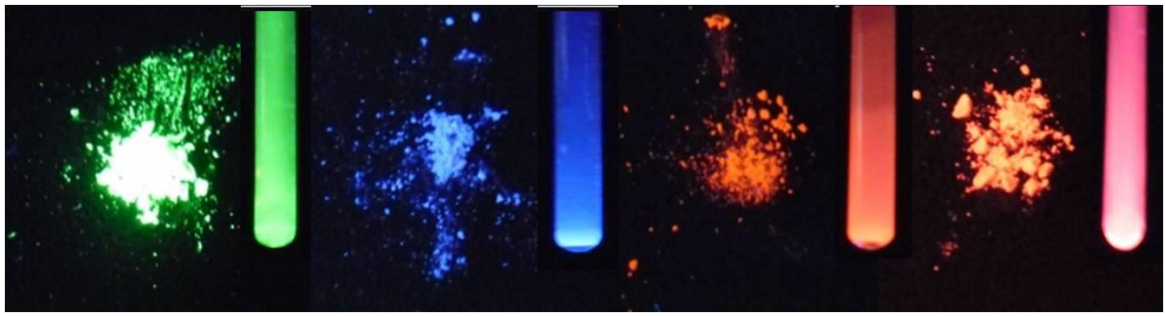

Figure 2.7. Photographs of **1Tb**, **2Tb**, **1Eu** and **2Eu** in the solid state and in THF solutions under upon irradiation at 365 nm.

Complexes **1Tb**, **2Tb**, **1Eu** and **2Eu** display very bright green, blue, red and pink luminescence, respectively, in both solution and the solid state (Figure 2.7). Emission spectra for the four lanthanide complexes in THF solution are plotted in Figure 2.8.

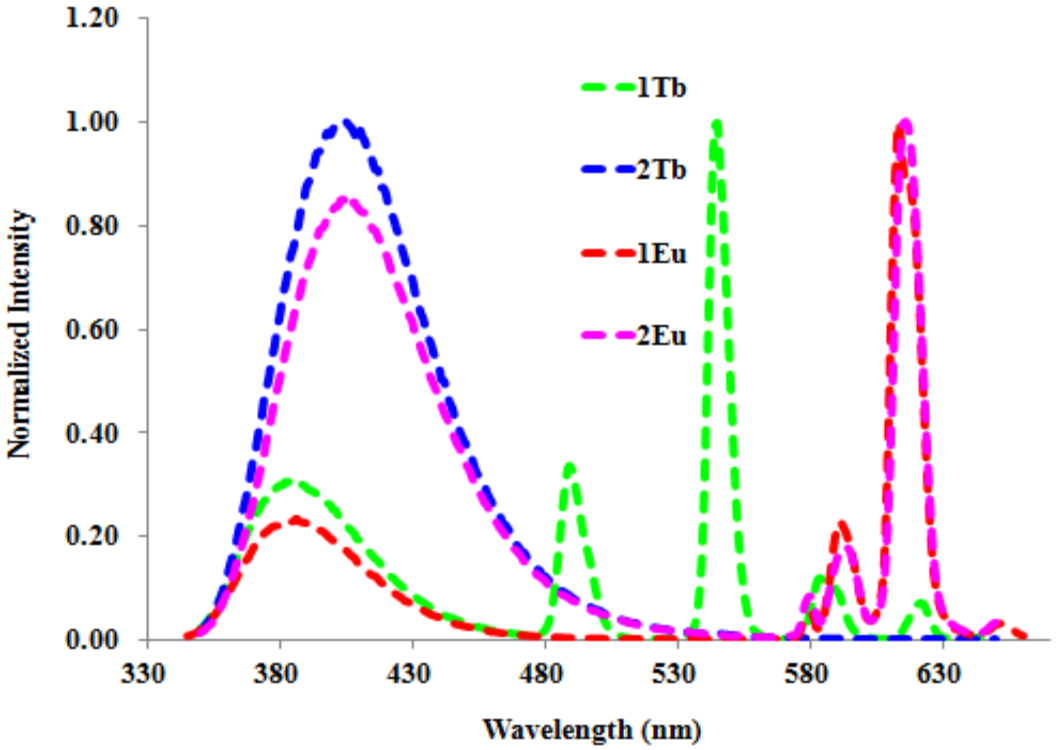

Figure 2.8. Normalized luminescence spectra of **1Tb**, **2Tb**, **1Eu** and **2Eu** complexes in THF at 298 K.

The complex **1Tb** exhibits exceptionally bright luminescence with characteristic Tb(III) emission bands in addition to the free ligand peak at λ_{em} = 489 nm, 545 nm, 585 nm and 612 nm, corresponding to the $^5D_4 \rightarrow {}^7F_n$ transitions with n = 6, 5, 4 and 3 respectively.[16] In contrast, **2Tb** does not display any Tb(III) emission bands in solution, this observation proposes the report that ligand **1** is highly effective in activating Tb(III) emission while ligand **2** is not effective.

For the **1Eu** and **2Eu** complexes, emission bands at λ_{em} = 579 nm, 590 nm and 617 nm from the $^5D_0 \rightarrow {}^7F_n$ transitions with n = 0, 1 and 2 from the Eu(III) ion were observed in addition to

their respective ligand peaks, indicating that ligands **1** and **2** are capable of activating Eu(III) emission, albeit much less efficient, compared to **1Tb**. The ligand's emission band contributes significantly in both Eu(III) compounds. Because of the blue emission band of ligand **2**, the overall emission color of **2Eu** appears to be pink. The **1Eu** compound has the characteristic red emission color of Eu(III) because ligand **1** emits in the near UV region, thus imposing less interference on the overall emission color of the complex.

In order to examine the luminescence emission and calculate quantum yield of the four lanthanide complexes in the solid state, the four compounds were doped into PMMA (10% wt) polymer to create thin films on quartz slides whose emissive properties could be recorded using an integration sphere. The emission observed by eye under UV radiation (365 nm) can be observed to be similar to that recorded in solution, as shown in Figure 2.9.

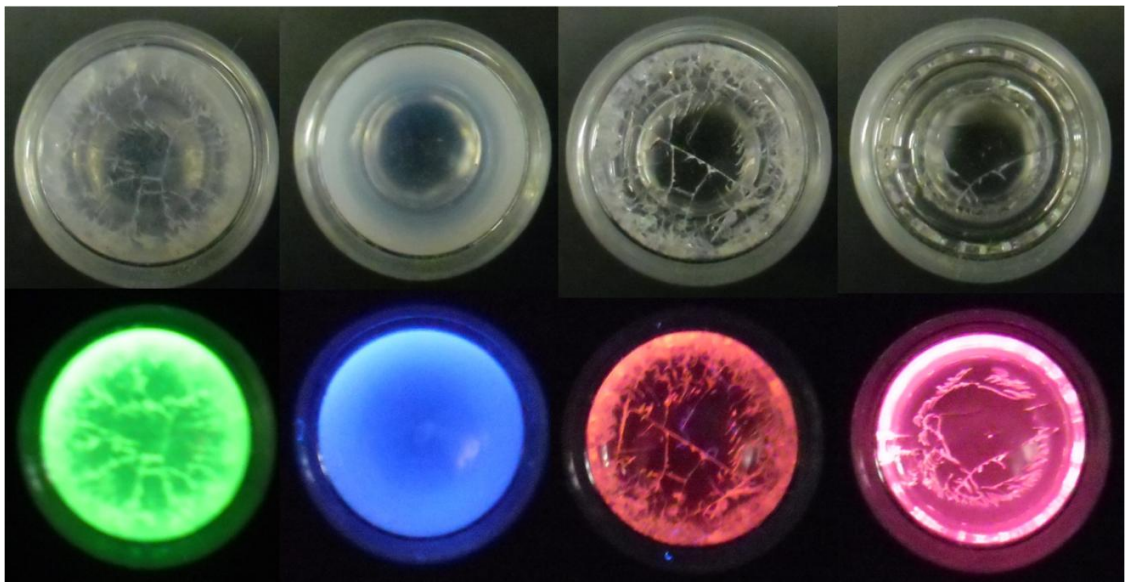

Figure 2.9. Photographs of **1Tb**, **2Tb**, **1Eu** and **2Eu** in PMMA (10wt%) (top) under visible light and under 365 nm UV irradiation (bottom).

Solid state emission spectra recorded for the four lanthanides in PMMA are plotted in Figure 2.10 and are quite similar to the spectra acquired in solution but with some differences. For complex **1Tb**, the emission band from the ligand becomes very small for and the quantum efficiency for **1Tb** was determined to be 0.70 for all emission bands and 0.56 for Tb(III) emission band (80% of the total emission).

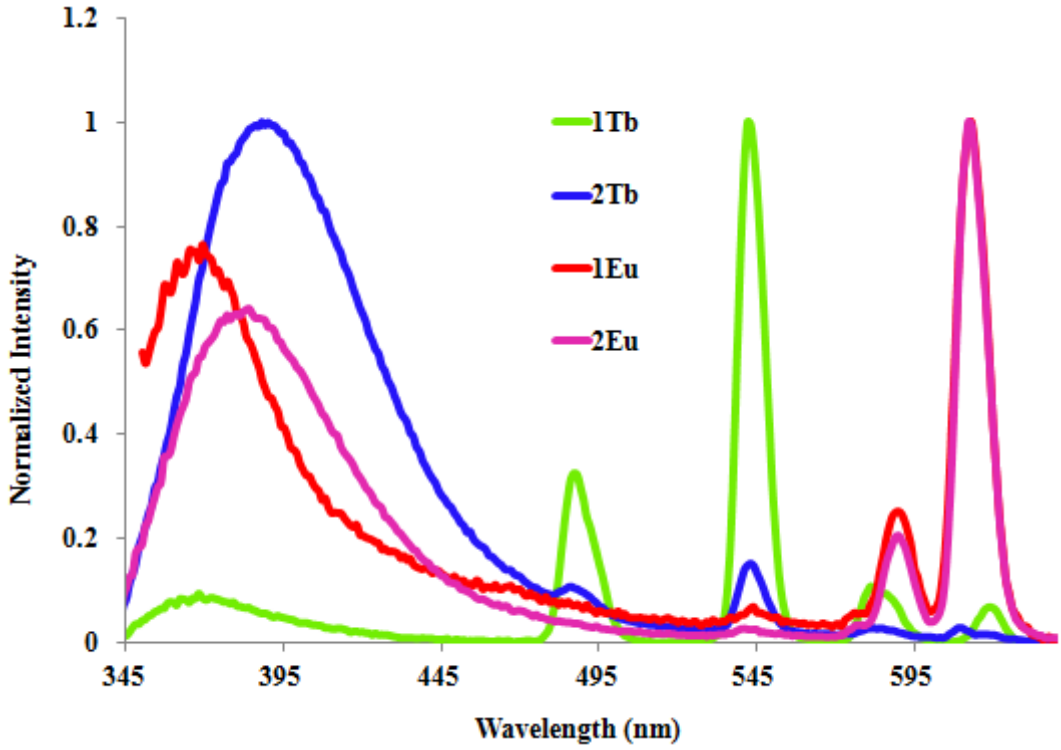

Figure 2.10. Solid state fluorescence emission spectra of the four lanthanide compounds doped in PMMA film (10% wt).

Complex **2Tb** shows very weak Tb(III) emission bands at λ_{em} = 489 nm, 545 nm, 585 nm and 612 nm that were not present in solution. The Tb(III) emission bands in **2Tb** has less than 10% contributions to the total emission of the complex (total quantum efficiency for **2Tb** is 0.41). The ligand based emission band for **1Eu** has a greater contribution in the solid state emission spectrum than that in solution as it makes up for 29% of the total emission. The total emission

quantum efficiency of **1Eu** is 0.14. The solid state emission spectrum for **2Eu** is almost identical to the spectrum acquired in THF solution, where the ligand-based emission is calculated to contribute 21% of the total complex emission and of its quantum yield of 0.48.

It is deduced from the luminescence data acquired for the four lanthanide complexes and their calculated quantum yields that ligand **1** efficiently sensitizes both Tb(III) and Eu(III) luminescence while ligand **2** efficiently activates only Eu(III) emission. Further photophysical studies were carried out to determine the cause for these observations.

2.3.5 Lanthanide Sensitization

In order to determine the significance of the boron moiety within the chelating ligand on the luminescence of the Tb(III) and Eu(III) ions, we performed the titration experiments of $Tb(Bz)_3$ and $Eu(Bz)_3$ by ligands **1** and **2**, respectively (Bz = benzoate) using luminescence emission measurements in THF at 298 K. As shown in Figure 2.11, the addition of ligand **1** to the solution of $Tb(Bz)_3$ or $Eu(Bz)_3$ led to a drastic intensity increase of the lanthanide emission bands. The exchange of ligand **1** with benzoate clearly enhances the emission of the lanthanide ions.

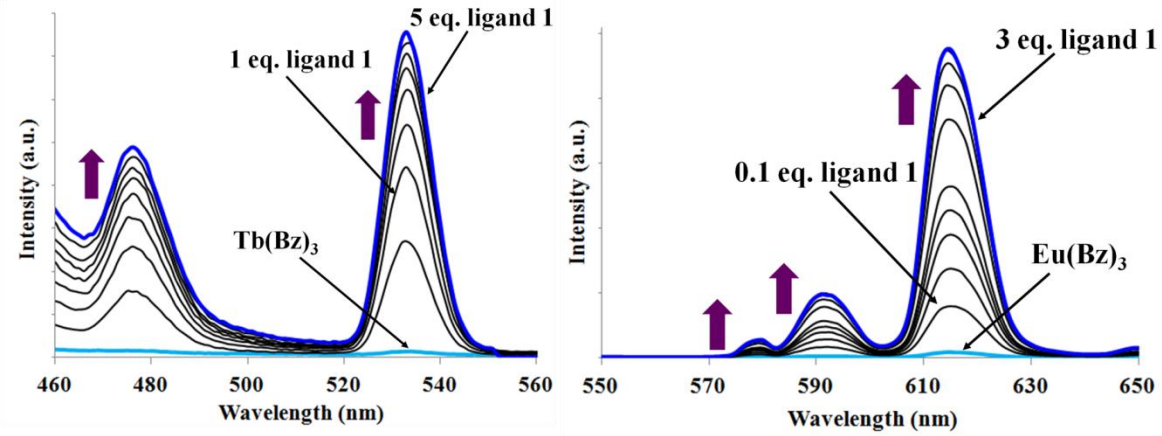

Figure 2.11. Luminescence titration spectra of $Tb(Bz)_3$ (λ_{ex} = 300 nm, left) and $Eu(Bz)_3$ (λ_{ex}= 330 nm, right) with 1 in THF (1.0×10^{-5} M) at 298 K.

A similar phenomenon was also observed for the addition of ligand **2** to the solution of $Eu(Bz)_3$, as shown in Figure 2.12. The presence of the $BMes_2$ group in the ligand is clearly critical in activation Tb(III) or Eu(III) emission.

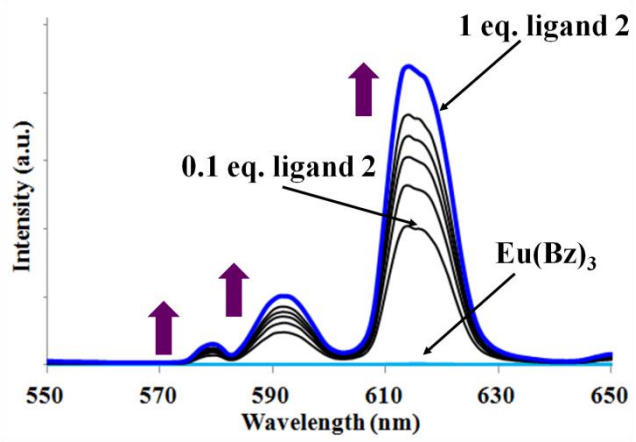

Figure 2.12. Luminescence titration spectra of $Eu(Bz)_3$ (λ_{ex}= 300 nm, left) and $Eu(Bz)_3$ (λ_{ex}= 330 nm, right) with 2 in THF (1.0×10^{-5} M) at 298 K.

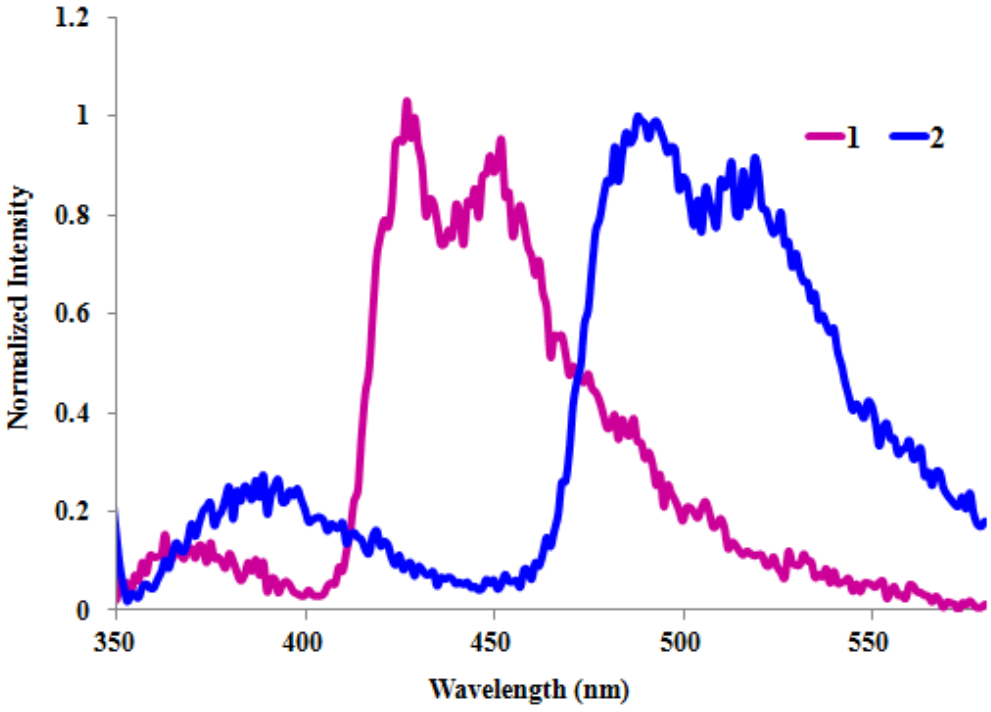

Figure 2.13. Normalized phosphorescence spectra of ligands **1** and **2** at 77K in THF.

The fact that ligand **1** can activate both Tb(III) and Eu(III) emission while ligand **2** can only activate Eu(III) emission can be explained by the triplet energy difference of the two ligands. It has been well established before that in order to activate lanthanide ion emission, the ligand's triplet energy should be close to and above that the emissive state of the lanthanide ion. To determine the triplet excited energy level of the ligands, the phosphorescence spectra for **1** and **2** at 77 K were recorded in THF, shown in Figure 2.13.

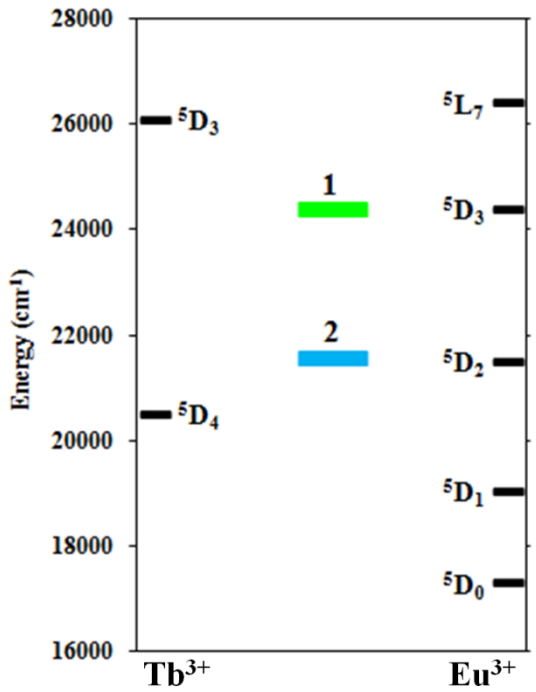

Figure 2.14. Triplet (T_1) energy levels for ligands **1** and **2** and ion energy levels in free Tb(III) and Eu(III).

The T_1 triplet energy level was calculated[17] to be 24,398 cm^{-1} and 21,563 cm^{-1} respectively, which are above the lowest excited resonance levels (or the emissive states) $^5D_4$ of Tb(III) (20,500 cm^{-1}) and $^5D_0$ of Eu(III) (17,300 cm^{-1}), as shown in Figure 2.14. The ineffective sensitization of the Tb(III) ion with ligand **2** may be attributed to the T_1 level of the ligand being

too close to the lanthanide $^5D_4$ resonance level ($\Delta\nu$ = 1,063 cm^{-1}) resulting in an inefficient energy transfer. The relatively low Eu(III) emission quantum efficiencies of **1Eu** and **2Eu** may be caused by the very large energy difference of the ligand's triplet state and the $^5D_0$ that is also known to result in low emission efficiency due to non-radiative deactivation of the lanthanide emitting state.[18]

2.4 Lanthanide Complexes as Luminescent Sensors

All solution titrations were conducted in 3 mL of dry THF solution at a concentration of 10^{-5} M of lanthanide complex to which 1μL (or 0.1 molar eq.) increments of 3×10^{-3} M of analyte (DPA, F^- or CN^-) solution in THF were added. All titrations were measured in a quartz cuvette at 298 K.

2.4.1 Lanthanide Complexes as DPA Sensors in Solution

All pyridine-2,6-dicarboxylic acid (DPA) titrations were conducted using the procedure described above. Herein titrations results for both fluorescence emission and UV-Vis absorption spectra are discussed.

Titration of **1Tb** with DPA yielded a distinct emission spectral change, as shown in Figure 2.15. Upon the addition of DPA to the lanthanide complexes, immediate quenching of the Tb(III) emission at λ_{em} = 489 nm, 545 nm, 585 nm and 612 nm was observed while the ligand's emission band gained some intensity without red shift. Significant emission color change under UV irradiation is observed from bright green to weakly purple-blue (not detected by the camera).

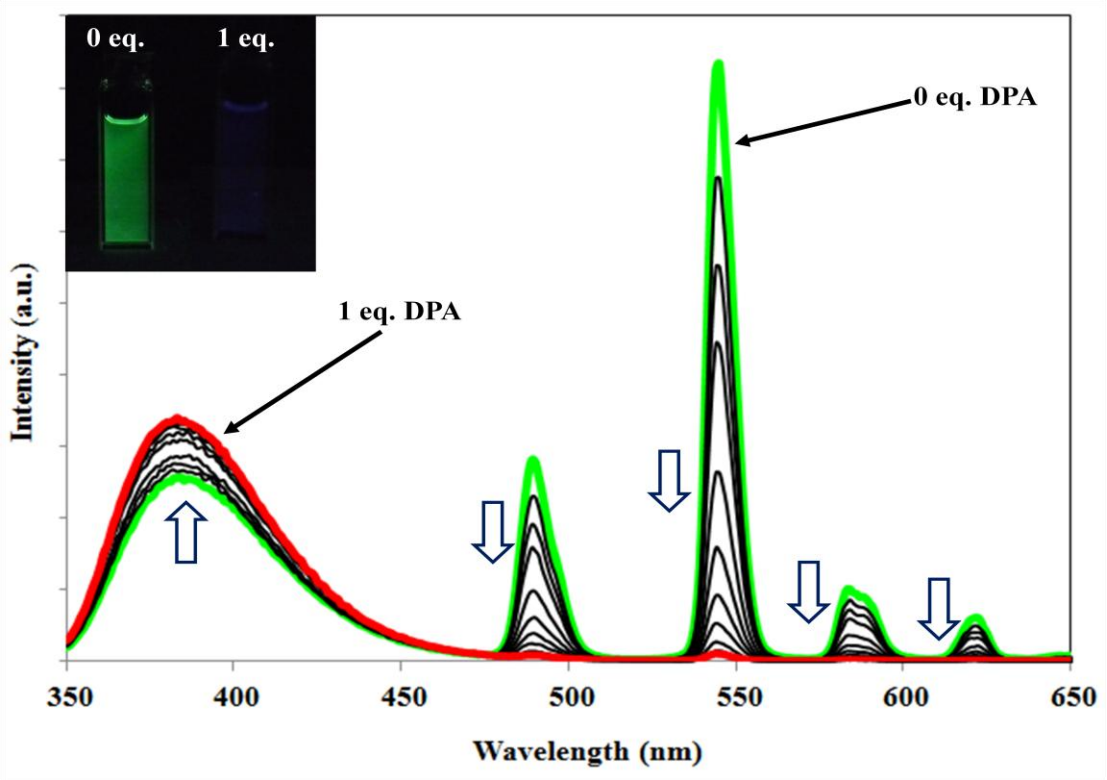

Figure 2.15. The luminescence titration spectra of **1Tb**, (1×10^{-5} M) by DPA in THF at 298 K.

A Stern-Volmer plot for the DPA emission titration of **1Tb** for λ_{max}= 545 nm, shown in Figure 2.16, indicates that full emission quenching is complete with the addition of 1 eq. DPA to the **1Tb** complex, consistent with the replacement of ligand **1** by DPA that deactivates the lanthanide emission indicating that DPA is a less efficient sensitizer for Tb(III) luminescence compared to ligand **1**.

UV-Vis absorption titration of **1Tb** with DPA showed no significant changes to the original complex spectrum with addition of DPA.

Because ligand **2** is not effective in sensitizing Tb(III) luminescence, complex **2Tb** does not demonstrate any Tb(III) emission bands and is therefore, not tested as a luminescent sensor for DPA.

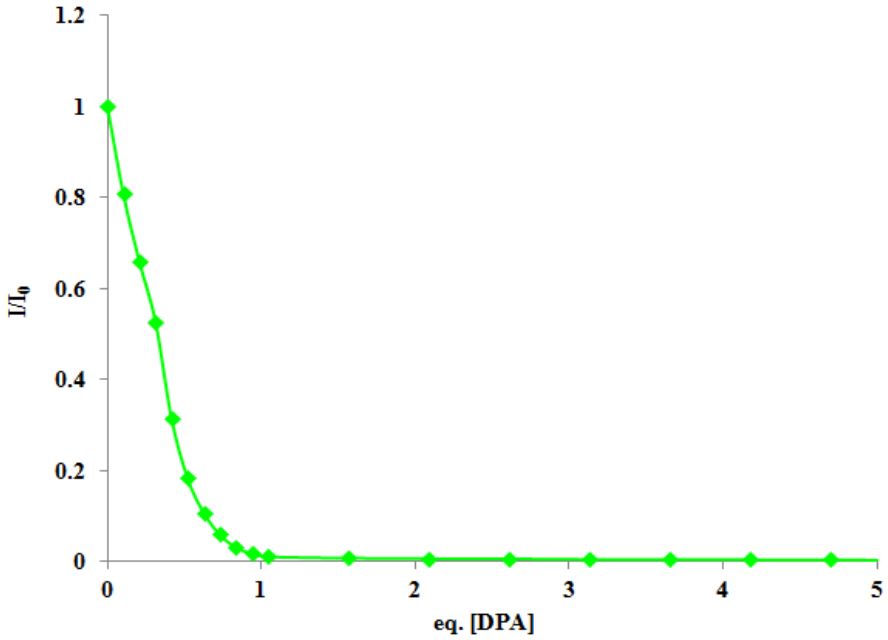

Figure 2.16. Stern-Volmer Plots of **1Tb** (λ_{max}= 545 nm) in THF at 298 K when titrated with DPA.

DPA titrations for complexes **1Eu** and **2Eu**, shown in Figures 2.17 and 2.18 respectively, yielded observations similar to those recorded for the addition of DPA to **1Tb** whereas the Eu(III) peaks at λ_{em} = 579 nm, 590 nm and 617 nm show quenching along with simultaneous ligand emission band intensity gain without any red-shift. These are indicative of DPA displacement of the triarylboron ligands from the Eu(III) metal, causing emission color change of **1Eu** from red to no color and from pink to blue for **2Eu**. This demonstrates again that DPA is less efficient at sensitizing Eu(III) than the boron ligands **1** and **2**. Blue luminescence is observed for the **2Eu** complex after addition of excess DPA due to the ligand peak at 406 nm playing such an important role in the complex's luminescence, resulting in the observation of blue emission.

UV-Vis absorption spectra of the titration of both complexes **1Eu** and **2Eu** with DPA demonstrate no photophysical changes with the addition of the DPA analyte and are therefore not included herein.

Stern-Volmer plots for the DPA titrations of both **1Eu** and **2Eu**, shown in Figures 2.19 and 2.20 respectively, indicate that the lanthanide peak (λ_{max} = 615 nm) luminescence is fully quenched with the addition of 1.0 eq. of DPA. This information supports the theory conceived previously with the results acquired from the DPA titration of **1Tb** that the DPA chelates displace the triaryboron ligands completely from their respective lanthanide centers to form a 1:1 complex with inferior emission.

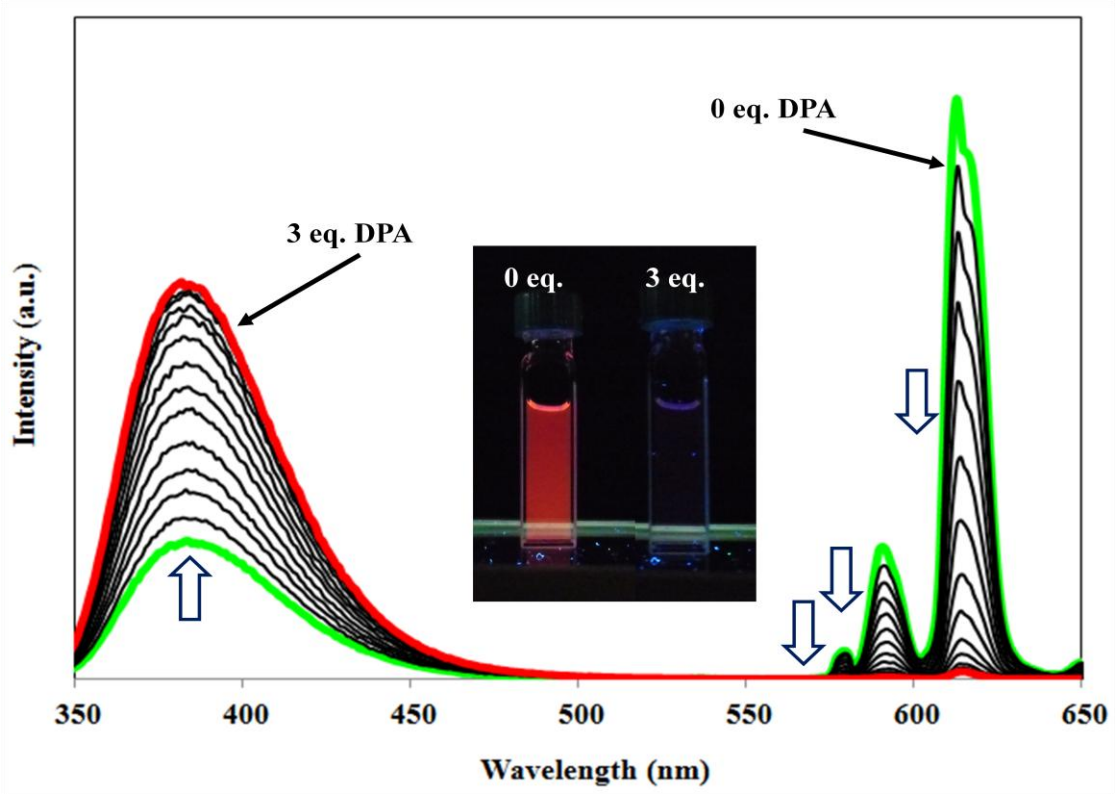

Figure 2.17. The fluorescence titration spectra of **1Eu** (1×10^{-5} M) by DPA in THF at 298 K.

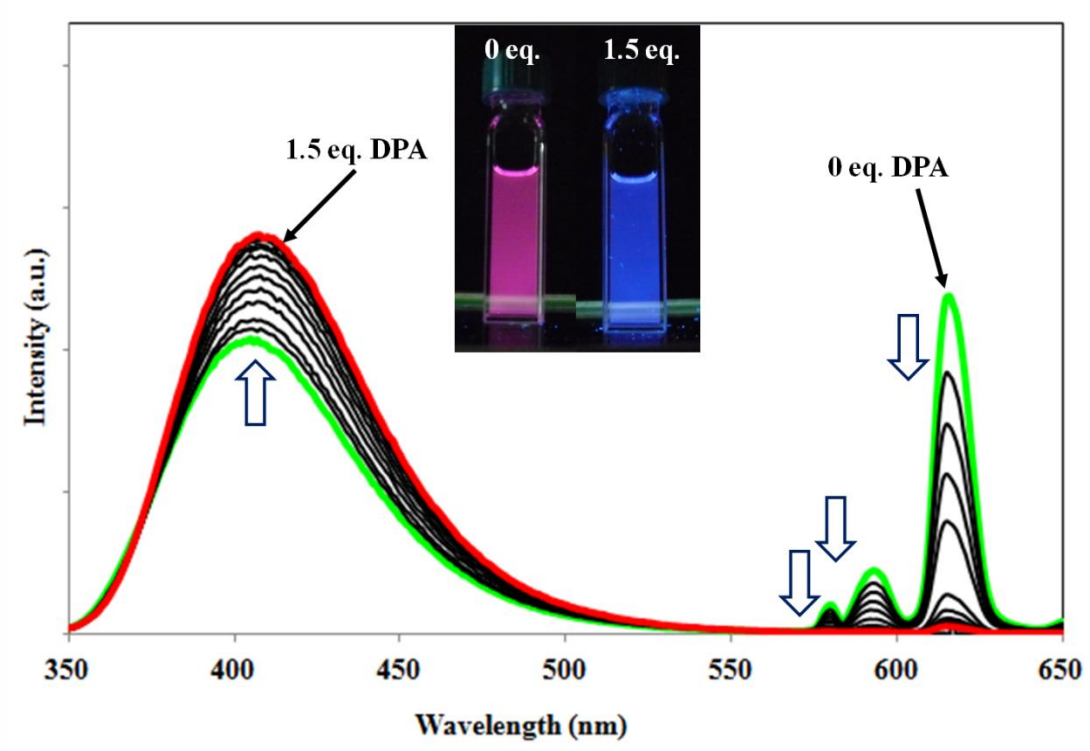

Figure 2.18. The fluorescence titration spectra of **2Eu** (1×10^{-5} M) by DPA in THF at 298 K.

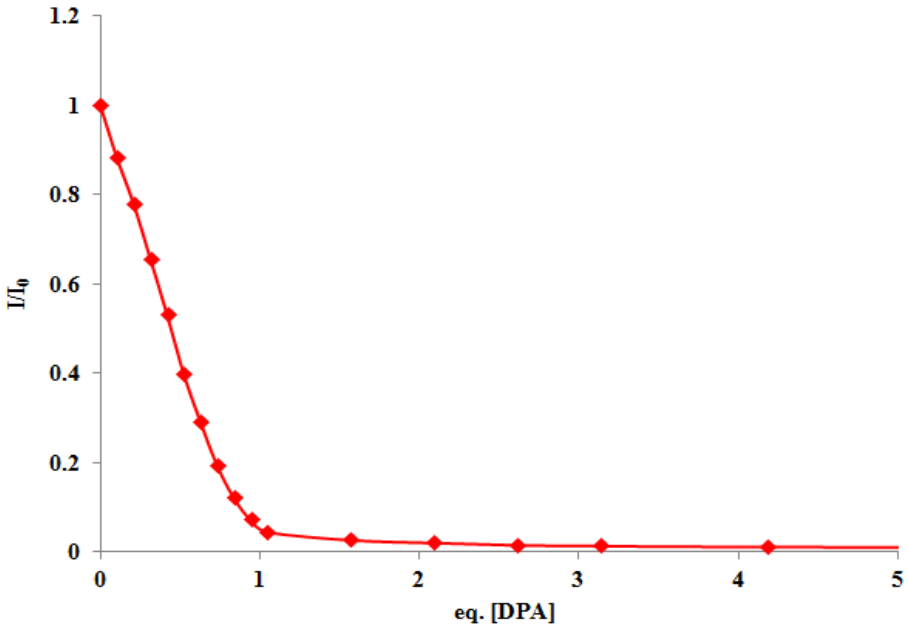

Figure 2.19. Stern-Volmer Plots of **1Eu** (λ_{max} = 615 nm) in THF at 298 K when titrated with DPA.

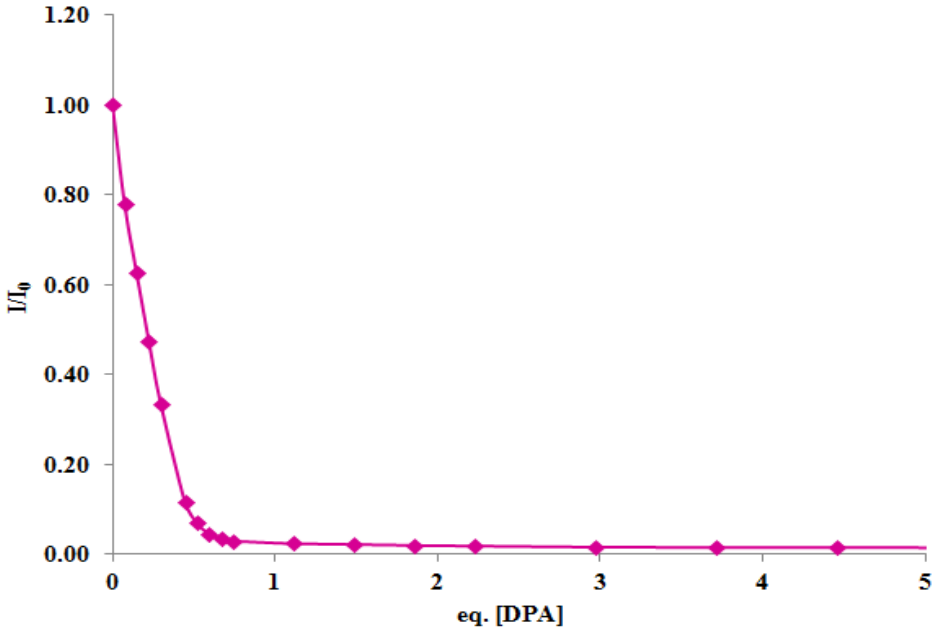

Figure 2.20. Stern-Volmer Plots of **2Eu** (λmax = 615 nm) in THF at 298 K when titrated with DPA.

2.4.2 Lanthanide Complexes as Anion Sensors in solution

To further probe the impact of $BMes_2$ on the lanthanide emission and the possible use of the lanthanide compounds in detecting anions such as fluoride and cyanide, we examined the absorption and luminescence spectral change of complexes **1Tb**, **1Eu** and **2Eu** in response to the addition of NBu_4F (TBAF) and NBu_4CN (TBACN) in THF.

For the titration **1Tb**, the addition of TBAF caused a general decrease of the Tb(III) emission bands and a red shift of the ligand's fluorescence band from ~385 nm to 430 nm, leading to the emission color change from green to blue, as shown in Figure 2.21. The absorption spectrum of **1Tb** shows a similar change of the ligand-based absorption band, shown in Figure 2.22, as the absorption peak at ~330 nm undergoes a red-shift to ~365 nm.

The quenching of the Tb(III) emission bands upon addition of F^- can be explained by the decrease of the first excited state energy of the ligand that lowers the triplet energy substantially, leading to the diminished emission intensity of the Tb(III) ion. The decrease of the first excited state energy of ligand **1** upon the addition of F^- to the boron center is caused by the low energy charge transfer transition of the $BMes_2X$ (X = F^- or CN^-) to the carboxylate, which is in agreement with the behavior of the free ligand.

Stern-Volmer plot of the **1Tb** titration with TBAF, shown in Figure 2.23, demonstrates a singular binding event, indicating that full quench of the lanthanide emission band at λ_{max} = 545 nm occurs upon addition of roughly 3 eq. of F^-.

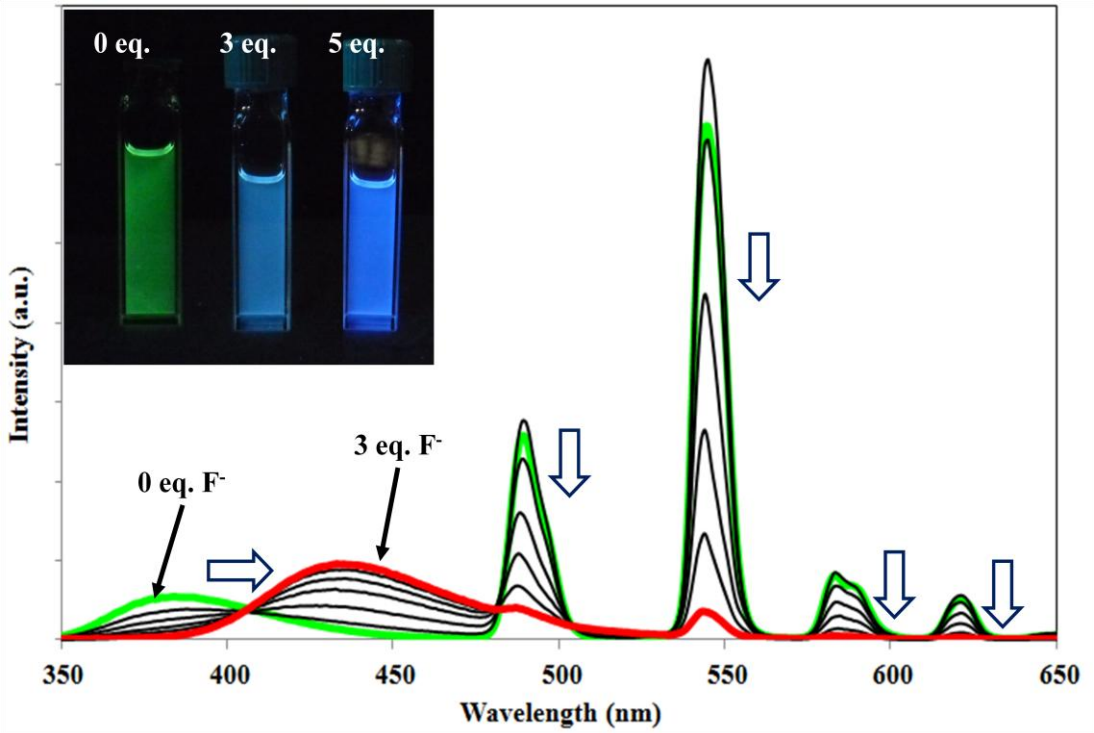

Figure 2.21. The fluorescence emission titration spectra of **1Tb** (1×10^{-5} M) by TBAF in THF at 298 K.

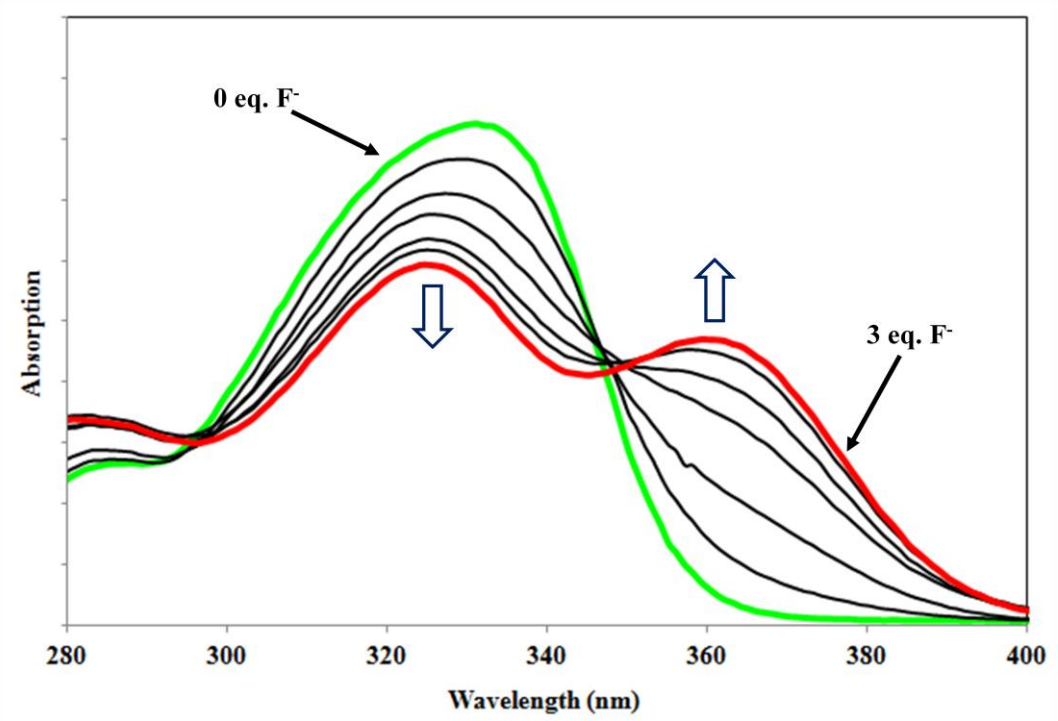

Figure 2.22. The UV-Vis absorption titration spectra of **1Tb** (1×10^{-5} M) by TBAF in THF at 298 K.

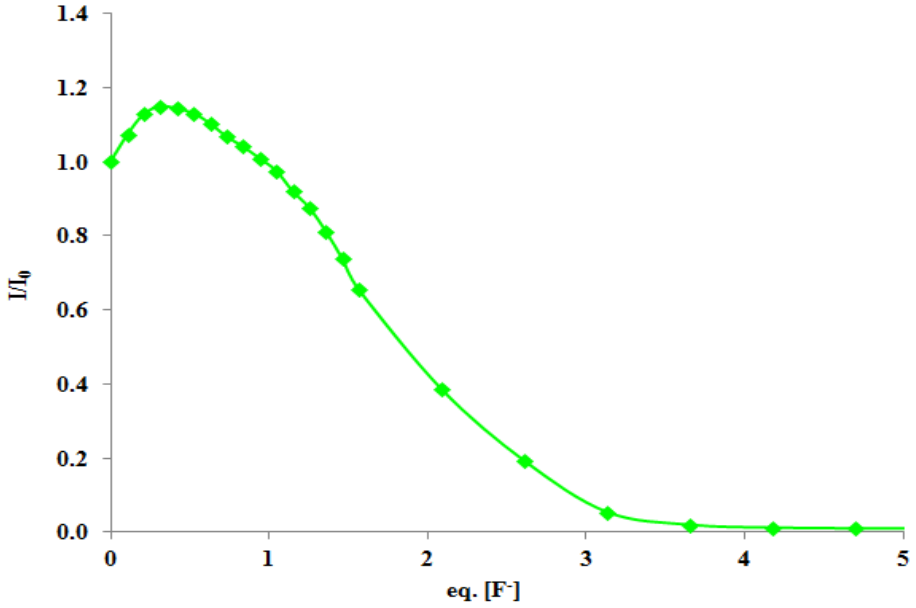

Figure 2.23. Stern-Volmer Plots of **1Tb** (λmax = 545 nm) in THF at 298 K when titrated with TBAF.

For the TBAF titration of **1Eu**, the addition of fluoride causes the luminescence of the solution to undergo multi-stage of color change. As shown in Figure 2.24, the addition of F^- to the solution of **1Eu** changes the emission color from red to pink, lavender, and finally blue, a consequence of the combined change of the ligand-based fluorescence band and the Eu(III) emission bands. The fluorescence emission changes observed for **1Eu** are similar to the ones recorded for **1Tb**, whereas quenching of the Eu(III) and simultaneous red-shift of the ligand peak is observed. UV-Vis absorption TBAF titration spectra of **1Eu**, plotted in Figure 2.25 similarly shows a red shift of the absorption band at ~335 nm to ~365 nm, following the same pattern observed for the **1Tb** complex.

It is noteworthy that the addition of F^- anions to the **1Eu** causes first a drastic increase of the Eu(III) emission peaks and only after the addition of more than 2 eq. of the anion, the Eu(III) peaks experiences intensity decrease. The initial intensity gain may be attributed to the lowering of the triplet state of the ligand after anion binding to the B atom, making it more compatible for Eu(III) emission activation. The subsequent quenching can be attributed to the replacement of carboxylate ligand by the anion.

The initial emission intensity gain observed in Figure 2.24 is also aparent in the Stern-Volmer plot for the TBAF titration of **1Eu** shown in Figure 2.26. After the intensity gain peaks at 1 eq. of added F^- anions, it is followed by a downward slope data line indicating full lanthanide emission band quenching at around 4 eq. of TBAF added.

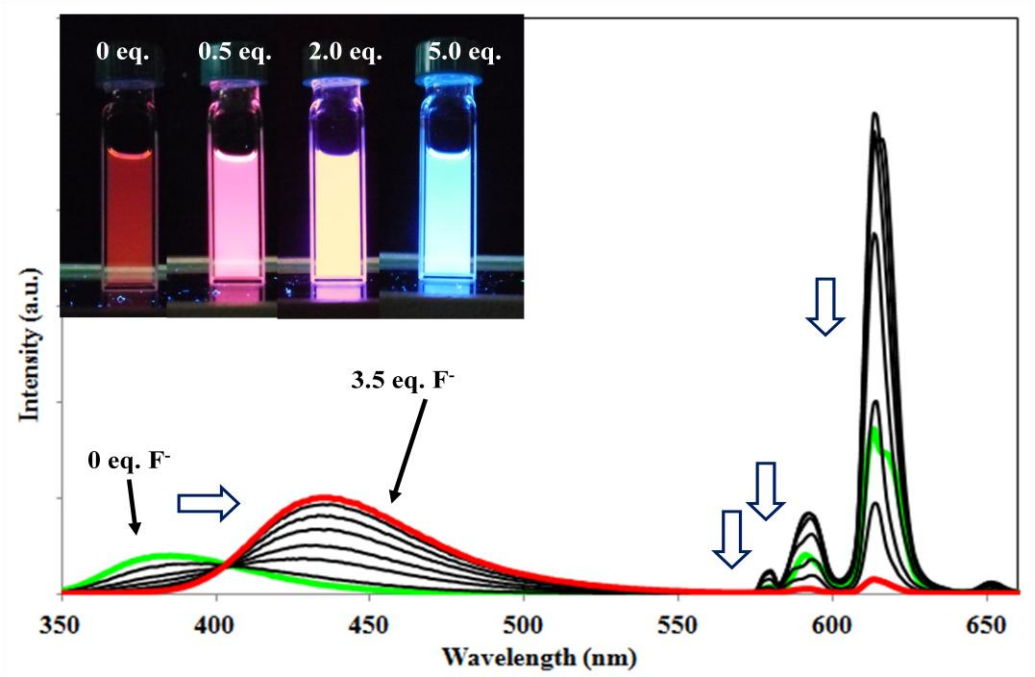

Figure 2.24. The fluorescence titration spectra of **1Eu** (1×10^{-5} M) by TBAF in THF at 298 K.

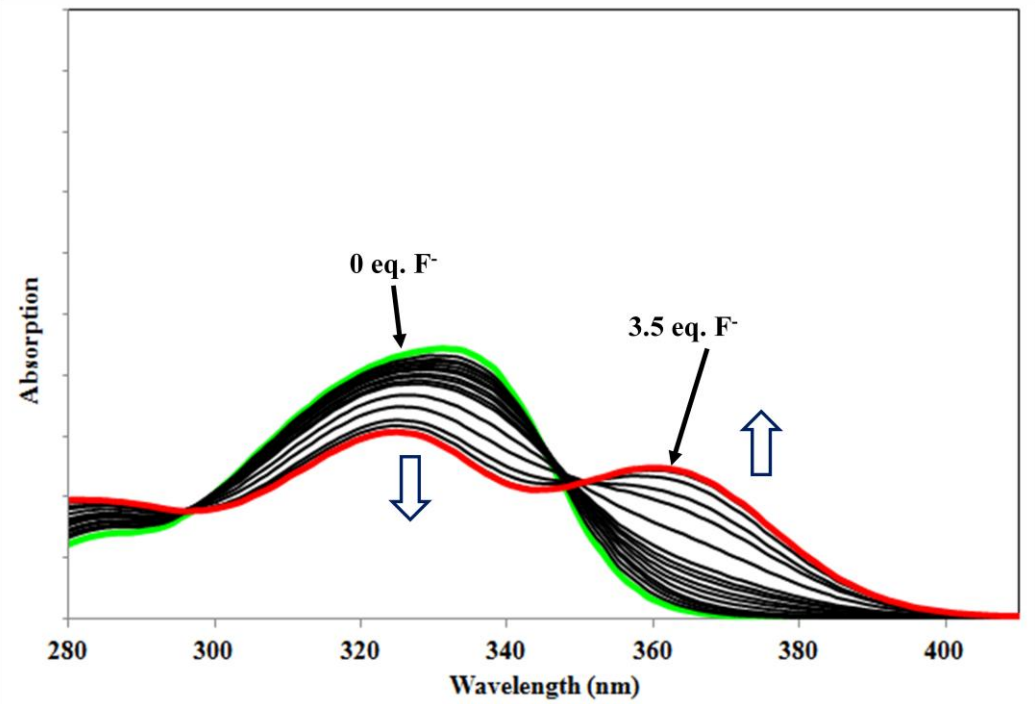

Figure 2.25 The UV-Vis absorption titration spectra of **1Eu** (1×10^{-5} M) by TBAF in THF at 298 K.

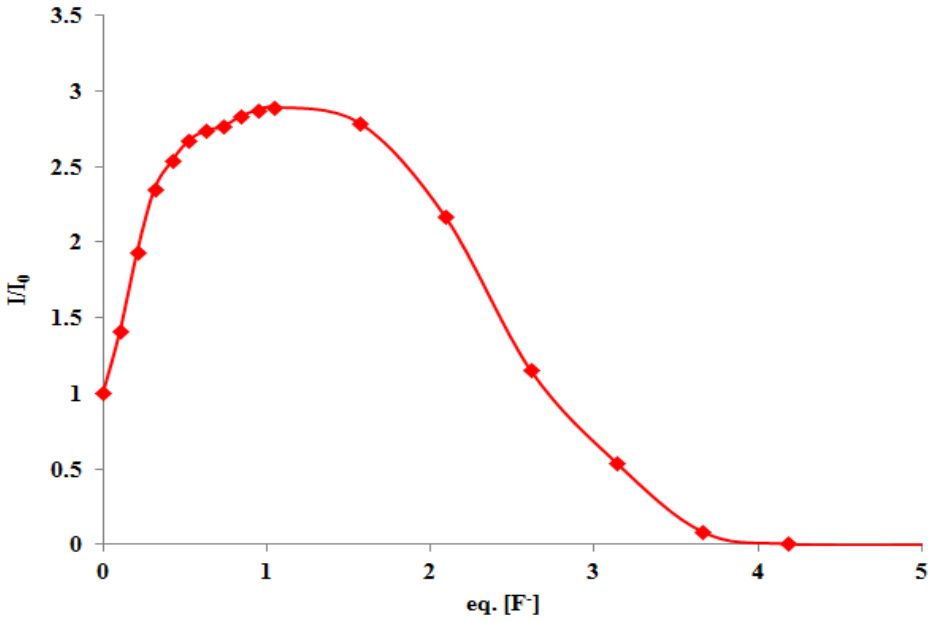

Figure 2.26. Stern-Volmer plot of **1Eu** (λ_{max}= 615 nm) in THF at 298 K when titrated with TBAF.

The TBAF titration spectra acquired for **2Eu** show similar changes as its **1Eu**. After an initial increase in emission band intensity, full quenching is observed for the Eu(III) emission peaks as shown in Figure 2.27. The ligand emission bands, unlike **1Eu**, do not undergo red-shift at all but experience complete luminescence quenching instead as it is saturated by F^- anions causing an emission color change from pink, to red-pink to non-emissive. The accompanying Stern-Volmer plot for this titration, plotted in Figure 2.29 at λ= 615 nm, sustains the initial lanthanide emission intensity growth from 0 to 5 eq. of TBAF added, followed by a downward slope data line with full lanthanide emission quench at 20 eq. of F^- added.

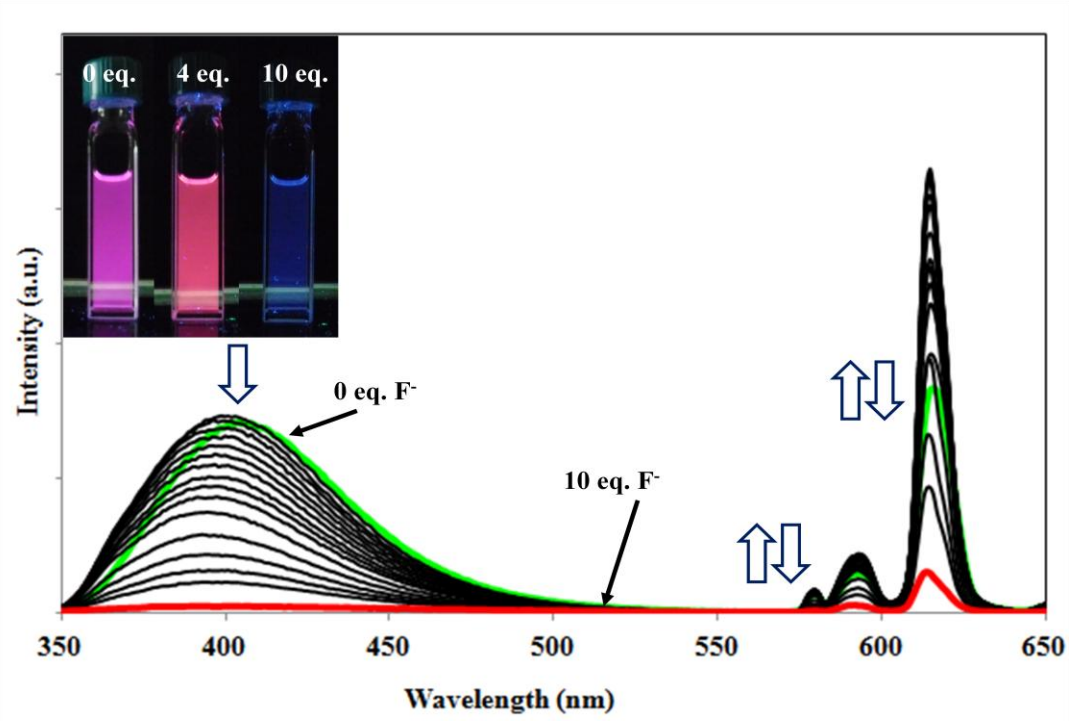

Figure 2.27. The fluorescence emission titration spectra of **2Eu** (1×10^{-5} M) by TBAF in THF at 298 K.

This behavior is similar to that of the respective paddlewheel Cu(II) complexes of both ligands when exposed to various molar increments of TBAF, as observed by a study previously done in our group.[19] The ligand **2** Cu(II) complex fluorescence titration with TBAF demonstrated quenching of the emission peak at ≈400 nm with addition of F^- anions while the Cu(II) complex of ligand **1** exhibited red-shift of the emission peak from ≈375 nm to ≈430 nm.

The UV-Vis absorptions spectra, plotted in Figure 2.28, show a blue-shift of the absorption band at 335 nm to 290 nm, unlike the red-shift observed for the two previous complexes. These results are also observed for the paddlewheel Cu(II) complexes discussed above for both ligands **1** and **2**. Ligand **1** Cu(II) complex emission peak undergoes red-shift as

TBAF molar equivalents are added to the solution while the Cu(II) complex for ligand **2** exhibits an emission peak blue-shift as F^- anions are added.

These results could be be explained by the ligand emission peak being attributed to through-space charge transfer between the triarylboron and carboxylate moieties. Due to the spacer between these two moieties changing from a duryl group for ligand **1** to a longer biphenyl group for ligand **2**, it is suggested that the larger spacer induces the addition of anions to the complex to produce quenching instead of red-shift.

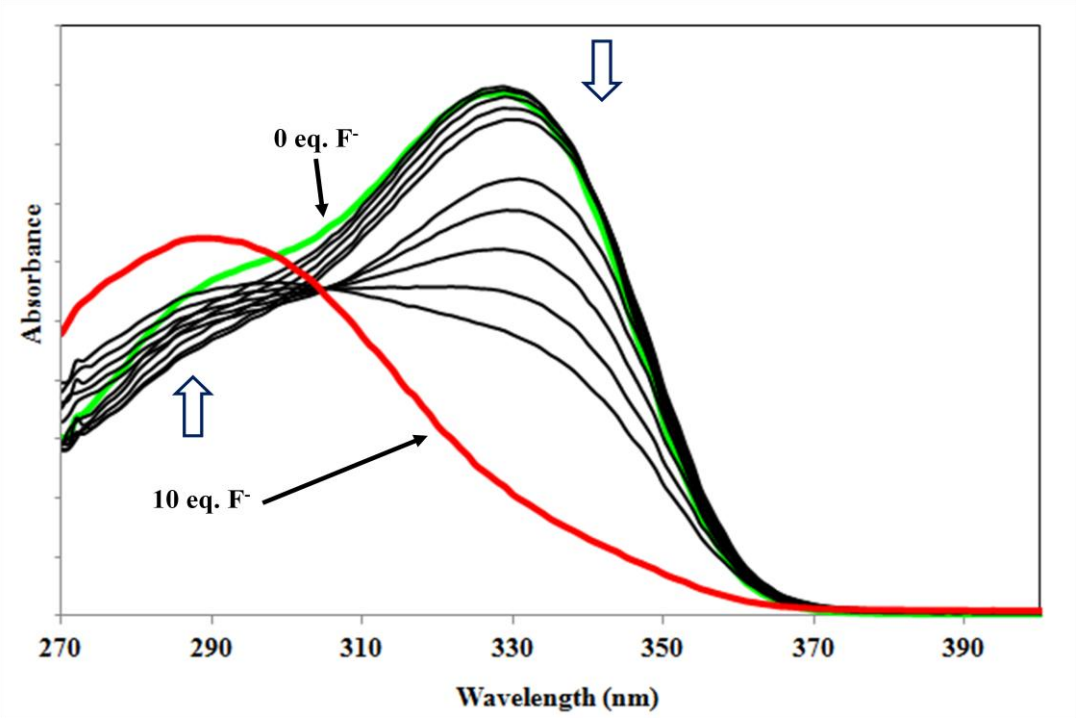

Figure 2.28. The UV-Vis absorption titration spectra of **2Eu** (1×10^{-5} M) by TBAF in THF at 298 K.

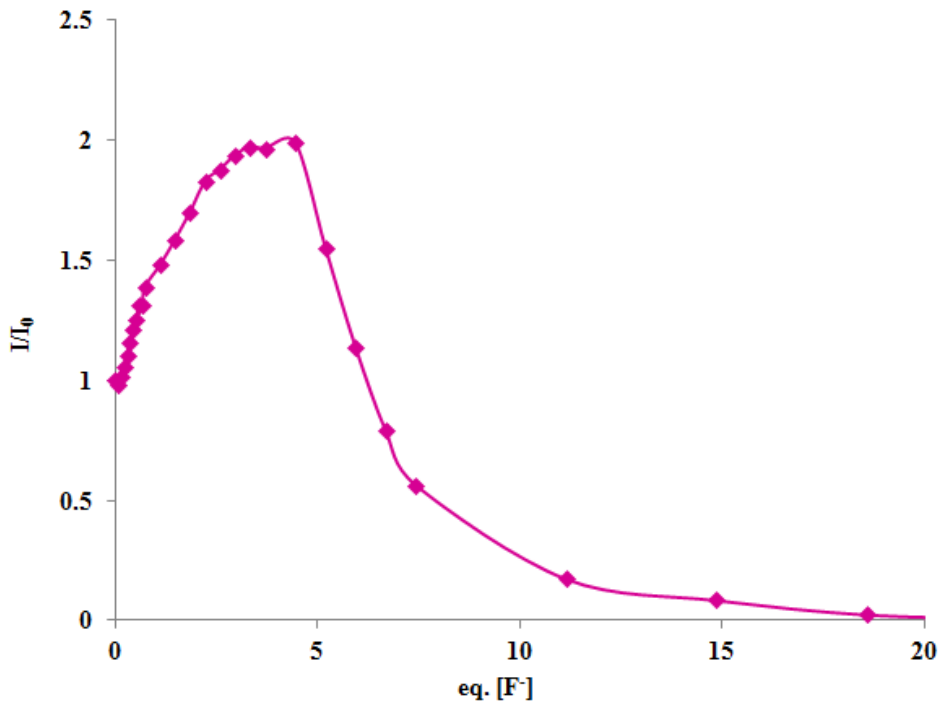

Figure 2.29. Stern-Volmer plot of **2Eu** (λ_{max} = 615 nm) in THF at 298 K when titrated with TBAF.

The fluorescence emission and UV-Vis absorption titration spectra for **1Tb**, **1Eu** and **2Eu** with TBACN proved to show features identical to the ones observed for the titrations with TBAF shown above. These spectroscopic patterns indicate that both CN^- and F^- anions affect the lanthanide complexes in the same way, as expected, by the coordination of the anion to the boron center causing a decrease in the first excited state energy of the ligand. This decrease in energy causes de-activation of the Tb(III) emission and of Eu(III) emission bands with simultaneous red-shift or quenching of the ligand's fluorescence band.

The fluorescence emission reaction of **1Tb** when subjected to TBACN shows a change in emission from green to sky blue, then to blue, shown in Figure 2.30, demonstrating the same emission pattern witnessed with TBAF. Stern-Volmer plot for the titration, illustrated in Figure

2.32, indicates a similar binding pattern than the one observed with F^- anions, with saturation reached at the addition of 5 eq. of TBACN. The UV-Vis spectra, plotted in Figure 2.31, exhibit absorption band red shift from 335 nm to 365 nm, similar to that of fluoride titration.

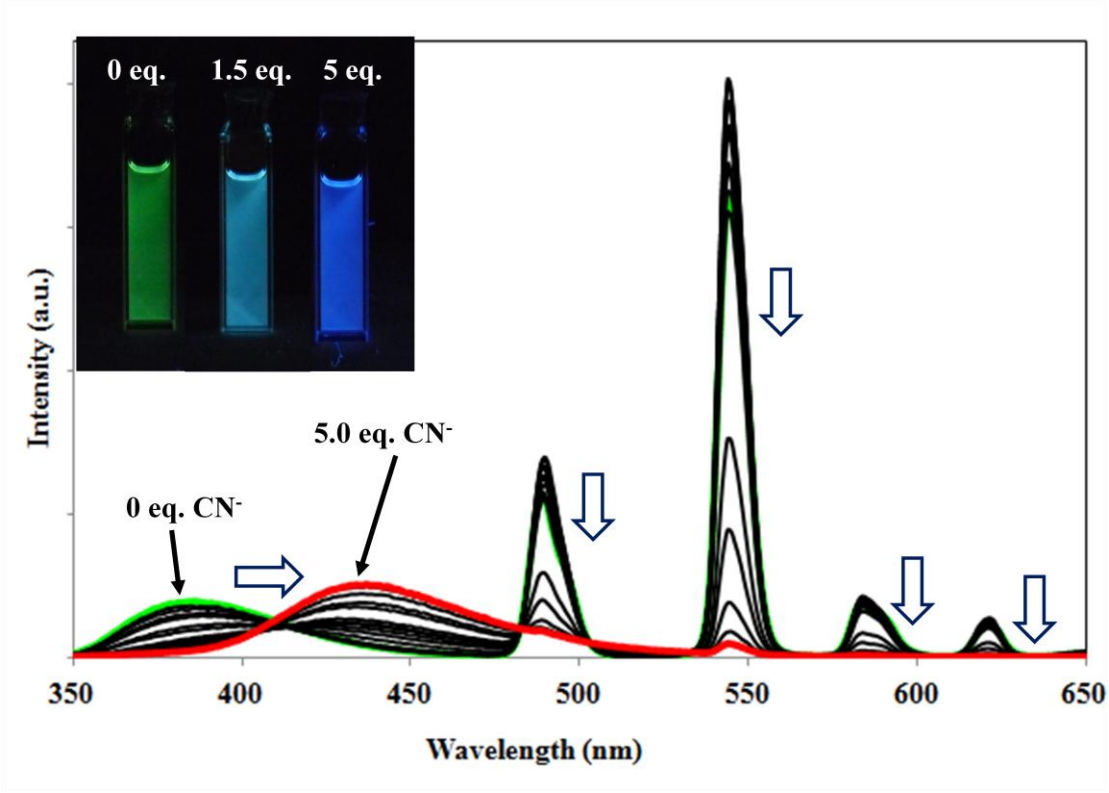

Figure 2.30. The fluorescence titration spectra of **1Tb** (1×10^{-5} M) by TBACN in THF at 298 K.

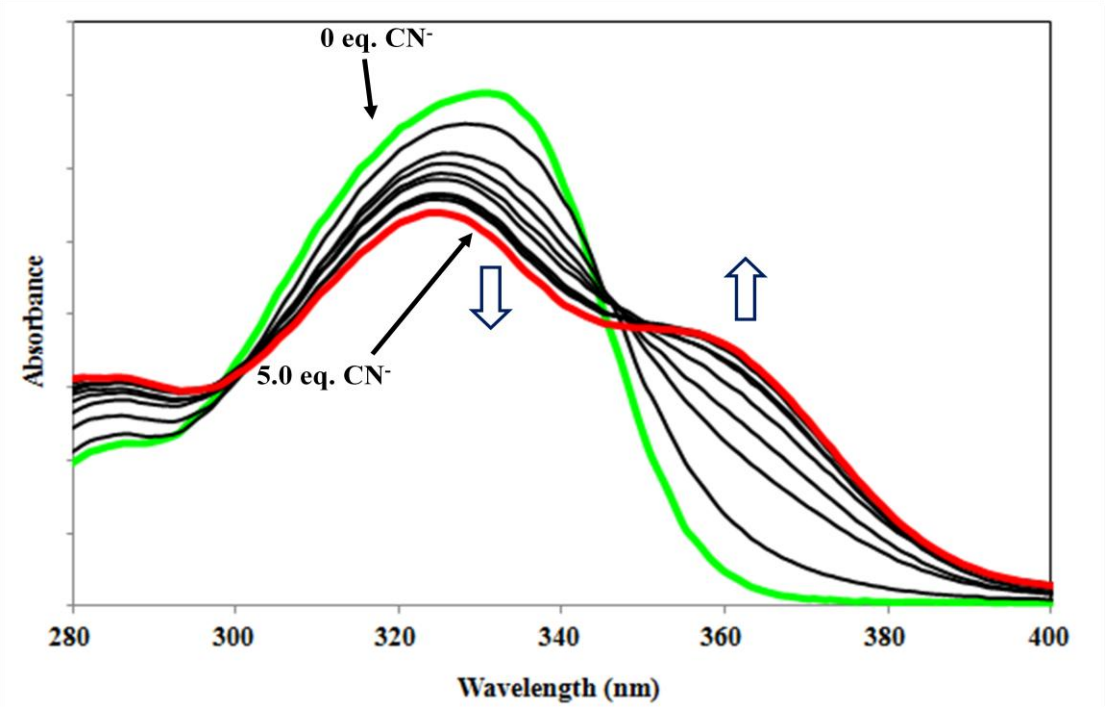

Figure 2.31. The UV-Vis absorption titration spectra of **1Tb** (1×10^{-5} M) by TBACN in THF at 298 K.

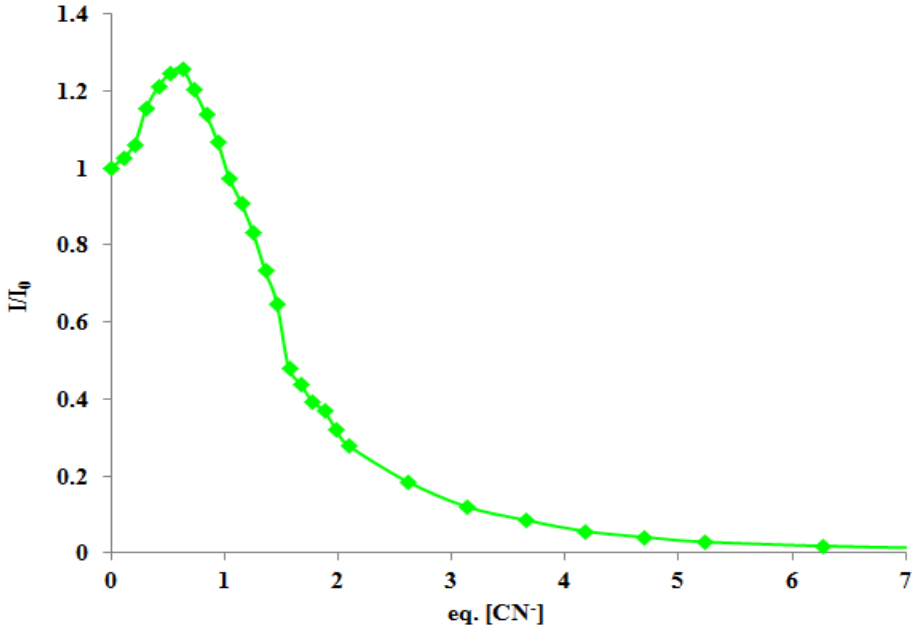

Figure 2.32. Stern-Volmer Plots of **1Tb** (λmax= 545 nm) in THF at 298 K when titrated with TBACN.

Both **1Eu** and **2Eu** complexes behave in the same way when exposed to CN^- as with F^-, as shown by the spectral change in Figures 2.33 to 2.38. **1Eu** shows luminescence color change from weak red to brighter red, then to blue luminescence along with an UV-Vis absorption band red-shift from 335 nm to 365 nm, shown in Figure 2.34. Full saturation is observed when 7 eq. of CN^- anions added, as demonstrated by the Stern-Volmer plot in Figure 2.35.

Emission color change from pink to brighter pink, then to no luminescence was observed for the titration of **2Eu** with TBACN, shown in Figure 2.36, with saturation being reached after 10 eq. of CN^- anions are added as demonstrated by the Stern-Volmer plot in Figure 2.38. UV-Vis absorption spectra, plotted in Figure 2.37, of the same titration exhibits the identical blue shift from 335 nm to 290 nm observed in the titration with TBAF discussed above.

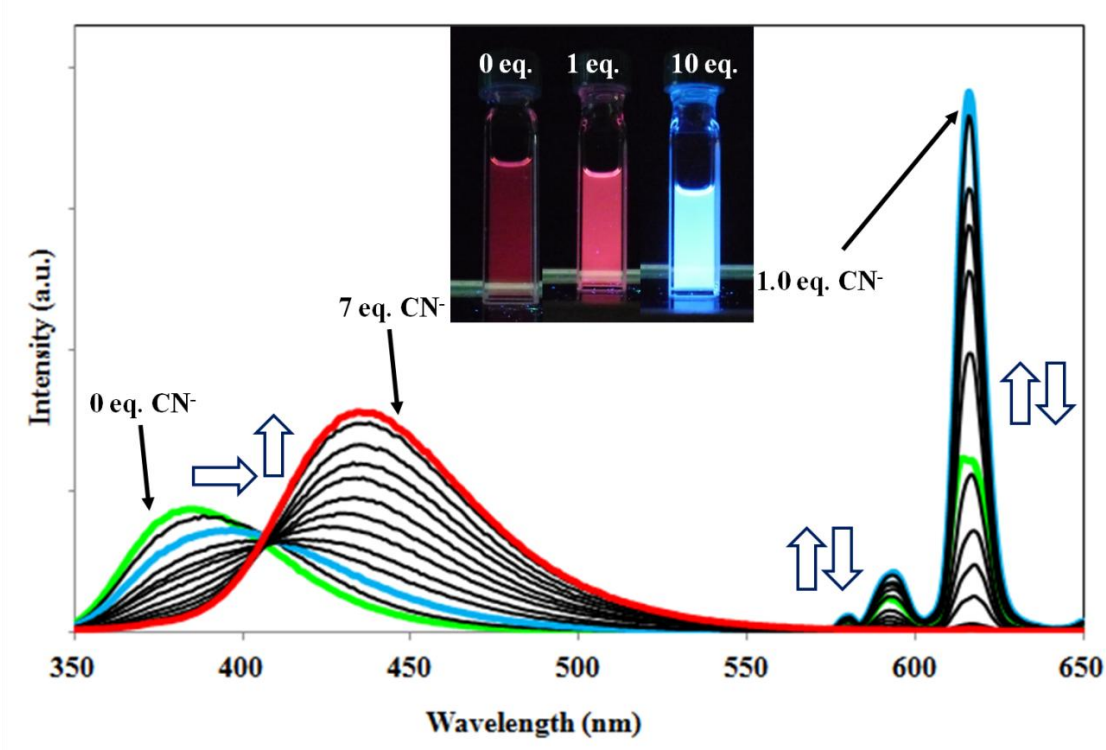

Figure 2.33. The fluorescence titration spectra of **1Eu** (1×10^{-5} M) by TBACN in THF at 298 K.

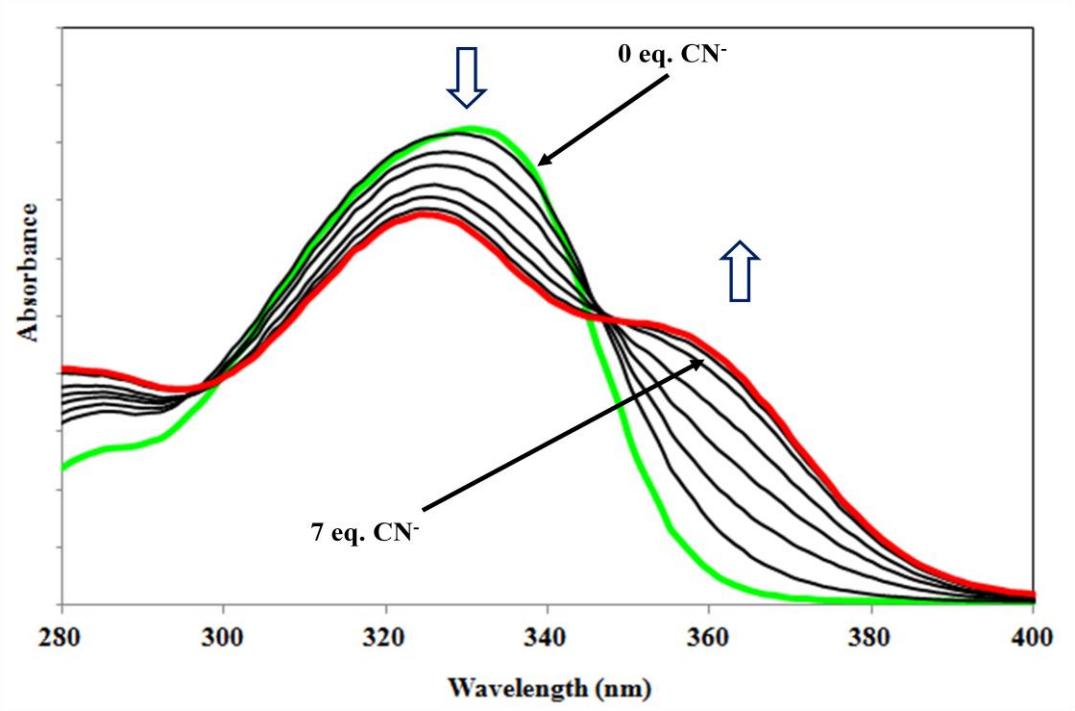

Figure 2.34. The UV-Vis absorption titration spectra of **1Eu** (1×10^{-5} M) by TBACN in THF at 298 K.

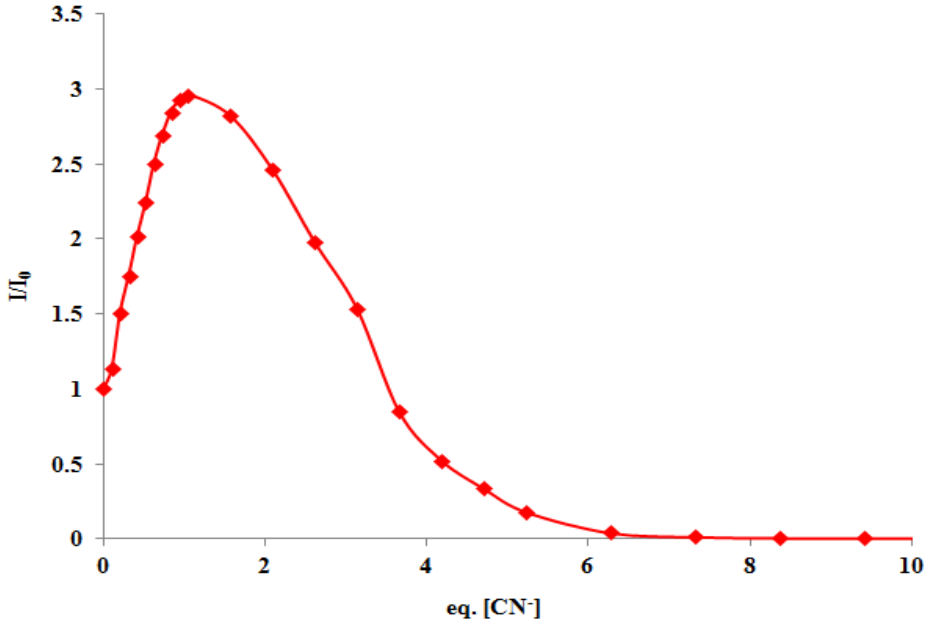

Figure 2.35. Stern-Volmer plot of **1Eu** (λmax= 615 nm) in THF at 298 K when titrated with TBACN.

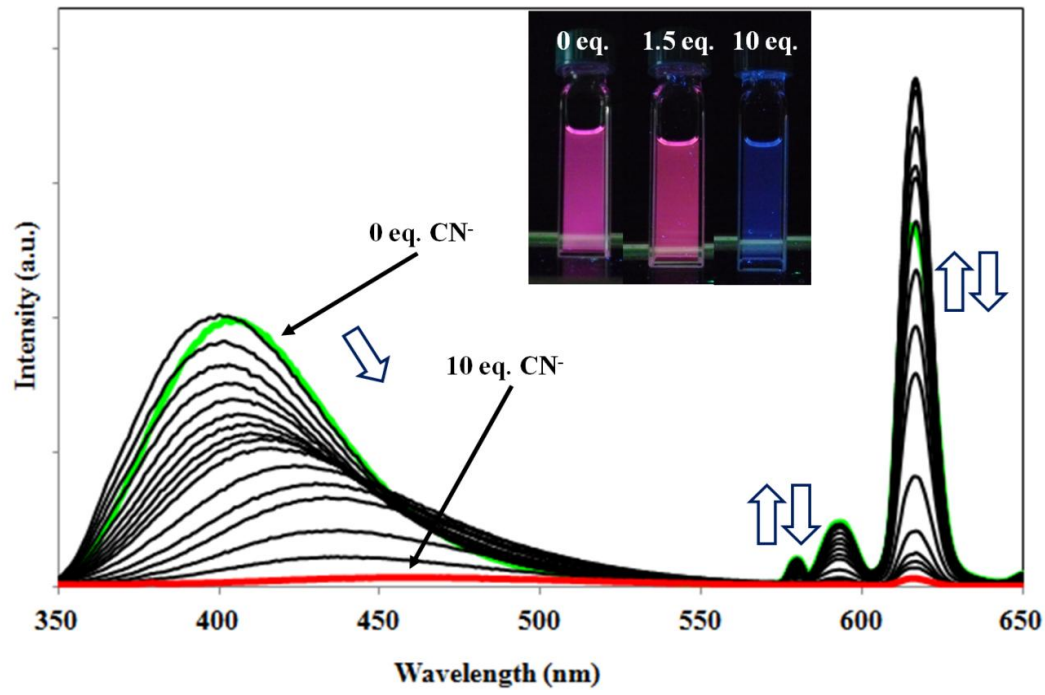

Figure 2.36. The fluorescence titration spectra of **2Eu** (1×10^{-5} M) by TBACN in THF at 298 K.

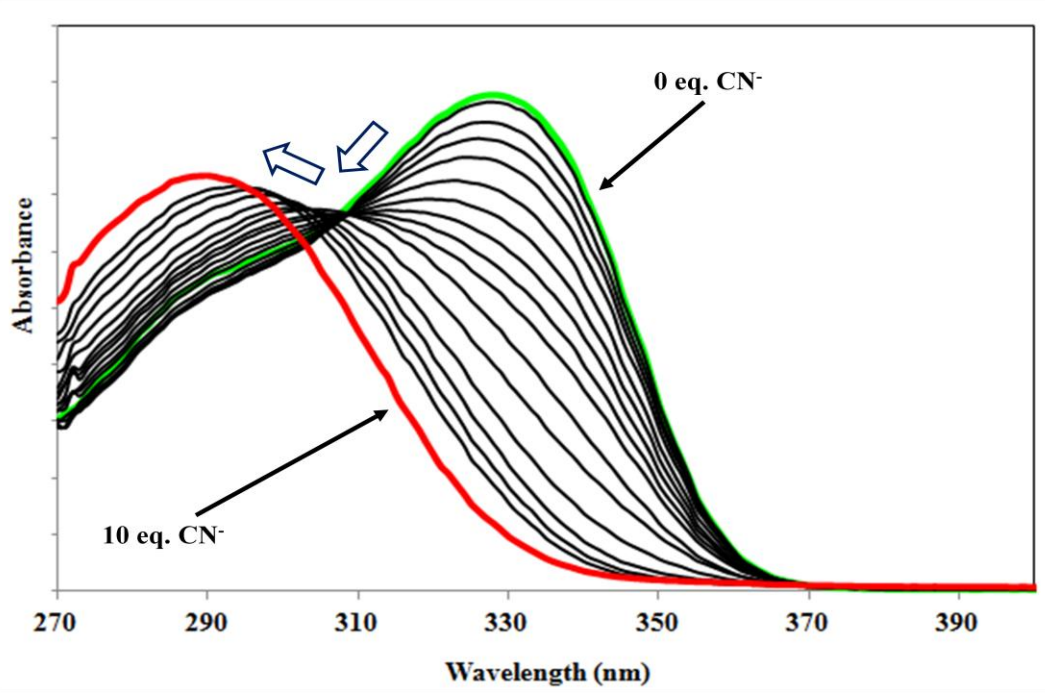

Figure 2.37. The UV-Vis absorption titration spectra of **2Eu** (1×10^{-5} M) by TBACN in THF at 298 K.

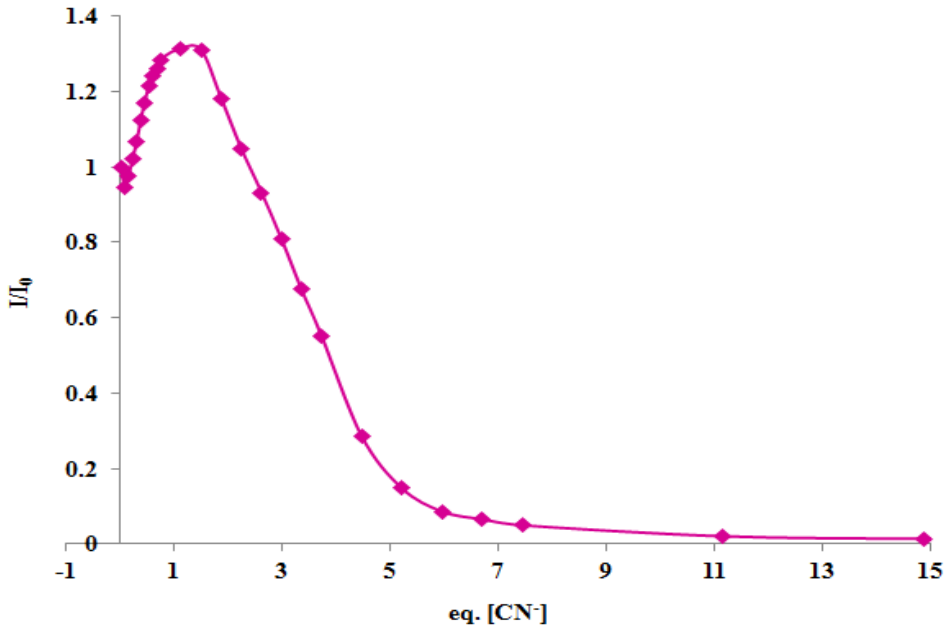

Figure 2.38. Stern-Volmer plot of **2Eu** (λ_{max} = 615 nm) in THF at 298 K when titrated with TBACN.

To verify that the initial luminescence and absorption spectral changes of the 3 lanthanide complexes upon contact with F^- and CN^- anions are indeed caused by anion complexation with the triaryl boron atom but not the lanthanide ion, we performed a similar titration experiment of **1Tb** with Cl^- anions. As mentioned in chapter 1 of this thesis, though small anions such as F^- and CN^- interact with the triarylboron moiety to trigger photophysical changes, larger anions such as Cl^- are too big for this interaction to occur due to the steric bulk of the mesityl functional groups. Chloride ions can however bind to lanthanide ions. A control experiment with **1Tb** being titrated by TBACl, illustrated in Figure 2.39, shows that the Tb(III) emission peaks did not display any appreciable quenching until more than 10 eq. of TBACl was added and the ligand's fluorescence peak did not show any significant change, thus further supporting that the initial color and spectral change of **1Tb** with the addition of F^- or CN^- is indeed caused by selective binding of the anion to the B center.

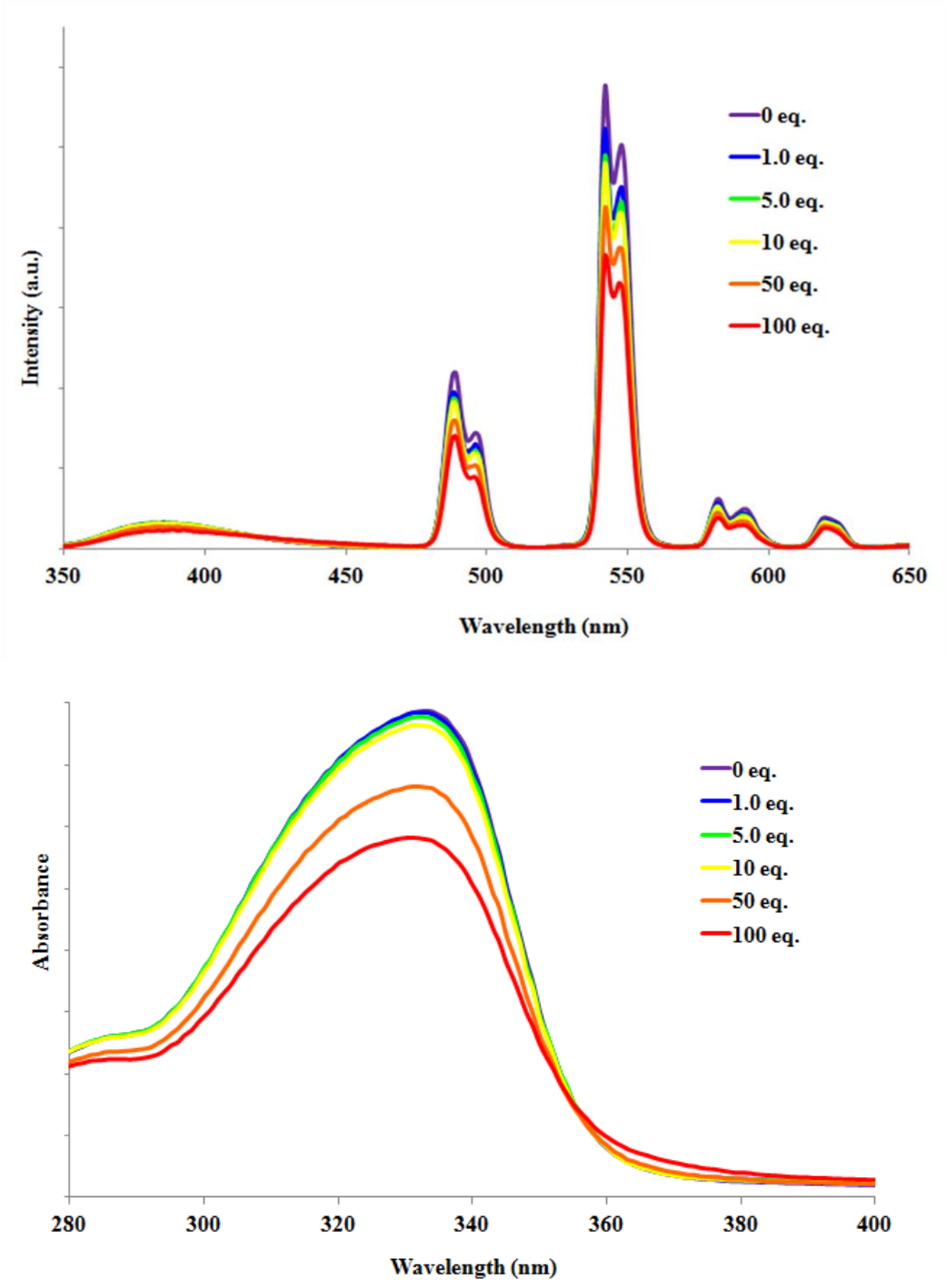

Figure 2.39. The fluorescence (top) and UV-Vis absorption (bottom) titration spectra of **1Tb** (1×10^{-5} M) by TBACl in THF at 298 K.

These experiments confirmed that the boryl group has indeed a strong impact on the emission of the lanthanide ions, which in turn can be used for anion sensing/detection by monitoring the lanthanide emission bands.

2.4.3 Lanthanide Complexes as Luminescent Sensors using Solid Substrates

The three complexes **1Tb**, **1Eu** and **2Eu** have demonstrated to be efficient luminescent sensors for DPA and the F^- and CN^- anions in organic solvents such as THF. However, for practical application, it is highly desirable to have an easy-to-use sensing platform that uses a solid substrate, simplifying the detection process for users and allowing for quick and efficient measurements. Efforts were therefore made to test the two most luminescent complexes, **1Tb** and **1Eu** for anion sensing on different solid substrates.

Preliminary tests were carried out by doping the complexes into either PMMA or PDMS polymer films (10% wt) and dropping excess amounts aqueous (>100 ppm) of DPA, KCN and KF in media on the polymer surface. No emission changes were observed for the doped polymer films and it was therefore concluded that these films are not suitable for sensing the selected analytes which may be attributed to the hydrophobic nature of the films.

Next we changed the substrate to filter papers by loading the complex unto Whatman grade 1qualitative filter papers with 11μm size pores and a diameter of 7.0 cm. The filter papers were loaded with 2 mL of lanthanide complex in THF solution at a concentration of 10^{-3} M. The papers were left to absorb the complex solution and dry for an hour. The substrate was then tested by spotting it with 10 μL of analyte solution in either water or MeOH, as described below.

We examined the filter papers' response to aqueous excess analyte solutions (>100 ppm), using the same procedure described above. Though no observable change was detected using

DPA and KCN in aqueous media, the lanthanide-loaded filter papers displayed a visual response toward KF solution. As shown by the photographs of the filter paper loaded with **1Tb** and spotted with aqueous KF solution and water as a control in Figure 2.40, noticeable emission color change from green to blue under 365 nm irradiation was observed where the F^- anions come into contact with the lanthanide complex. Photographs taken for the **1Eu**-loaded filter paper, shown in Figure 2.41, exhibit similar noticeable emission change from red to brighter pink under 365 nm in the area where aq. KF solution came into contact with the lanthanide complex.

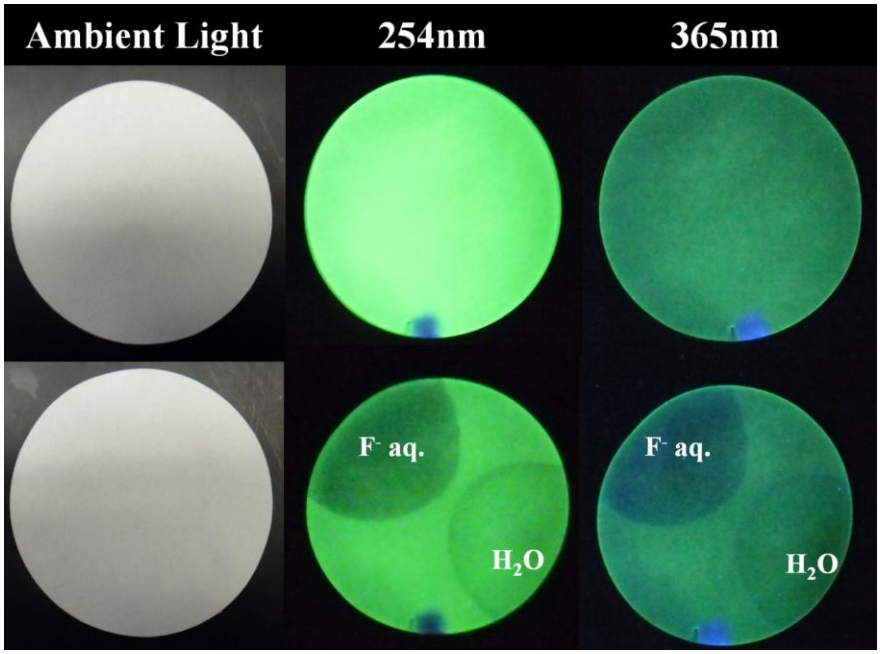

Figure 2.40. Photographs taken under irradiation wavelength stated above of **1Tb**-loaded filter paper (top) before and (bottom) after spotting with aq. KF solution.

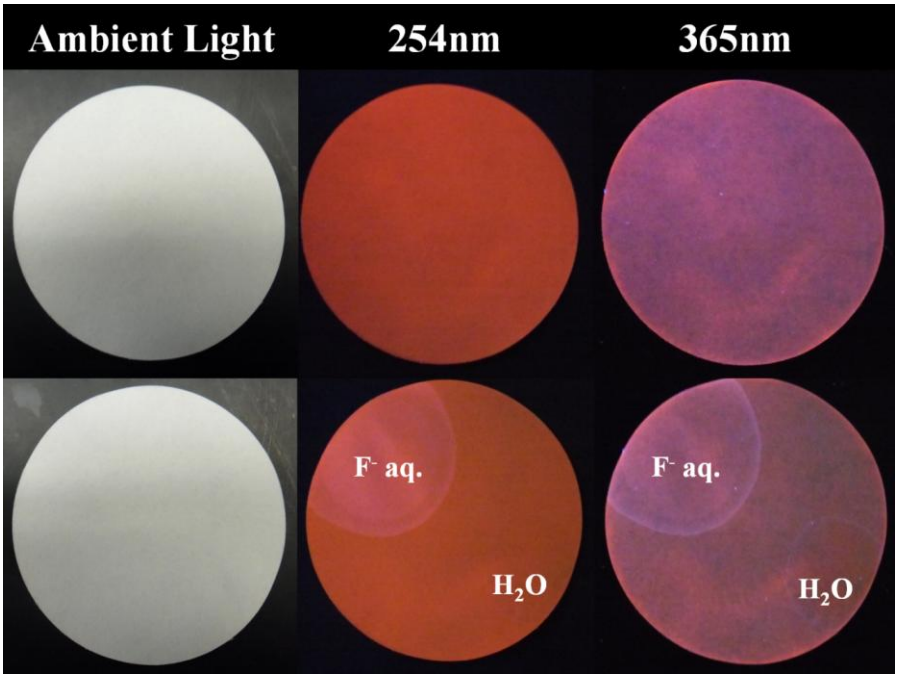

Figure 2.41. Photographs taken under irradiation wavelength stated above of **1Eu**-loaded filter paper (top) before and (bottom) after spotting with aq. KF solution.

In order to improve the emission color response, we repeated the same experimental procedure by using TBAF as a source of F^- in MeOH solution. The **1Tb** complex-loaded filter paper, shown in Figure 2.42, exhibits a remarkably sharp response when exposed to excess TBAF in MeOH, with an emission color change from green to dark blue observable under irradiation at both 254 nm and 365 nm. This improved response clearly is caused by the improved binding and delivering of fluoride anions to the lanthanide complex in methanol. It must be emphasized that all lanthanide compounds are insoluble in methanol. The emission change observed is consistent with luminescence observed in the solution state once excess F^- anions are added to **1Tb**.

Results observed for **1Eu**-loaded filter paper were similar to those recorded for **1Tb** in the solid state. As shown in figure 2.43, there is a noticeable emission color change from pink to dark blue under both 254 nm and 365 nm irradiation after TBAF in methanol was added. The observations are consistent with emission color changes observed in THF solution for **1Eu** saturated with F^- anions.

Emission color change for both complexes in the filter papers toward F^- source is instant. Determining the detection limit for this response would now be an important study to characterize the lanthanide complex's application as solid-state luminescent sensors for F^- anions in alcohol medium. An experimental procedure was designed to determine the detection limit for both complexes by loading them into a filter paper, as done before. The filter paper was then cut into strips which were dipped in to methanol solutions with TBAF concentrations varying from 100, 50, 25 and 10 ppm.

The results acquired for both **1Tb** and **1Eu** are shown in Figure 2.44 and 2.45 respectively. The data indicate an obvious color response from their initial emission color to dark blue at 100 ppm. No color change was observed for any of the lower concentrations. It was

therefore deduced that the detection limit for both **1Tb** and **1Eu** is 100 ppm of F^- anions in alcohol solvents.

Similar tests using solid substrate **1Tb** and **1Eu** luminescent sensors for CN^- and DPA in MeOH were carried out using TEACN as a source of CN^- and the same procedure outlined above. The results acquired for both **1Tb** and **1Eu** with excess CN^- are shown in Figure 2.46 and Figure 2.47, respectively. Results for the two tests show emission color change from their respective colors to blue, an observation that is similar to that noted for the detection of TBAF however, less evident. Detection limit tests of both lanthanide complex solid substrates for CN^- support these observations as they indicate no emission changes for the substrate at up to and including 100 ppm of CN^- in MeOH. It is deduced that the lanthanide complexes exhibit a less sensitive response for the CN^- analyte than for F^- anions.

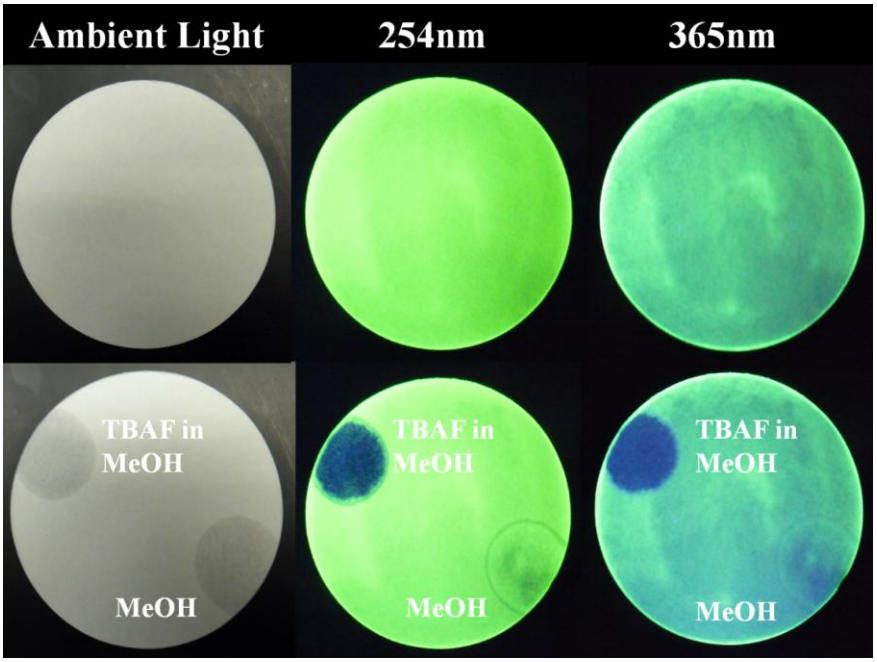

Figure 2.42. Photographs taken under irradiation wavelength stated above of **1Tb**-loaded filter paper (top) before and (bottom) after spotting with TBAF solution in MeOH.

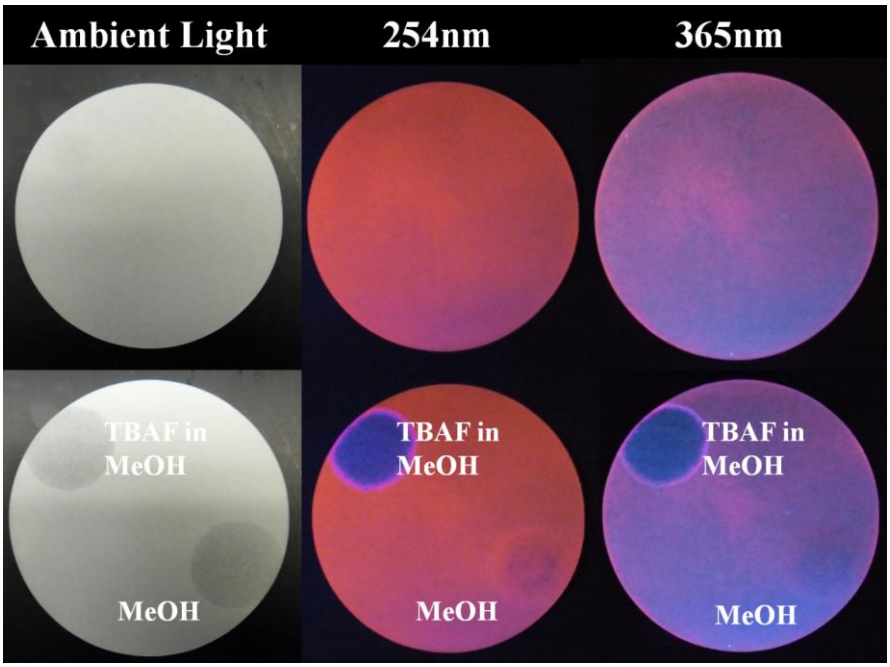

Figure 2.43. Photographs taken under irradiation wavelength stated above of **1Eu**-loaded filter paper (top) before and (bottom) after spotting with TBAF solution in MeOH.

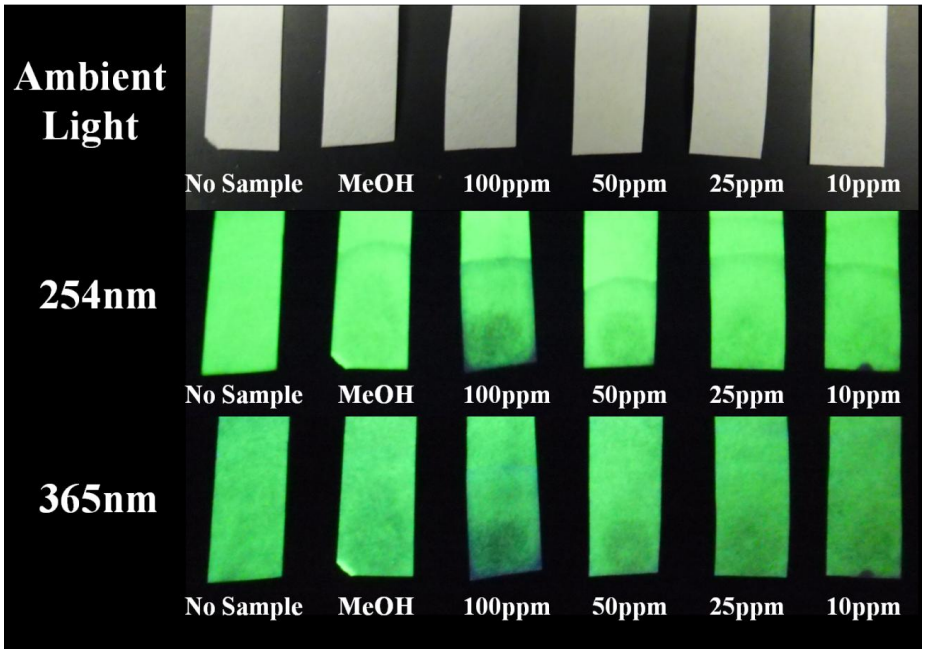

Figure 2.44. Photographs taken under irradiation described above to deduce the detection limit of **1Tb** doped filter paper for F^- anions in MeOH.

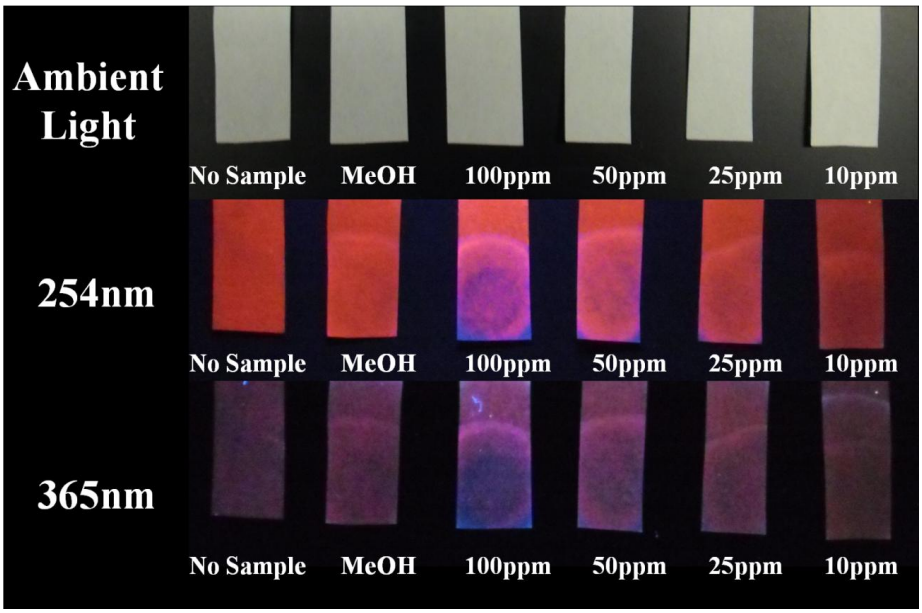

Figure 2.45. Photographs taken under irradiation described above to deduce the detection limit of **1Eu** doped filter paper for F^- anions in MeOH.

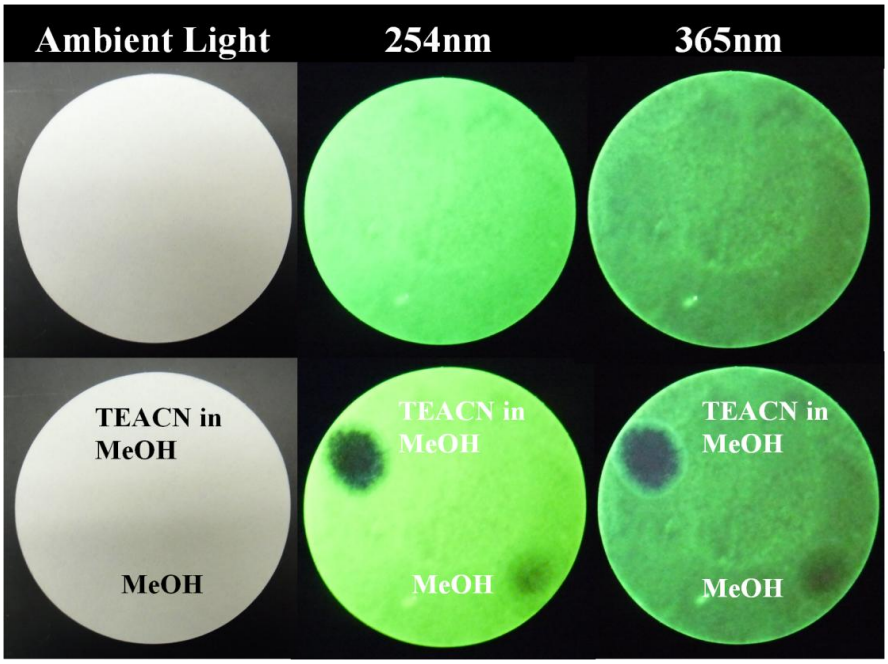

Figure 2.46. Photographs taken under irradiation wavelength stated above of **1Tb**-loaded filter paper (top) before and (bottom) after spotting with TEACN solution in MeOH.

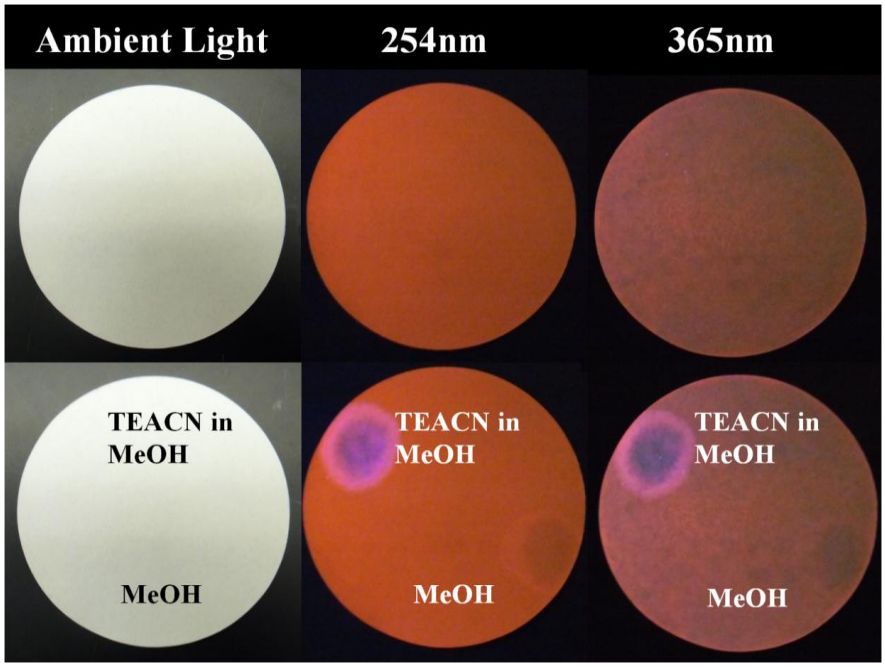

Figure 2.47. Photographs taken under irradiation wavelength stated above of **1Eu**-loaded filter paper (top) before and (bottom) after spotting with TEACN solution in MeOH.

DPA detection using **1Tb** and **1Eu** lanthanide complex solid substrates was also examined utilizing the same procedure outlined for the previous two analytes. The results acquired for both **1Tb** and **1Eu** with excess DPA in MeOH are shown in Figure 2.48 and Figure 2.49, respectively. Substrate **1Tb** exhibits color change from green emission to blue emission under 254 nm irradiation and to no emission under 365 nm irradiation when exposed to excess DPA in MeOH. Substrate **1Eu** demonstrates emission color change from green to pink under under 254 nm irradiation and to blue emission under 365 nm irradiation when exposed to excess DPA in MeOH. These results differ greatly to those attained for the two small anions tested previously as the interaction mechanism for DPA and the lanthanide complexes is different. Tests to determine the detection limit for DPA using the lanthanide substrates were undergone and no response was observed for DPA in MeOH up to and including 100 ppm. It is deduced that the lanthanide solid substrates are not an ideal sensitive method for detection of small amounts of DPA.

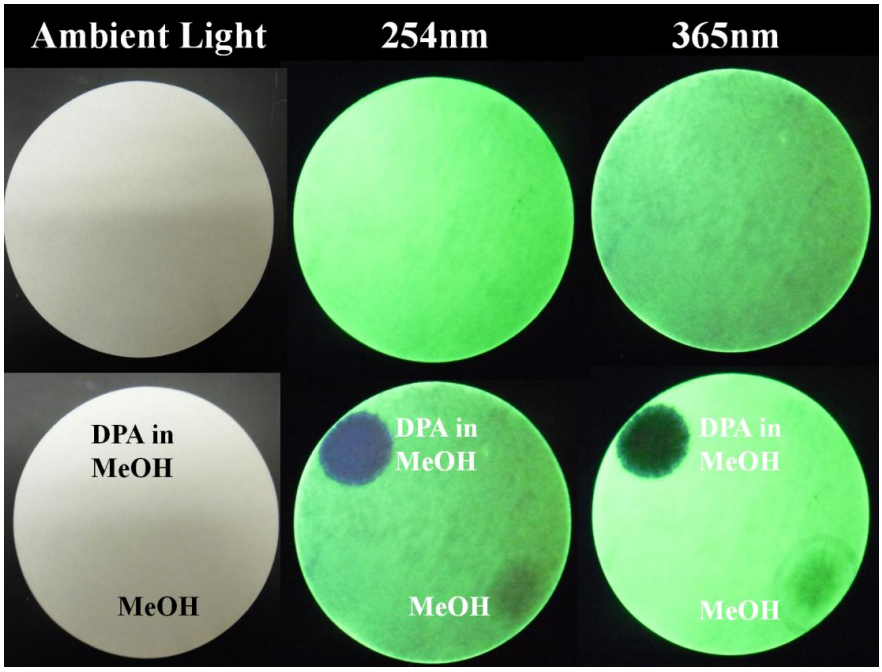

Figure 2.48. Photographs taken under irradiation wavelength stated above of **1Tb**-loaded filter paper (top) before and (bottom) after spotting with DPA solution in MeOH.

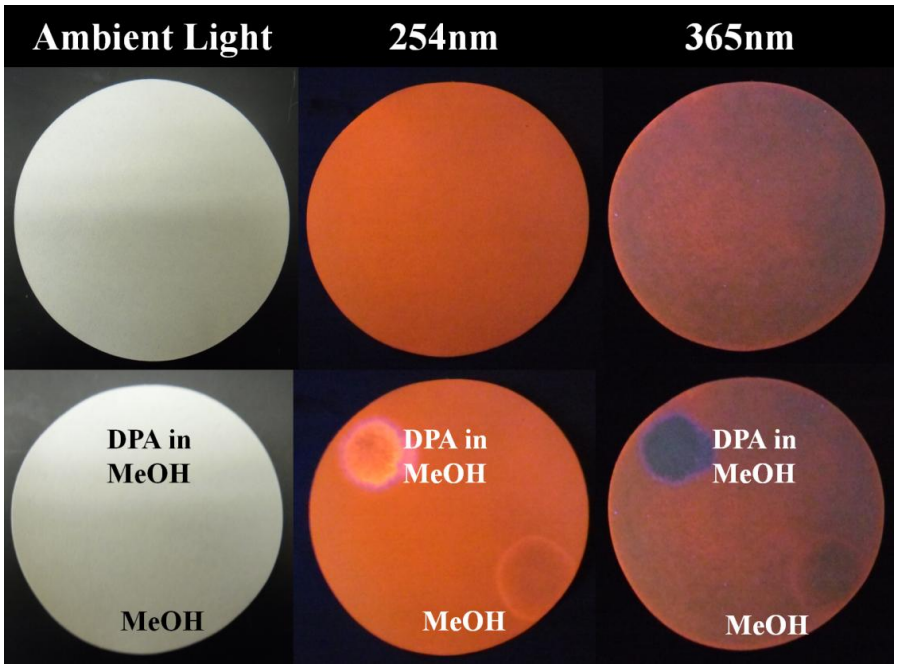

Figure 2.49. Photographs taken under irradiation wavelength stated above of **1Eu**-loaded filter paper (top) before and (bottom) after spotting with DPA solution in MeOH.

2.5 Conclusion

In summary, the first examples of multifunctional triarylboron functionalized Tb(III) and Eu(III) compounds have been achieved. Two mesityl-functionnalized triarylboron ligands and their respective lanthanide complexes were successfully synthesized and characterized using standard spectroscopic methods. The triarylboron ligand **1** has been found to be highly effective in activating Tb(III) and Eu(III) emissions exhibiting bright green and red luminescence respectively, and high quantum yields. Ligand **2** was demonstrated to efficiently sensitize Eu(III) luminescence exhibiting bright pink emission but was unable to do the same for Tb(III). This observation was explained by the calculated lowest excited energy levels of both the two triarylboron ligands and the lanthanide ions. Due to the ligand **2**'s lowest excited state being too close to that of the Tb(III) ion, sensitization was shown to be inefficient and no characteristic Tb(III) green emission was recorded.

The new lanthanide complexes were shown to be promising as luminescent sensors/probes for CN^- and F^- as well as for DPA. Solution titration tests for all three analytes showed distinct spectral and color change upon contact with the potential luminescent sensors at very low concentrations in organic solvents of below 0.1 ppm, indicating potential for application. Testing of the new lanthanide complexes as luminescent sensors in the solid state yielded encouraging results for fluoride detection.

2.6 References

[1] J. Georges, *Analyst.*, **1993**, 118, 1481.

[2] (a) M. A. El-Sayed and M. L. Bhaumik, *J. Phys. Chem.*, **1965**, 69, 275; (b) M. A. El-Sayed and M. L. Bhaumik, *J. Chem. Phys.*, **1963**, 39, 2391.

[3] *Advances in Inorganic Chemistry*; Elsevier: San Diego, **2011**; Collect. Vol. No. 63, pp10-30.

[4] E. P. Diamandis and T. K.Christopoulos, *Anal. Chem.*, **1990**, 62, 1149A.

[5] M. Bredol, U. Kynast and C. Rhonda, *Adv. Mater.*, **1991**, 3, 361.

[6](a) J. Kido and Y. Okamoto, *Chem. Rev.*, **2002**, 102, 2357; (b) J. Kido, W. Ikeda, M. Kimura and K. Nagai, *Jpn. J. Appl. Phys.*, **1996**, 35, 394.; (c) T. Sano, M. Fujita, T. Fujii, Y. Hamada, K. Shibata and K. Kuroki, *Jpn. J. Appl. Phys.*, **1995**, 34, 1883.; (d) J. Kido, H. Hayase, K. Hongawa, K. Nagai and K. Okuyama, *Appl. Phys. Lett.*, **1994**, 65, 2124.

[7] C. M. G. dos Santos, A. J. Harte, S. J. Quinn and T. Gunnlaugsson, *Coord. Chem. Rev.*, **2008**, 252, 2512.

[8] A. Thibon and V. C. Pierre, *Anal. Bioanal. Chem.*, **2009**, 394, 107.

[9](a) V. Zlojutro, Y. Sun, Z. M. Hudson and S. Wang, *Chem. Commun.*, **2011**, 47, 3837; (b) F. Jäkle, *Chem. Rev.*, **2010**, 110, 3985; (c) Z. M. Hudson and S. Wang, *Acc. Chem. Res.*, **2009**, 42, 1584; (d) S. Yamaguchi and A. Wakamiya, *Pure Appl. Chem.*, **2006**, 78, 1413 (e) W. L. Jia, D. R. Bai, T. McCormick, Q. D. Liu, M. Motala, R. Y. Wang, C. Seward, Y. Tao and S. Wang, *Chem.–Eur. J.*, **2004**, 10, 994.

[10] (a) C. R. Wade, A. E. J. Broomsgrove, S. Aldridge and F. P. Gabbaï, *Chem. Rev.*, **2010**, 110, 3958, and references therein; (b) T. W. Hudnall, C. W. Chiu and F. P. Gabbaï, *Acc. Chem. Res.*, **2009**, 42, 388; (c) Y. Kubo, M. Yamamoto, M. Ikeda, M. Takeuchi, S. Shinkai, S. Yamaguchi

and K. Tamao, *Angew. Chem., Int. Ed.*, **2003**, 42, 2036; (d) S. Yamaguchi, S. Akiyama and K. Tamao, *J. Am. Chem. Soc.*, **2001**, 123, 11372.

[11] S. Yamaguchi, T. Shirasaka, and K. Tamao, *Org. Lett.* **2000**, 2(26), 4129.

[12] Y. Liu, X. Xu, F. Zheng and Y. Cui, *Angew. Chem. Int. Ed.* **2008**, 47, 4538.

[13]B. A. Blight, A. F. Stewart, N. Wang, J-S. Lu and S. Wang, *Inorg. Chem.* **2012**, 51, 778.

[14] C. Seward, N-X. Hu and S. Wang, *J. Chem. Soc. Dalton. Trans.*, **2001**, 134.

[15] H. Doi, M. Kinoshita, K. Okumoto and Y. Shirota, *Chem. Mater*., **2003**, 15, 1080.

[16] (a) T. L. Esplin, M. L. Cable, H. B. Gray and A. Ponce, *Inorg. Chem*., **2010**, 49, 4643.; (b) E. G. Moore, A. P. S. Samuel, and K. N. Raymond, *Acc. Chem. Res.*, **2009**, 42, 542; (c) M. Fujita, Y. J. Kwon, S. Washizu and K. Ogura, *J. Am. Chem. Soc*., **1994**, 116, 1151; (d) R. W. Gable, B. F. Hoskins and R. Robson, *J. Chem. Soc., Chem. Commun.*, **1990**, 1677; (e) S. Subramanian and M. J. Zaworotko, *Angew. Chem., Int. Ed.*, **1995**, 34, 2127.

[17] W. R. Dawson, J. L. Kropp and M. W. Windsor, *J. Chem. Phys*., **1966**, 45, 2410.

[18] (a) F. Gutierrez, C. Tedeschi, L. Maron, J. P. Daudey, R. Poteau, J. Azema, P. Tisnès and C. Picard, *Dalton. Trans*., **2004**, 9, 1334; (b) M. Latva, H. Takalob, V. M. Mukkala, C. Matachescuc, J. C. Rodriguez- Ubisd and J. Kankarea, *J. Lumin*., **1997**, 75, 149.

[19] A. Stewart, **2011**, *Triarylboron-containing Paddle-Wheel Complexes: Towards MOF-based Sensors for Small Anions*, B. Sc. H. Thesis, Queen`s University, Kingston, ON, Canada.

Chapter 3

Luminescent 8-Hydroxyquinoline Dipicolylamine Complexes as Sensors for Zinc(II) Ions

3.1 Introduction

The divalent cationic form of zinc is the second most abundant transition metal found in biological systems after iron, reaching quantities up to 2-3g.[1] Its roles in biological processes are far reaching including, but not limited to, enzyme regulation, DNA binding and recognition, neural transmission and its role as a structural cofactor in metalloproteins.[2] Approximately 90% of biological zinc ions are found in a protein-bound form involved in catalytic and structural functions,[3] while free Zn(II) ions are involved in regulation of programmed cell death (apoptosis).[4]

However, increased levels of free Zn(II) ions within an organism due to failed homeostasis introduce the potential for many problems. In recent years research has elucidated a strong correlation between various diseases and the levels of zinc ions found within respective tissues—in particular the high level of Zn(II) found in brain tissues of Alzheimer's patients.[2b] In a healthy biological system, Zn(II) occurrence in brain tissue allows for several important functions such as zinc-directed neural excitability modulation at inter-neuron synaptic clefts. On the other hand, in the event of faulty metabolization in the brain tissue, Zn(II) concentration irregularities have been linked to certain important neural disorders such as Alzheimer's, Parkinson's, epilepsy and dementia.[2,3,5]

Spatial and temporal *in* vivo tracking of these metal ions is, therefore, critical to understand, validate and rectify these concerns. Yet, due to the $3d^{10}4s^{0}$ electronic configuration of Zn(II), the ion does not possess any spectrophotometric characteristics rendering conventional spectrometric techniques useless for Zn(II) detection.[2b] Therefore, a new prominent area for zinc detection is the use of luminescent sensors consisting of a fluorescent ligand whose emission or absorption properties change during the coupling event with a free Zn(II) ion.[6]

The most widely used fluorescent Zn(II) chemosensors are 6-methoxy-8-(p-toluenesulfonamide) quinoline (TSQ) and its derivatives.[7] These sensors operate by using the photoinduced electron transfer (PET) mechanism wherein the molecule is comprised of a zinc-coupling receptor moiety such as di-2-picolylamine or N,N,N',N'-tetrakis(2-pyridylmethyl)-ethylenediamine (TPEN), and a fluorophore.[8] These zinc-coupling receptors transfer electron to the neighbouring fluorophore in the excited state quenching the moiety's emission, this mechanism is suppressed when a Zn(II) ion couples to the receptor at several binding sites, resulting in an increase of emission and a fluorescence 'turn-on' sensing system.

Studies have shown that coordination geometry for Zn(II) varies and that coordination numbers of 4, 5 and 6 are relatively common, depending on the medium.[9] Zn(II) tetrahedral geometry is favoured in proteins and enzymes[10] whilst octahedral geometry is preferred in aqueous media[11] and penta-coordination has been observed in certain catalytic binding sites.[12]

With the aim to develop potential fluorescent systems for Zn(II) detection, part of my research has focused on the synthesis of a novel compound, *5-(4-((bis(pyridin-2-ylmethyl)amino)methyl)phenyl)quinolin-8-ol* (**1-OH**), shown in Figure 3.1, composed of both an 8-hydroxyquinoline as and a dilypyridyl coupling site and its use in Zn(II) sensing. The 8-hydroxyquinoline compound has been historically used as a fluorophore and fluorescent marker

for Zn(II) as well as for other compounds including Mg(II), Pb(II), Sr(II) and Ca(II).[13] The dipyridyl site of the designed ligand is derived from the well known metal chelator TPEN, and has been a very popular chelating moiety for Zn(II) detection with 3 available coupling sites.[14]

Further work was applied to the **1-OH** ligand model by equipping the compound with both a four-coordinate boron group and a tris(8-hydroxyquinolinato)aluminum center. Four coordinate diphenylboron bidentate heterocyclic ligands have been studied in recent years for their applications as emitters in organic light emitting devices (OLEDs). Interest has been developed in BPh_2q compounds as an alternative to Alq_3 devices for several reasons, including their increased stability over aluminum centered compounds.[15] Most importantly in our study, the BPh_2q moiety was chosen due to its high luminescent quantum yield of 30%,[16] much superior to that of Alq_3.[17] A new Al(III) compound with ligand **1-**OH is also synthesized as part of the effort to create a strongly emitting Zn(II) tagging compound. The structures of the boron and aluminum compounds are also shown in Figure 3.1.

The ligand **1-OH** and its metal complexes were fully characterized by UV-Vis absorption spectroscopy, fluorescence spectroscopy, ^{1}H NMR, ^{13}C NMR, COSY and High Resolution Mass Spectrometry. Data was acquired for both the pure ligand, as well as in its complex interaction with the Zn(II) ion. DFT calculations and luminescence quantum yield measurements were further used in order to complete the characterization of the proposed luminescent sensors. The detail is presented in this chapter.

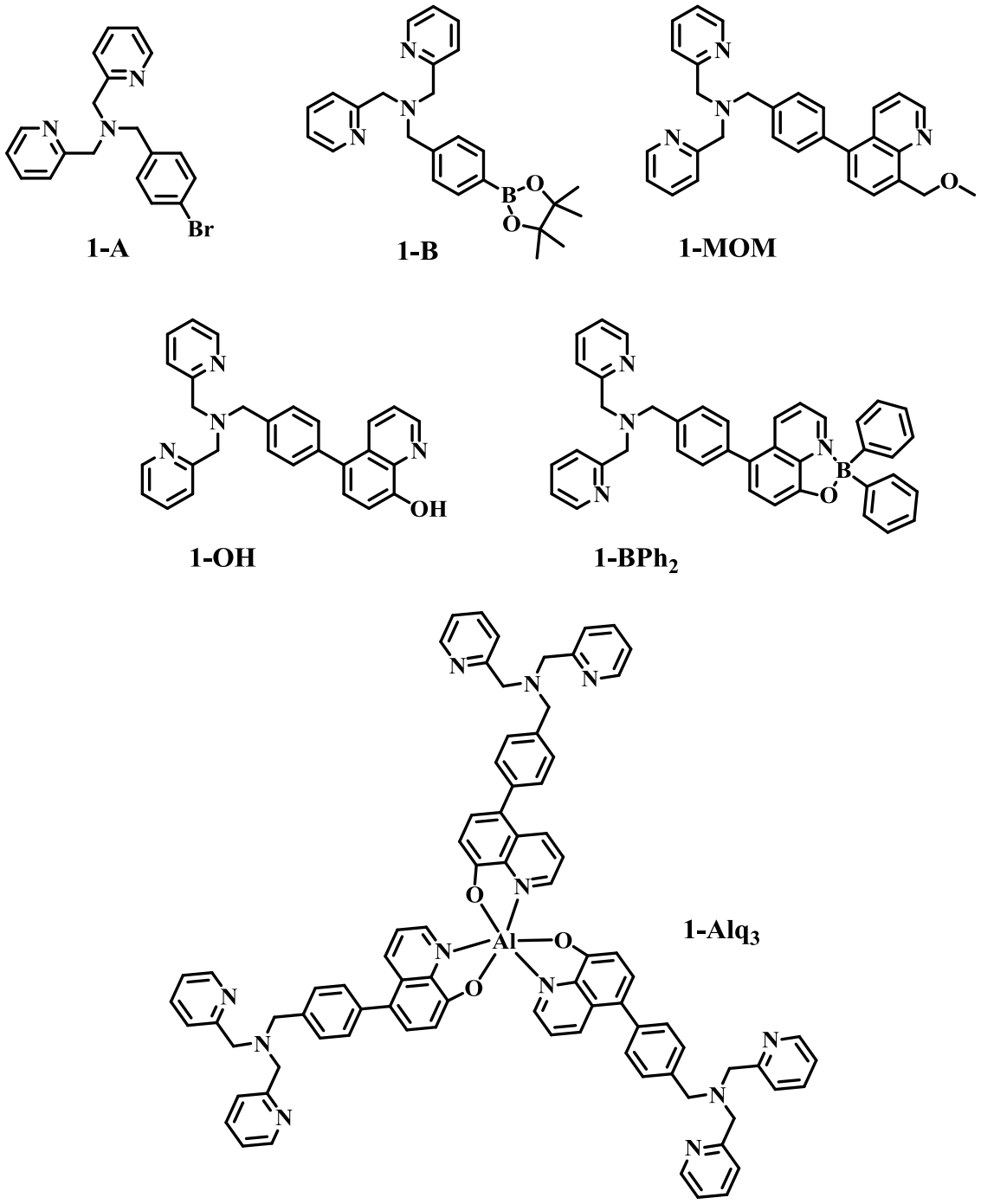

Figure 3.1. The molecular structures of compounds and synthesized and investigated in Chapter 3.

3.2 Experimental Section

Reagents for chemical synthesis were purchased from Aldrich Chemical Company with no further purification. Air-sensitive reactions were carried out under an inert N_2 atmosphere using standard Schlenk techniques in oven-dried clean glassware. Deuterated solvents $CDCl_3$ and CD_2Cl_2 acquired from Aldrich Chemical Company were used as received with no further drying. ^1H NMR and COSY spectra were acquired using Bruker Avance 300, 400 or 500 MHz spectrometers and ^{13}C NMR analyses were performed on Bruker Avance 400 or 500 MHz spectrometers.

Mass spectrometry measurements were acquired using a High Resolution ESI ZQ Single Quad instrument mass spectrometer. DFT calculations were carried out using the Gaussian 03 computing program[18] and the B3LYP/ 6-311G(d) level of theory. UV-Vis spectra were recorded using an Ocean Optics CHEMUSB4000 absorbance spectrophotometer. Excitation and emission spectra were obtained using a Photon Technologies International QuantaMaster Model 2 spectrometer. Quantum Yield measurements in the solid state were acquired using a PTFE-coated integrating sphere mounted into a Jobin Yvon Horiba Fluoromax-3 by means of known spectroscopic methods.[19]

Cyclic voltammetry measurements were acquired using a BAS CV-50W analyzer with a scan rate of 400 mV/sec. A sample concentration of approximately 3 mg in 3 mL of DMF at room temperature was used, using 50 mg of NBu_4PF_6 as the supporting electrolyte. A three-compartment cell consisting of a working Pt electrode, an auxiliary Pt electrode and an Ag/AgCl reference electrode was employed with a ferrocene/ferrocenium internal standard ($E_{1/2}{}^{ox}$=0.55 V).

3.2.1 Synthesis of 1-A

4.00 g (16.0 mmol) of 4-bromobenzylbromide, 2.91 g (14.6 mmol) of bis(2-pyridylmethyl)amine and excess NaOH pellets (5.00 g) were added to a 500 mL round bottom flask with magnetic stirring bar. 150 mL of THF was added to the flask and the mixture was stirred under reflux for 5 hours, at which point the heat was turned off and the flask contents were stirred for an additional 16 hours at room temperature. Extraction of the product was performed by using diethyl ether and water, isolating the organic layer and drying it with $MgSO_4$ before decanting. Excess solvent was removed by rotary evaporation. The product was purified by distillation at 260°C giving an orange-yellow viscous oil in 92% yield. ^{1}H NMR ($CDCl_3$, δ, ppm): 8.52 (dt, J=0.9 Hz, 2.4 Hz, 2H), 7.66 (td, J=1.8 Hz, 5.7 Hz, 2H), 7.53 (d, J=7.8 Hz, 2H), 7.43 (d, J=8.4 Hz, 2H), 7.28 (d, J=8.4 Hz, 2H), 7.15 (td, J= 0.9 Hz, 5.1 Hz, 2H), 3.79 (s, 2H), 3.63 (s, 2H)

3.2.2 Synthesis of 1-B

KOAc (4.50 mmol, 0.44 g) and 4-Br-$C_6H_4CH_2N(CH_2$-2-py$)_2$ (1.50 mmol, 0.55 g) were added to an oven-dried schlenk flask with a magnetic stir bar and vacuumed dry for about half an hour. A 3% mol equivalent of (dppf)Pd(II)Cl_2 catalyst and 2.20 mmol (0.57 g) of bis(pinacolato)diboron were added to the flask in inert atmosphere. 15 mL of dry DMF was de-oxygenated by freeze-pump thawing using liquid nitrogen before being added to the reaction flask by cannulation once it had warmed back up to room temperature. The reaction flask was next stirred and heated to 100 °C overnight. Excess solvent was removed from the reaction flask under vacuum and the residue was then extracted using CH_2Cl_2 and water. The organic layer was collected and dried using $MgSO_4$. The product was purified using column chromatography and eluted with ethyl acetate to produce a beige solid in 74% yield. ^{1}H NMR ($CDCl_3$, δ, ppm): 8.51

(dd, J=0.9 Hz, 3.3 Hz, 2H), 7.76 (d, J=7.8 Hz, 2H), 7.65 (td, J=1.8 Hz, 6.0 Hz, 2H), 7.57 (d, J=7.5 Hz, 2H), 7.43 (d, J=7.8 Hz, 2H), 7.13 (td, J=1.2 Hz, 5.1 Hz, 2H), 3.80 (s, 4H), 3.71 (s, 2H)

3.2.3 Synthesis of 1-MOM

Boronic ester (0.75 mmol, 0.36 g), 5-bromo-8-hydroxyquinoline (0.50 mmol, 0.14 g), potassium phosphate (0.50 mmol, 0.40 g), palladium acetate (5% eq., 0.01 g) and 2-dicyclohexylphosphino-2',6'-dimethoxybiphenyl (10% eq., 0.02 g) were all incorporated into an oven-dried schlenk flask with a magnetic stir bar under N_2. 10 mL of toluene were added to the mixture, and the entire flask was freeze-pump thawed. After equilibrating back to room temperature, the reaction was stirred under reflux overnight. The product was purified by extraction using water and CH_2Cl_2. The organic layer was collected and dried using $MgSO_4$. Excess solvent was removed under reduced pressure. The product was further purified by column chromatography and eluted with 5-10% MeOH in ethyl acetate giving **1-MOM** as dark brown oil in 37% yield. ^{1}H NMR ($CDCl_3$, δ, ppm): 8.95 (dd, J=1.8 Hz, 2.4 Hz, 1H), 8.54 (d, J=4.8 Hz, 2H), 8.21 (dd, J=1.5 Hz, 6.9 Hz, 1H), 7.66 (m, 2H), 7.52 (d, J=8.1 Hz, 2H), 7.46 (d, J=8.1 Hz, 2H), 7.37 (m, 2H), 7.15 (td, J=0.9 Hz, 2.4 Hz, 2H), 5.50 (s, 2H), 3.89 (s, 4H), 3.79 (s, 2H), 3.60 (s, 3H) ^{13}C NMR ($CDCl_3$, δ, ppm): 159.85, 152.63, 149.62, 149.30, 149.05, 148.75, 140.54, 138.24, 136.63, 136.27, 134.61, 133.61, 128.93, 127.84, 122.91, 122.46, 121.84, 112.03, 95.36, 68.10, 60.24, 58.39 High Res. ESI MS: Calc. 477.2291 Exp. 477.2293

3.2.4 Synthesis of 1-OH

1-MOM ligand (0.19 mmol, 0.09 g) was dissolved in 15 mL of 2:1 MeOH : CH_2Cl_2 in a round bottom flask with a magnetic stir bar. Flask contents were stirred as 0.5 mL of concentrated HCl was slowly added to the swirling contents after which the reaction mixture was stirred under reflux for 24 hours. A solution of $NaHCO_3$ in water was used to neutralize the acidic flask.

Extraction was carried out using water and CH_2Cl_2. The organic layer was collected and dried using $MgSO_4$ to produce a dark green solid **1-OH** in quantitative yield. ^{1}H NMR ($CDCl_3$, δ, ppm): 8.81 (dd, J=1.2 Hz, 2.4 Hz, 1H), 8.58 (d, J=5.1 Hz, 2H), 8.29 (dd, J=1.2 Hz, 7.2 Hz, 1H), 7.71 (m, 4H), 7.56 (d, J=8.1 Hz, 2H), 7.43 (m, 4H), 7.22 (m, 4H), 3.93 (s, 4H), 3.82 (s, 2H) ^{13}C NMR ($CDCl_3$, δ, ppm): 159.81, 151.68, 149.08, 147.69, 138.38, 138.21, 137.99, 136.52, 134.76, 130.75, 130.07, 129.04, 128.24, 126.79, 122.90, 122.05, 121.76, 109.53, 68.01, 60.18, 58.35, High Res. ESI MS: Calc. 433.2028 Exp. 433.2028

3.2.5 Synthesis of 1-BPh_2

1-OH (0.18 mmol, 0.08 g) and BPh_3 (0.18 mmol, 0.05 g) were added to an oven-dried schlenk flask with a magnetic stir bar under N_2 before adding 10 mL of toluene. The flask mixture was stirred at 80 °C for 12 hours. Extraction was undergone using water and CH_2Cl_2. The organic layer was collected and dried using $MgSO_4$ to yield the dark-green oily product in 78% yield. ^{1}H NMR ($CDCl_3$, δ, ppm): 8.61 (m, 4H), 7.73 (m, 4H), 7.63 (d, J=7.2 Hz, 3H), 7.56 (d, J=6.3 Hz, 5H), 7.47 (d, J=6 Hz, 2H), 7.33 (m, 9H), 4.01 (s, 4H), 3.90 (s, 2H) ^{13}C NMR ($CDCl_3$, δ, ppm): 159.00, 158.49, 149.18, 139.74, 138.19, 138.02, 137.43, 137.26, 133.36, 132.36, 129.92, 127.95, 127.35, 127.08, 126.32, 123.56, 123.19, 122.70, 120.20, 116.20, 109.95, 60.03, 58.57 High Res. ESI MS: Calc. 597.2833, Exp. 597.2854

3.2.6 Synthesis of 1-Alq_3

1-OH (0.23 mmol, 0.10 g) was measured out in an oven dried schlenk flask with a magnetic stir bar. The flask was evacuated and refilled with argon gas three times to thoroughly dry the starting material. In a separate flask containing dry molecular sieves, toluene was freeze pump thawed before being transferred to the reaction flask via cannulation under argon gas after its temperature equilibrated to 298 K. 2.0 M $AlMe_3$ in toluene (0.077 mmol, 39.00 μL) was added

drop-wise to the schlenk flask under nitrogen, stirring the solution throughout the process. Reaction was left to stir under argon overnight. Hexanes solvent was slowly added to the stirring solution the next day to induce precipitation of the product. Product was collected by centrifugation and rinsed with hexanes before being dried under vacuum to produce a green solid in 65% yield. ^{1}H NMR ($CDCl_3$, δ, ppm): 8.96 (d, J=3.9 Hz, 1H), 8.89 (d, J=4.5 Hz, 1H), 8.53 (m, 8H), 8.39 (t, J=6.6 Hz, 2H), 7.65 (m, 13H), 7.50 (m, 12H), 7.35 (m, 7H), 7.13 (m, 12H), 3.87 (s, 12H), 3.76 (s, 6H) ^{13}C NMR ($CDCl_3$, δ, ppm): 160.11, 160.07, 160.01, 158.64. 158.57, 158.16, 149.33, 149.30, 145.42, 144.95, 142.81, 140.26, 139.69, 138.82, 138.55, 138.30, 138.15, 137.96, 137.87, 137.74, 136.82, 132.19, 131.86, 131.62, 130.97, 130.30, 130.15, 129.46, 129.34, 129.28, 128.53 128.21, 128.05, 127.77, 125.83, 125.68, 125.61, 125.45, 125.39, 123.16, 122.33, 122.04, 121.40, 113.65, 113.04, 112.58, 68.26, 60.42, 60.38, 58.62, 53.80, 31.89, 30.65, 30.00, 25.92, 22.96, 21.77, 14.44, High Res. ESI MS: Calc 1321.5509, Exp 1321.5522

3.2.7 Molecular Orbital Calculations

DFT calculations were performed on all four synthesized compounds **1-MOM**, **1-OH**, **1-BPh_2** and **1-Alq_3**. The calculations were executed using the Gaussian03 program at the B3LYP/6-31G* level of theory.

3.3 Results and Discussion

3.3.1 Synthesis

3.3.1.1 Synthesis of ligands 1-MOM and 1-OH

As shown in Scheme 3.1, 4-Br-$C_6H_4CH_2N(CH_2$-2-py$)_2$ was synthesized by condensation reaction in THF with excess NaOH from 4-bromobenzylbromide and bis(2-pyridylmethyl)amine

in 92% yield. Boronic ester **1-B** was synthesized by Suzuki-Miyaura coupling of 4-Br-$C_6H_4CH_2N(CH_2$-2-py) with bis(pinacolato)diboron in DMF in 74% yield.

MOM-protected 5-bromo-8-hydroxyquinoline was provided by Dr. Yi Sun and previously synthesized according to literature.[20] Ligand **1-MOM** was synthesized using Pd catalyzed Suzuki-Miyaura coupling of the boronic ester **1-B** and the MOM protected 5-bromo-8-hydroxyquinoline moiety in 37% yield. Ligand **1-OH** was produced through a de-protection reaction of **1-MOM** using HCl stirred under reflux in a MeOH/water mixture.

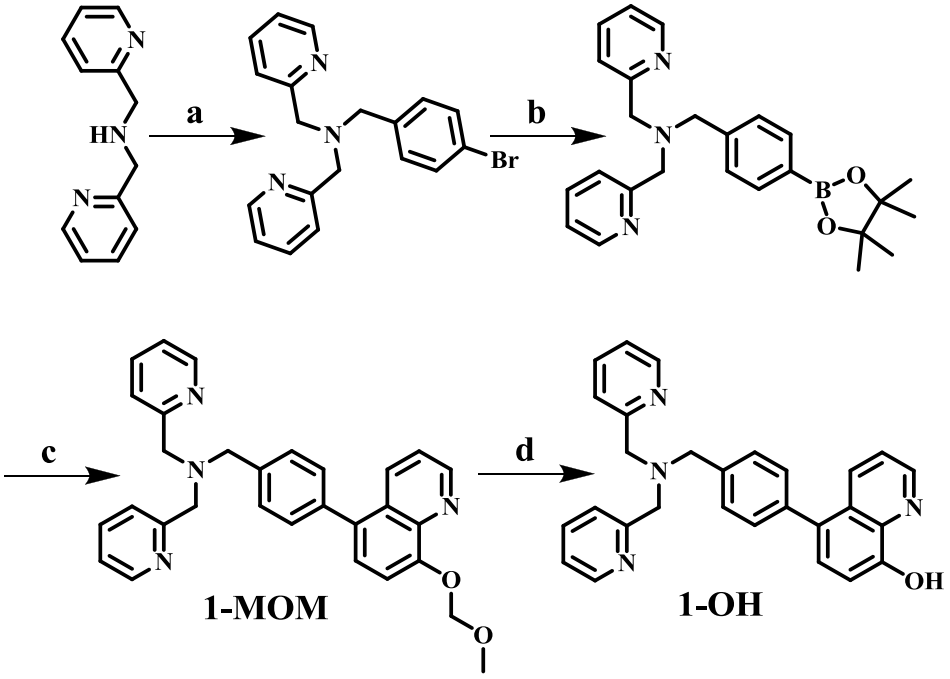

Reagents and conditions: a) 1-bromo-4-(bromomethyl)benzene, NaOH, THF, reflux, 7h; b) bis(pinacolato)diboron, KOAc, (dppf)Pd(II)Cl_2, DMF, 100°C, 12h; c) 5-bromo-8-(methoxymethoxy)quinoline, $Pd(OAc)_2$, K_3PO_4, 2-dicyclohexylphosphino-2',6'-dimethoxybiphenyl, toluene, reflux, 12h; d) (i) HCl, 2:1 (MeOH: CH_2Cl_2), reflux, 24h; (ii) $NaHCO_3$, H_2O, rt, 1h.

Scheme 3.1. Synthetic procedures for ligands **1-OH** and **1-MOM**.

3.3.1.2 Synthesis of compounds 1-BPh_2 and 1-Alq_3

Both ligands **1-BPh_2** and **1-Alq_3** were synthesized from ligand **1-OH** in conditions outlined in Scheme 3.2. The compound 1-BPh_2 was synthesized by a reaction between **1-OH** and triphenylborane in toluene at 80°C. Benzene was eliminated and the reaction mixture was allowed to stir overnight to yield the army green solid product in 78% yield. Ligand **1-OH** was reacted with $Al(CH_3)_3$ at room in toluene in order to synthesize compound **1-Alq_3**. The reaction mixture was left to stir overnight followed by addition of hexanes to the reaction flask to precipitate and isolate the green solid product in 63 % yield.

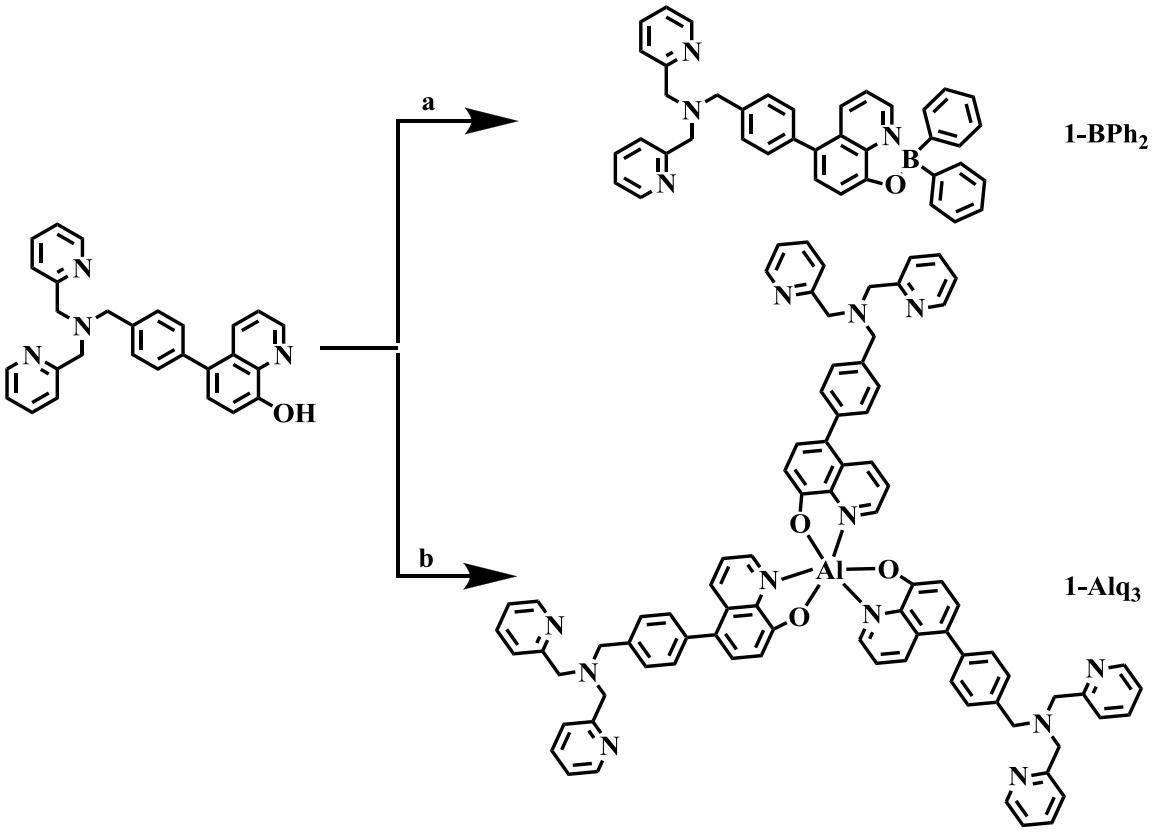

Reagents and conditions: a) BPh_3, toluene, reflux, 12h; b) $Al(CH_3)_3$, toluene, 12h.

Scheme 3.2. Synthetic procedures for complexes **1-BPh_2** and **1-Alq_3**.

Ligands **1-OH**, **1-MOM**, and compounds **1-BPh$_2$** and **1-Alq$_3$** were characterized by ^{1}H and ^{13}C NMR and high resolution ESI mass spectrometry. All four compounds are air-stable both in solid state and in solution. However, **1-BPh$_2$** was stored under argon in the fridge as a precaution due to the cumbersome nature of the synthetic procedure for this ligand.

3.3.2 UV-Vis Absorption Spectra

In order to gain a better understanding of their electronic properties, UV-Vis spectra were acquired for all 4 compounds (**1-MOM**, **1-OH**, **1-BPh$_2$** and **1-Alq$_3$**) and are illustrated in Figure 3.2. All comppounds have exhibit a significant overlap in absorption range in the same 225-300 nm wavelength region due to π-π* transitions attributed to the aromatic moiety that is present in all compounds. The highest ε value is attributed to 1-Alq$_3$ at 265 nm, the peak is both stronger and slightly red-shifted when compared to the other ligands due to the presence of three **1-OH** ligands, creating an amplified π-skeleton.

Furthermore, analysis of the spectra leads to the observation of a weak yet distinct peak for **1-Alq$_3$** compound at 420 nm. This peak is similar to the π-π* absorption maxima for the Alq$_3$ standard compound with an expected absorption peak at 383 nm.[21] Due to the aryl group attachment to the central Alq$_3$ compound, the π-π* absorption maximum undergoes a discrete bathochromic shift as can be explained by the extension of conjugation caused by the added aryl group[22].

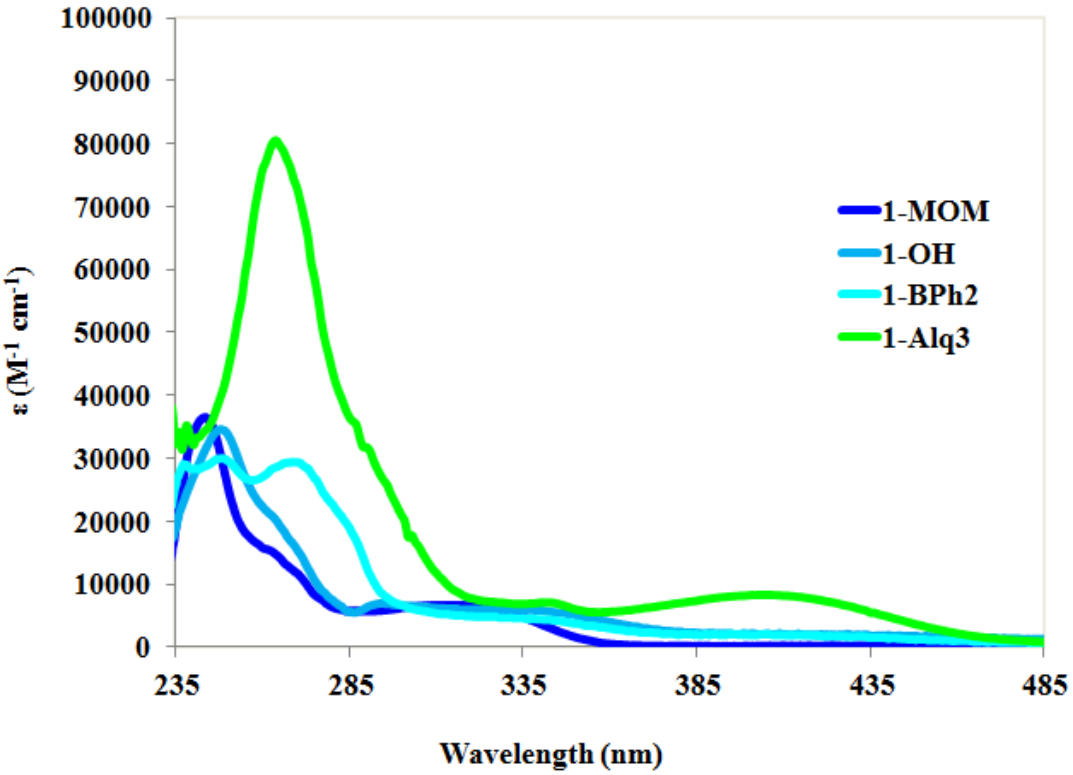

Figure 3.2. Absorption spectra acquired for 10^{-5} M **1-MOM**, **1-OH**, **1-BPh$_2$** and **1-Alq$_3$** ligands at room temperature in THF.

3.3.3. Luminescence

Fluorescence emission spectra acquired for the four molecules in THF at room temperature are shown in Figure 3.3. Blue fluorescence is observed for **1-MOM** and **1-OH** while green fluorescence is displayed for **1-BPh$_2$** and **1-Alq$_3$** in solution.

The emission energy is noted to be analogous for **1-MOM** and **1-OH** due to the similarity in binding targets on the hydroxyquinoline side of the molecule. Both the ligands have a free nitrogen binding site while the oxygen site differs between the two. The oxygen binding site is blocked only in the **1-MOM** ligand, while in the case of **1-OH** the oxygen is simply protonated.

1-BPh_2 and **1-Alq_3** have a similar emission wavelength, which can be attributed to the **1-OH** ligand being attached to BPh_2 and the Al(III) center, respectively. The binding of **1-OH** to both BPh_2 or Al(III) produces a red-shift in the emission wavelength, which can be attributed to the Lewis acidic nature of both the boron and the aluminum centers to which the hydroxyquinoline is bound as they lower the LUMO level and narrow the band gap of the compound.[23] The analogous nature of the two electron-withdrawing group XIII elements explains why their emission peaks overlap**.** A summary of the absorption and luminescent properties are presented in Table 3.1.

Table 3.1. Absorption and luminescence data.

Compound Ligand	**UV-Vis, nm (ε, M^{-1} cm^{-1})**	**λ_{em}[a], nm THF, 298K**	**Φ_{fl}[b], CH_2Cl_2**	**Φ_{ss}[c]**
1-MOM	243 (36,600)	399	0.43	0.03
1-OH	248 (34,500)	400	0.01	0.02
1-BPh_2	248 (30,000), 269 (29,400)	531	0.10	0.20
1-Alq_3	265 (79,700), 406 (8,400)	528	0.08	<0.01

[a] in CH_2Cl_2 at 1.0×10^5M. [b] Relative to 9, 10-diphenylanthracene= 0.95. [c] Measured using an integration sphere.

To examine if the solvent polarity has any impact on the fluorescence of the four compounds, fluorescence emission spectra were acquired and are shown in Figure 3.4. It was determined that **1-BPh_2** and **1-Alq_3** do not show significant emission wavelength change with solvent polarity. However, **1-MOM** and **1-OH** do demonstrate weak positive solvatochromism, indicating a difference in the dipole moment between the ground and excited states of the two molecules with their excited state being slightly more polar than their ground state. The BPh_2 and Al(III) moieties

present in the **1-BPh$_2$** and **1-Alq$_3$** compounds diminish the influence of solvent polarity on the emission of the compounds.

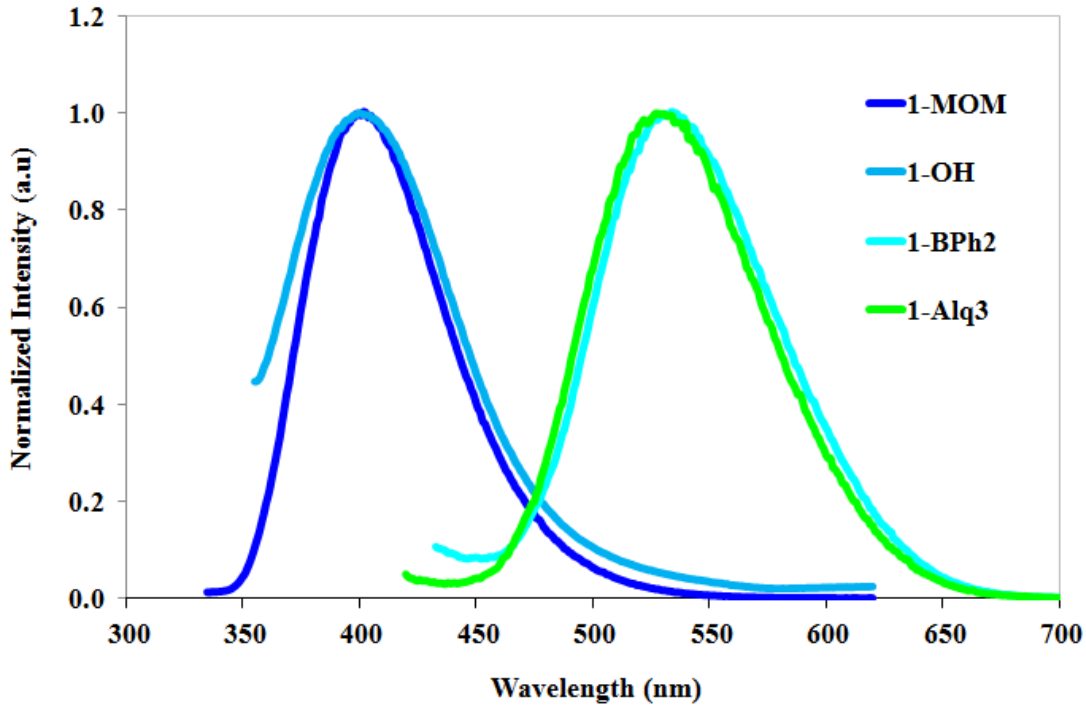

Figure 3.3. Normalized fluorescence spectra of compounds **1-MOM**, **1-OH**, **1-BPh$_2$** and **1-Alq$_3$** at rt in THF.

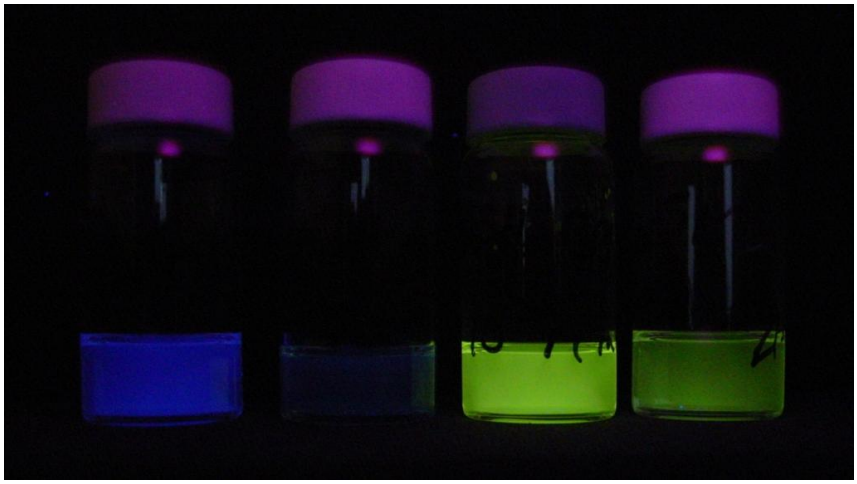

Figure 3.3a. Photograph, under 365 nm irradiation, of the compounds **1-MOM**, **1-OH**, **1-BPh$_2$** and **1-Alq$_3$**.

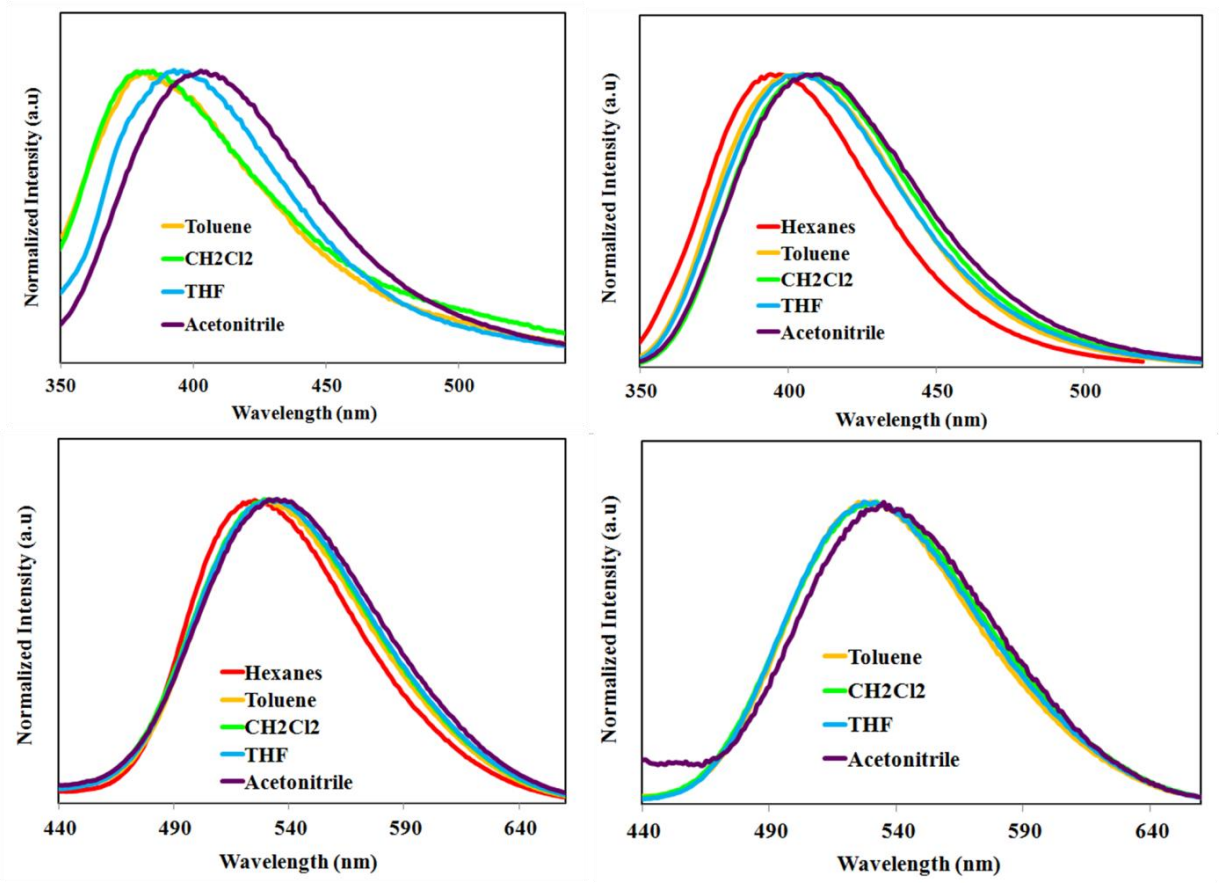

Figure 3.4. Normalized fluorescence spectra of the four compounds in various solvents: compound (Top Left) **1-OH**, (Top Right) **1-MOM**, (Bottom Left) **1-BPh$_2$** and (Bottom Right) **1-Alq$_3$** at rt.

3.3.4 Fluorescent Quantum Yield

Quantum yield measurements in solution for the ligands **1-MOM**, **1-OH**, **1-BPh$_2$**, and **1-Alq$_3$** were calculated using 9,10-diphenylanthracene as a standard in CH_2Cl_2 at 298 K ($\Phi = 0.95$). Quantum yield calculations were performed using previously known procedures on free ligand samples in CH_2Cl_2.[24] Solid state quantum yield was recorded using a previously published

procedure.[25] Calculation results for all four compounds are presented in Table 3.1. Ligand **1-OH** was shown to have the lowest quantum yield of all the compounds tested both in solid state and solution, (Φ_{ss} = 0.02) and (Φ_{fl}= 0.01) respectively. Its MOM-protected counterpart **1-MOM**, however, exhibits the highest calculated quantum yield in solution of the four compounds (Φ_{fl} = 0.43) besting even that of the two metal complexes **1-BPh$_2$** and **1-Alq$_3$**, (Φ_{fl} = 0.10) and (Φ_{fl} = 0.08), respectively. Interestingly, both compounds **1-Alq$_3$** and **1-MOM** have stronger quantum yield in solution state, while complex **1-BPh$_2$** exhibits stronger quantum yield in solid state. This observation could be due to a higher degree of molecule planarity and subsequent molecular stacking being present in solid state for molecules **1-Alq$_3$** and **1-MOM**, leading to self-quenching. The tetrahedral nature of the four-coordinated boron moiety of the **1-BPh$_2$** molecule would disturb the degree of planarity of the molecule and would impede solid-state self quenching, yielding a stronger quantum yield in the solid state (Φ_{ss} = 0.20) than in solution.

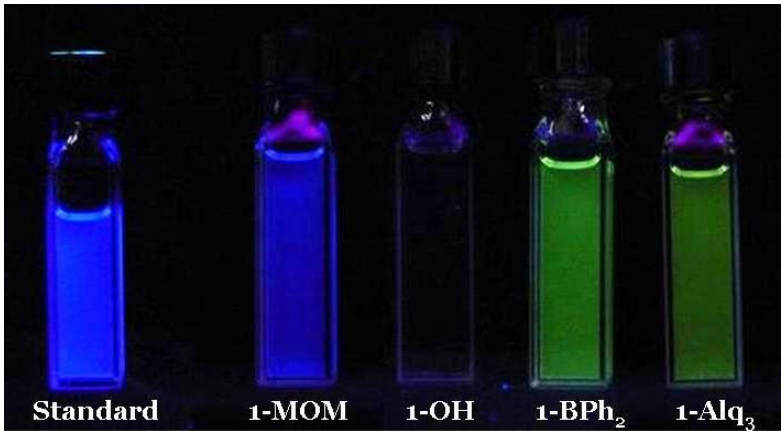

Figure 3.5. Quantum yield test cuvettes of all four 1-X compounds and the 9,10-diphenylathracene standard under UV light 365 nm irradiation.

3.3.5 Electrochemical Properties

Cyclic voltammetry measurements were recorded in dry DMF by using NBu_4PF_6 as the electrolyte and by using scan rates of 200-500 mV/sec. Recorded cyclic voltammetry data for sompounds **1-BPh$_2$** and **1-Alq$_3$** are shown in Figure 3.6 and Table 3.2.

Figure 3.6 indicates that both compounds are shown to possess a single quasi-reversible reduction peak. **1-BPh$_2$** has a reduction peak at -2.04 V (vs. $FeCp_2^{0/+}$) which can be attributed to the reduction of the chelating ligand. The resulting energy level values can be compared to previously recorded boron center cyclic voltammetry data of hydroxyquinoline diphenyl boron molecules with similar HOMO/LUMO energy levels.[26] The CV measurements acquired for compound **1-Alq$_3$** show a weaker reduction peak at -2.17 V. Experimental HOMO/LUMO energy levels acquired for **1-Alq$_3$** are shown to be similar to comparable electon-rich 5-substituted tris(8-quinolinolate) aluminum (III) complexes.[27] Measurements of **1-MOM** and **1-OH** did not produce any visible reduction peaks. The reduction peaks observed for 1-**MOM** and **1-OH** are indicative of the electron accepting and transporting ability of the **1-OH** molecule being enhanced by the existence of the boron and Al(III) centers. HOMO and LUMO energies of **1-Alq$_3$** and **1-BPh$_2$** were calculated using CV and UV-Vis and are illustrated in Figure 3.7.

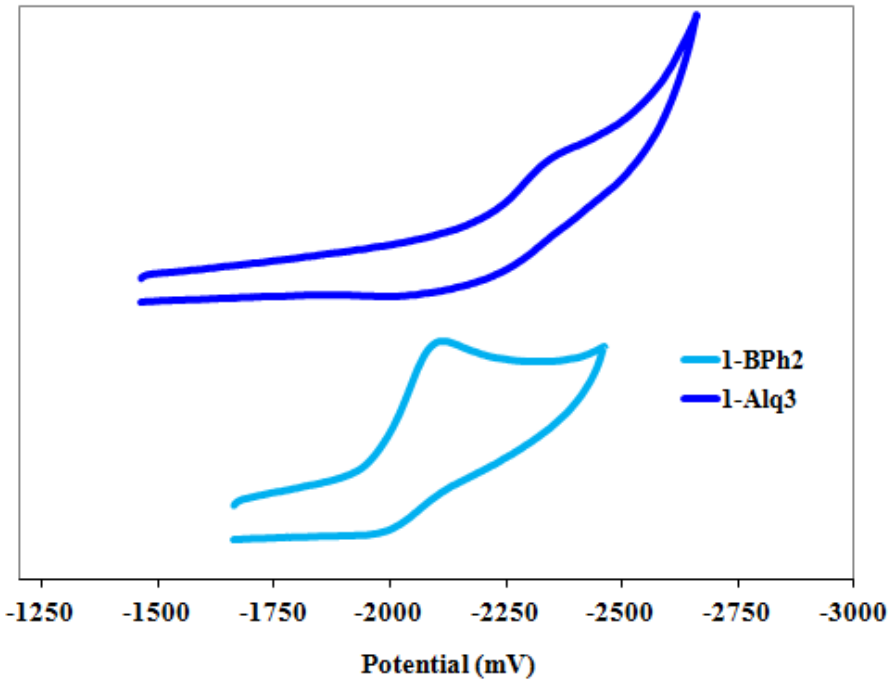

Figure 3.6. CV Diagrams for **1-BPh$_2$** and **1-Alq$_3$** recorded in DMF. Reference used for the potential measurement is $FeCp_2^{+/0}$.

3.3.6 DFT Calculations

The HOMO and LUMO diagrams along with the energy (a.u.) for each level are shown in Figure 3.8 with isocontour values of 0.02 au.

The molecular orbital diagrams in Figure 3.8 illustrate that in all four compounds, the HOMO level is composed of a π-orbital with contributions from both the hydroxyquinoline and the neighboring phenyl group of the ligand. In contrast, the LUMO levels of all four compounds, are composed of π*-orbital with contributions from the hydroxyquinoline ring alone. As can be observed from the molecular orbital diagrams, the lowest energy electronic transition expected is that of a π-π* transition centered on the hydroxyquinolate group. This phenomenon has been previously observed for hydroxyquinoline ligands and their metal compounds.[26b]

Table 3.2. HOMO and LUMO energy levels and gaps for all four **1-X** compounds.

	Calculated Energy (eV)[a]			Experimental Energy (eV)		
Compound Ligand	**HOMO**	**LUMO**	**Energy Gap**	**HOMO[b]**	**LUMO[c]**	**Energy Gap[d]**
1-MOM	-5.72	-1.57	-4.15	-	-	-3.40
1-OH	-5.63	-1.61	-4.03	-	-	-3.26
1-BPh_2	-5.67	-2.34	-3.32	-5.33	-2.75	-2.57
1-Alq_3	-4.82	-1.67	-3.15	-4.90	-2.63	-2.27

[a] Calculated using the Gaussian 03 program employing a split valence B3LYP/6-311G(d) basis set. [b] Calculated from experimental LUMO and the optical energy gap. [c] Calculated from reduction potential measurements in DMF. [d] Calculated from absorption edge of UV-Vis spectrum acquired for all four 1-X ligands.

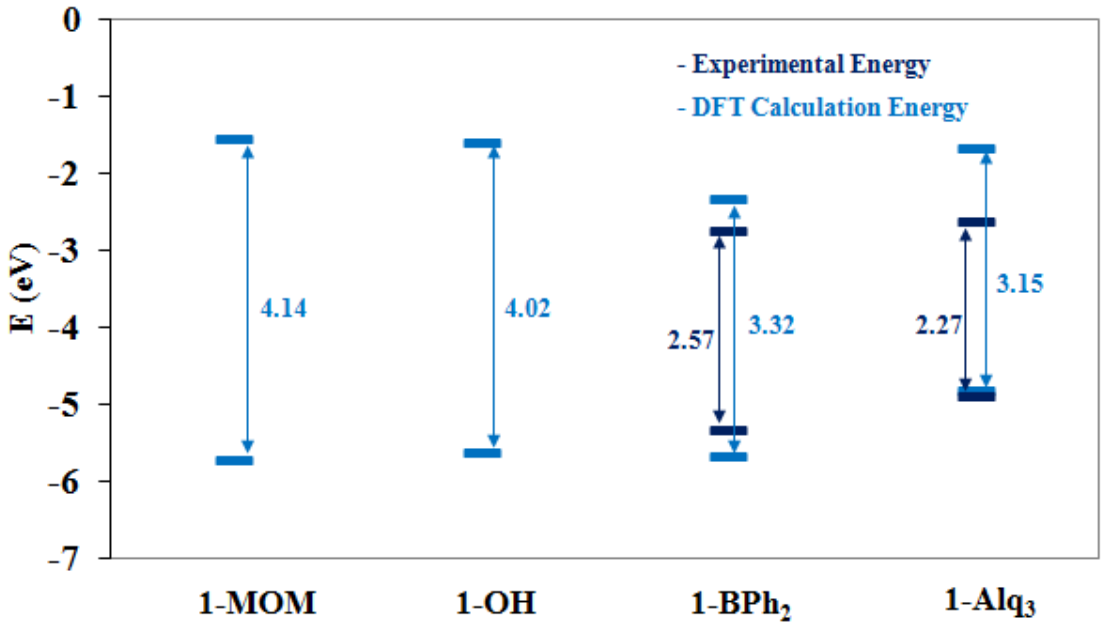

Figure 3.7. Experimental and calculated HOMO and LUMO levels of all **1-X** ligands.

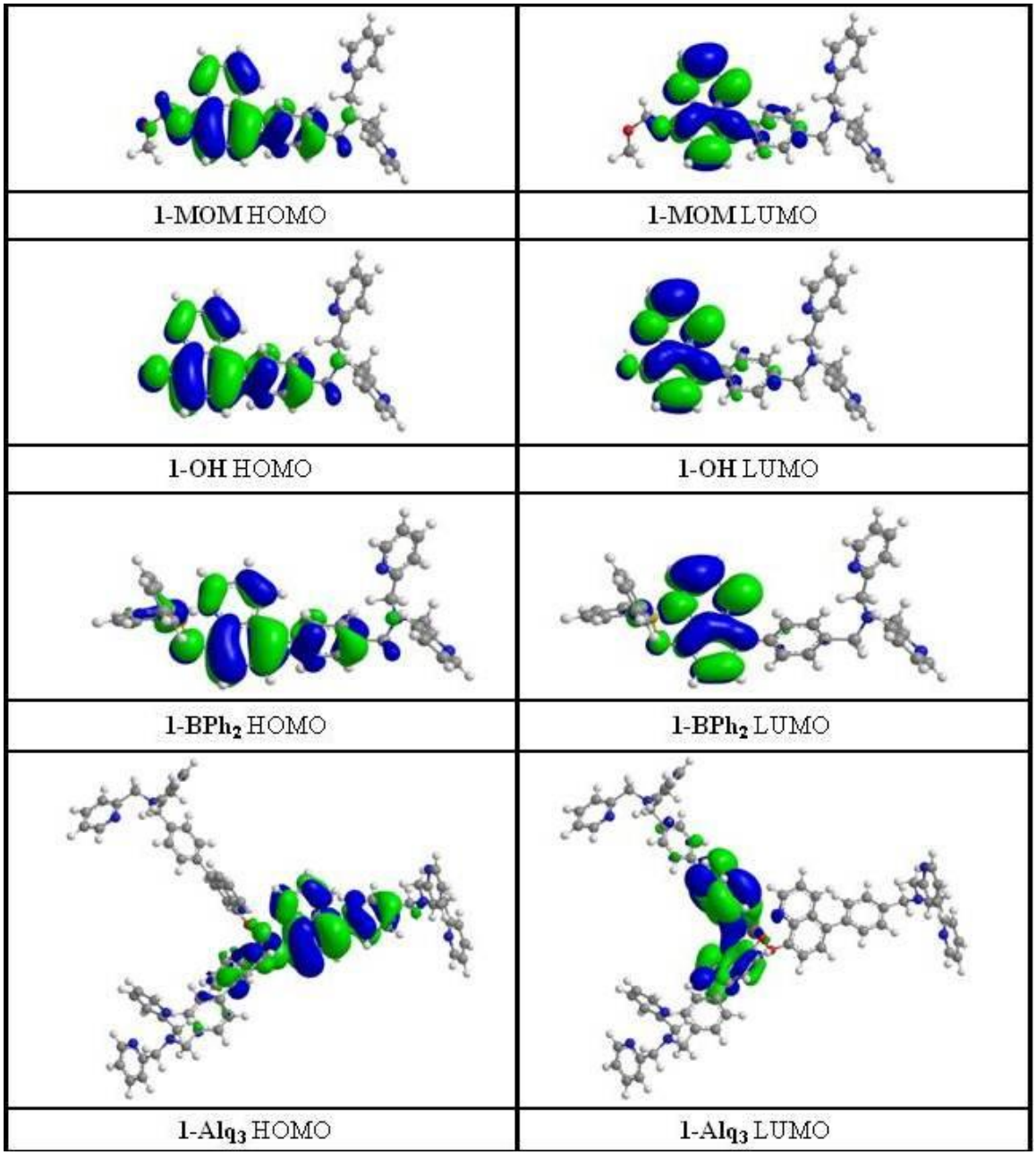

Figure 3.8. HOMO and LUMO Molecular diagrams for **1-MOM**, **1-OH**, **1-BPh$_2$** and **1-Alq$_3$** ligands.

3.3.7 1-MOM, 1-OH, 1-BPh_2 and 1-Alq_3 as Sensors for Zn(II)

To examine the potential of compounds **1-MOM**, **1-OH**, **1-BPh_2** and **1-Alq_3** as sensors for Zn(II) ions, titration experiments were performed using UV-Vis absorption and fluorescence emission spectroscopy. Titrations were performed for 10^{-5} M ligand solutions in THF with 3×10^{-3} M zinc perchlorate hexahydrate in THF using 3 mL spectroscopic cuvettes. This procedure allowed for 1 μL increments of zinc solution to be added to the ligand solution in order to produce a regular titration measurement adding up to molar equivalent zinc to ligand ratio after 10 μL.

The emission spectrum for pure **1-OH** ligand (Figure 3.9) exhibits a peak in the blue region of the spectrum. The emission peak undergoes a bathochromic shift of ~150 nm as Zn(II) is added yielding a distinct emission color change from blue to green, attributed to Zn(II) ions binding to the hydroxyquinoline site. Once 0.5 molar equivalence is achieved, the peak undergoes a blue-shift of ~100 nm, generating a blue green emission color, which can be attributed to Zn(II) binding to the dipyridyl site. Previous research on the subject indicates that the 8-hydroxyquinoline-Zn(II) complex has an emission peak in the 530-600 nm range.[26b] It is therefore deduced that the 8-hydroxyquinoline compound is the first site to bind to Zn(II) causing a red shift in the emission band to λ_{max}=550 nm up until 0.5 molar equivalence of Zn(II) . This is followed by binding of Zn(II) to the dipyridyl site as excess Zn(II) ions are added, thus explaining the appearance of the second peak in the blue-green spectral region at 455 nm in Figure 3.9.

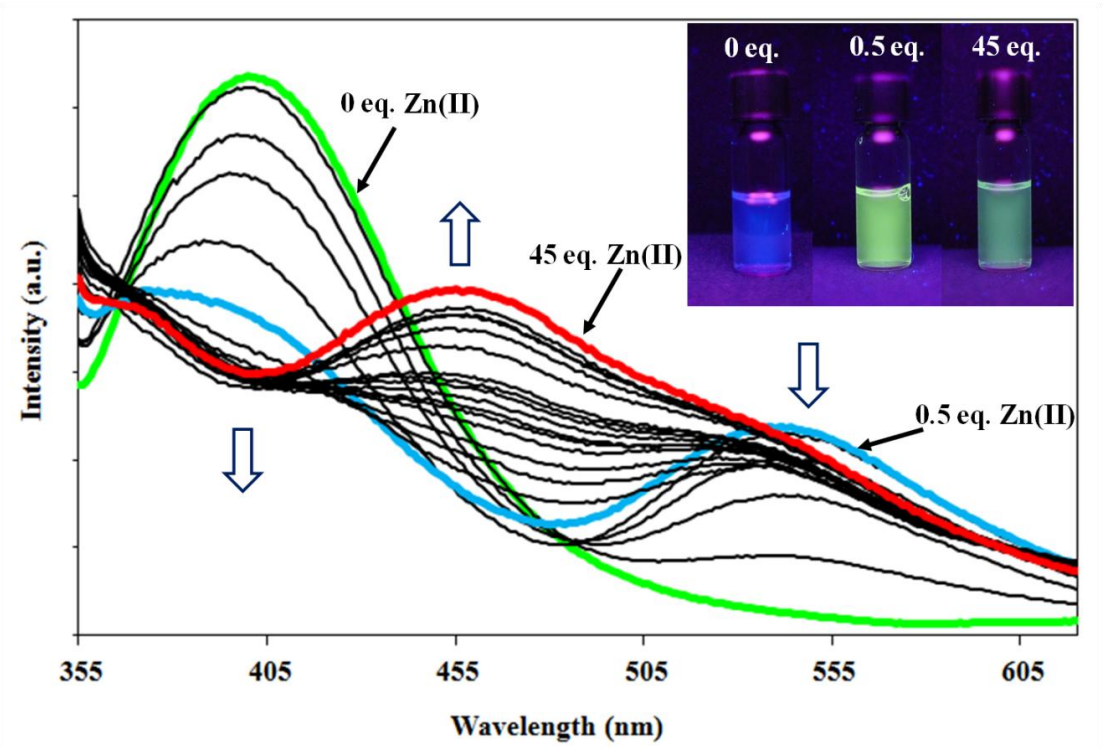

Figure 3.9. Fluorescence emission zinc titration for 10^{-5}M **1-OH** in THF from 0 to 45.5 molar eq. of Zn(II).

The UV-Vis absorption spectrum for the Zn(II) titration of ligand **1-OH** is shown in Figure 3.10. The peak at 247nm as molar increments of Zn(II) are added, followed by an slight increase in the peak at 262nm. Both observations are consistent with Zn(II) binding to the hydroxyquinoline moiety and the dipyridyl group of the ligand, though the spectral changes are not significant enough to use the UV-absorption spectrum as indicator for Zn(II) sensing.

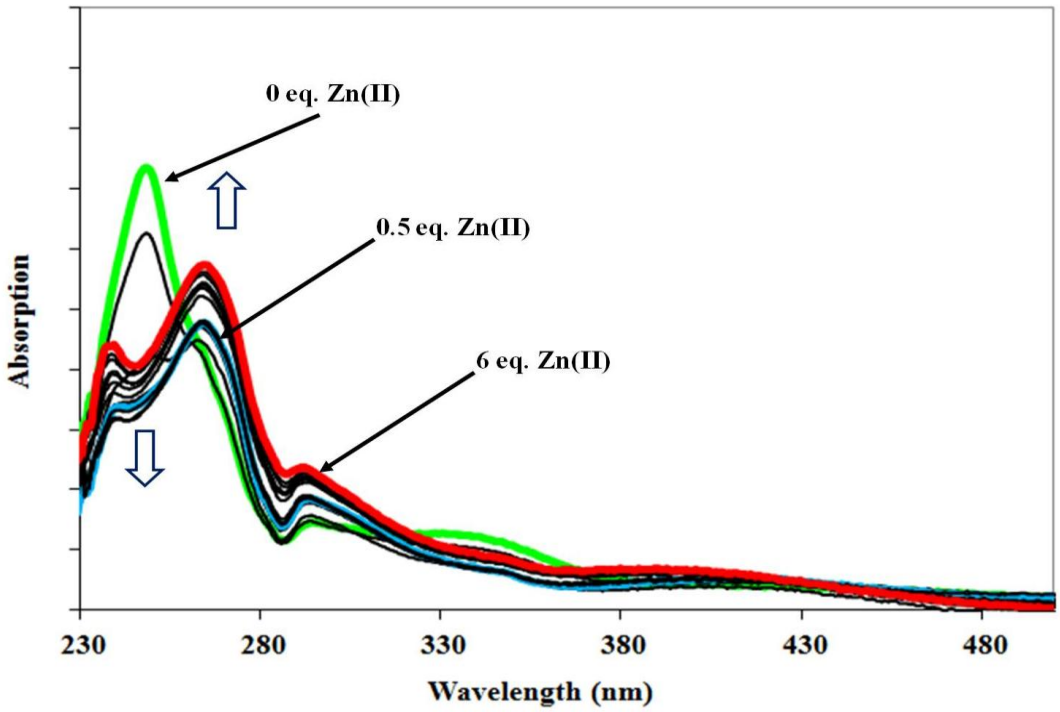

Figure 3.10. UV absorption zinc titration for 10^{-5}M **1-OH** in THF from 0 to 6 molar eq. of Zn(II).

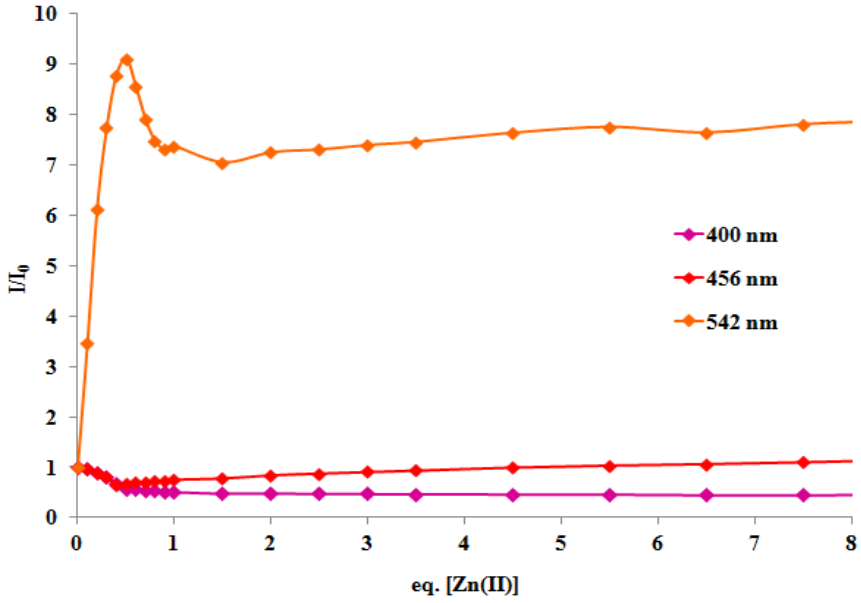

Figure 3.11. Stern-Volmer plot for Zn(II) fluorescence titration of ligand **1-OH** at 400 nm, 456 nm and 542 nm.

The Stern-Volmer plot for fluorescence Zn(II) titration of **1-OH** at 400 nm, 256 nm and 542 nm is shown in Figure 3.11 and indicates strong binding of Zn(II) ions to the ligand up until 0.5 eq. of Zn(II) is reached demonstrating coupling at the hydroxyquinoline moiety, as previously deduced. Slow ligand-metal coupling follows from 0.5 eq. up to 40 eq. of Zn(II) concentration and beyond added to the ligand, indicating a coupling equilibrium between 1-OH and Zn(II) at both dipyridyl and hydroxyquinoline binding sites due to such a high sensing limit. Stern-Volmer graph is shown plotted up to 10 eq. of Zn(II) ions for clarity. A proposed Zn(II) binding model for ligand 1-OH, as deduced from the acquired titration data is shown in Scheme 3.3.

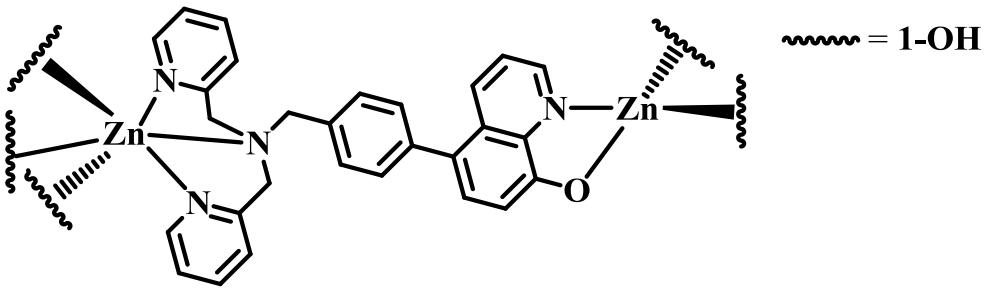

Scheme 3.3. Suggested binding model of Zn(II) ions to ligand **1-OH**.

The fluorescence spectral change for the **1-MOM** ligand with Zn(II) addition is shown in Figure 3.12. The ligand solution responds to the addition of Zn(II) with a red-shift yielding green emission**.** Comparisons of the zinc titration emission spectra for **1-OH** and **1-MOM** reveal that both spectra begin in the blue region of the spectrum at 400 nm. As Zn(II) is added to the **1-MOM** ligand, the peak undergoes a slow bathochromic shift of ~50 nm to 450 nm in the blue-green region as well as a simultaneous decrease in intensity. The ensuing peak at 450 nm as excess Zn(II) is added is reminiscent of the peak present at the same wavelength in the **1-OH** titration data, and is indicative of Zn(II) binding to the dipyridyl moiety on the **1-MOM**

molecule. Unlike the **1-OH** titration data, no hydroxyquinoline-bound Zn(II) peak is observed at 550 nm, indicating that no coupling occurs at the hydroxyquinoline moiety, possibly due to the MOM-protecting group shielding the binding site. A Stern-Volmer plot illustrating the peak decrease at 400 nm is for the Zn(II) titration of **1-MOM** is shown in Figure 3.14. A proposed of the Zn(II) binding model for ligand **1-MOM** in equilibrium, as deduced from the acquired titration data is shown in Scheme 3.4.

UV-Vis absorption titration spectra indicate subtle changes to both the peaks at 230-280 nm and 315 nm as can be observed in Figure 3.13. The peak at 243 nm experiences a decrease as well as a simultaneous rounding as Zn(II) equivalents are added to the sample while the peak at 315 nm experiences an initial increase followed by a decrease after 5 eq. of Zn(II) are added. No significant color changes are witnessed under ambient light.

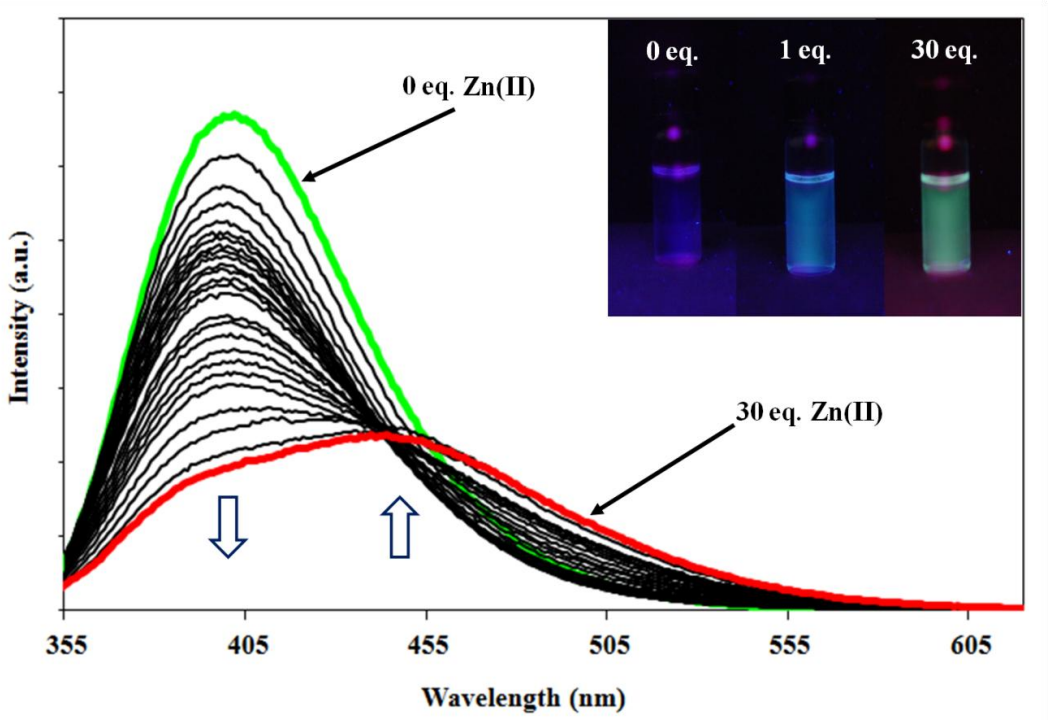

Figure 3.12. Fluorescence emission zinc titration for 10^{-5}M **1-MOM** in THF from 0 to 30 molar eq. of Zn(II).

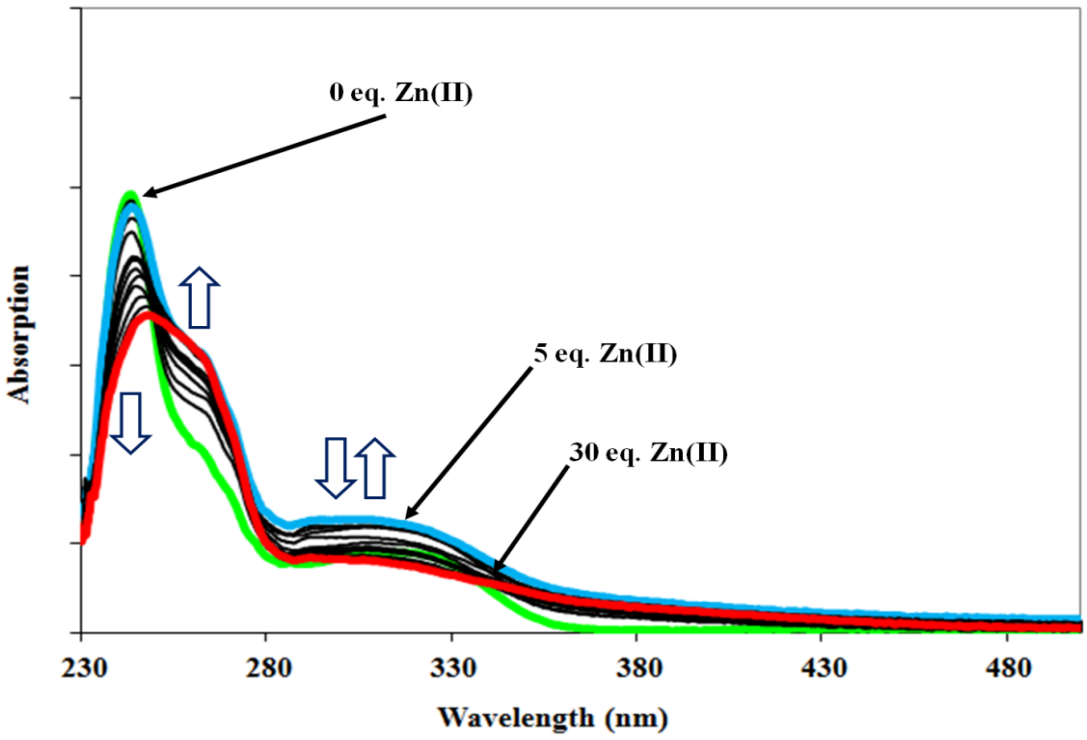

Figure 3.13. UV absorption zinc titration for 10^{-5}M **1-MOM** in THF from 0 to 30 molar eq. of Zn(II).

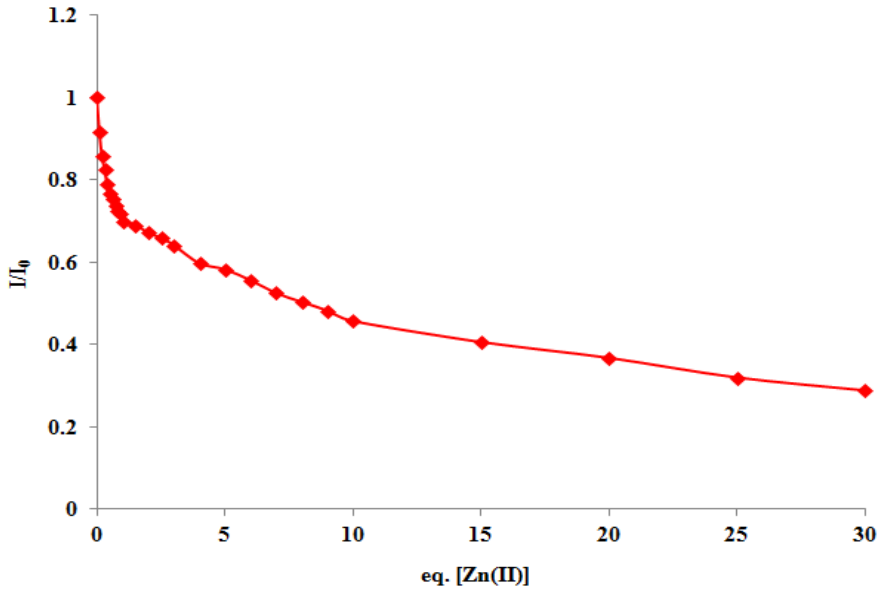

Figure 3.14. Stern-Volmer plot for Zn(II) fluorescence titration of ligand **1-MOM** at 400 nm**.**

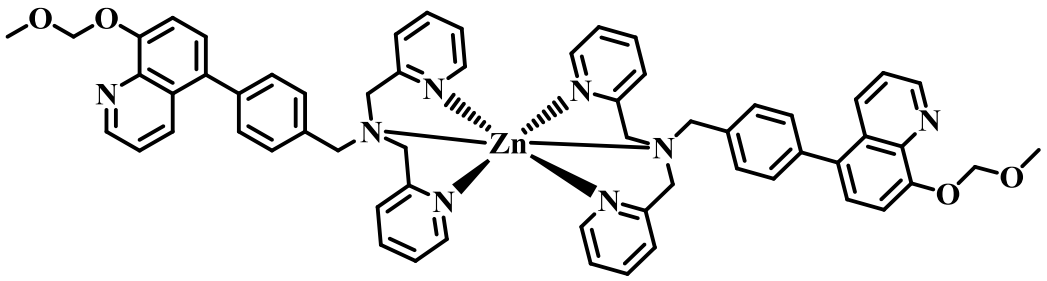

Scheme 3.4. Suggested binding model of Zn(II) ions to ligand **1-MOM**.

In order to establish the impact of Zn(II) binding to the dipyridyl amino site only, full hydroxyquinoline blocking was performed to create ligands **1-Alq$_3$** and **1-BPh$_2$.** Figure 3.15 illustrates that **1-BPh$_2$** in THF emits in the green region of the spectrum (λ_{max}=530 nm) and as Zn(II) is added to the THF solution, an increase in emission intensity is recorded. This emission enhancement can be explained by the intramolecular photoelectron charge transfer between the dipyridyl amino site and the boron-bound hydroxyquinoline site, an effect known to quench the fluorescence of the chromophore.[28] As the Zn(II) is added, the dipyridyl amino nitrogen atoms bind to the metal, thus blocking this intramolecular charge transfer, resulting in an increase in emission.

A Stern-Volmer plot for **1-BPh$_2$** (Figure 3.17) indicates full saturation of the ligand solution occurs when 0.5 molar equivalence is achieved, producing a complex of 2:1 ligand to Zn(II). A proposed Zn(II) binding model for compound **1-BPh$_2$**, as deduced from the acquired titration data is shown in Scheme 3.5. This pattern has been previously observed in Zn(II)-polypyridyl group binding studies resulting in a hexadentate metal-ligand model, which is also applicable in the case of **1-BPh$_2$** as the hydroxyquinoline is completely blocked.[29]

The UV-Vis absorption titration spectra, shown in Figure 3.16, illustrates no change to the absorption data as increments of Zn(II) are added to the sample.

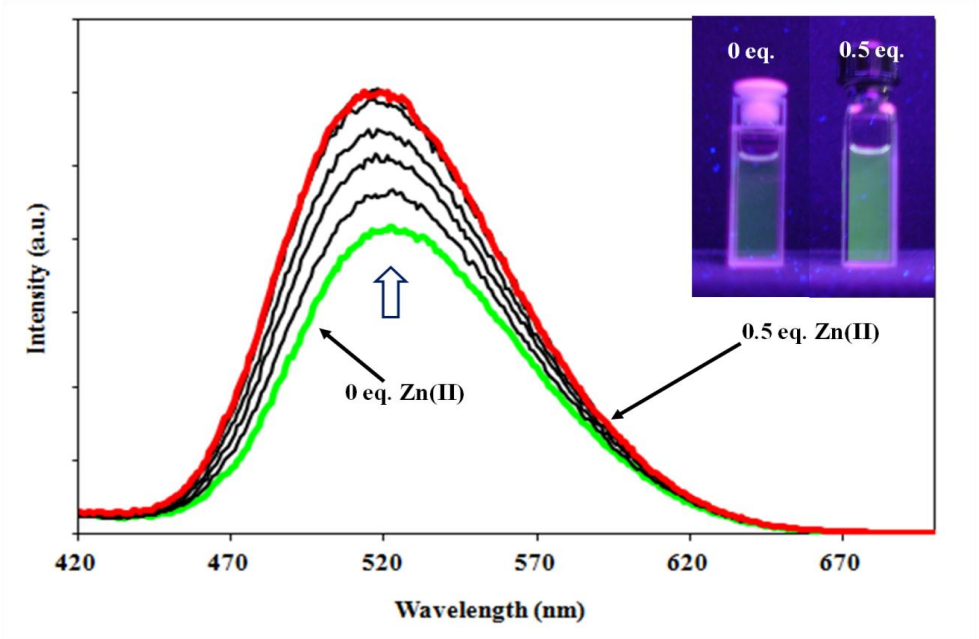

Figure 3.15. Fluorescence emission zinc titration for 10^{-5} M **1-BPh$_2$** in THF from 0 to 0.5 molar eq. of Zn(II).

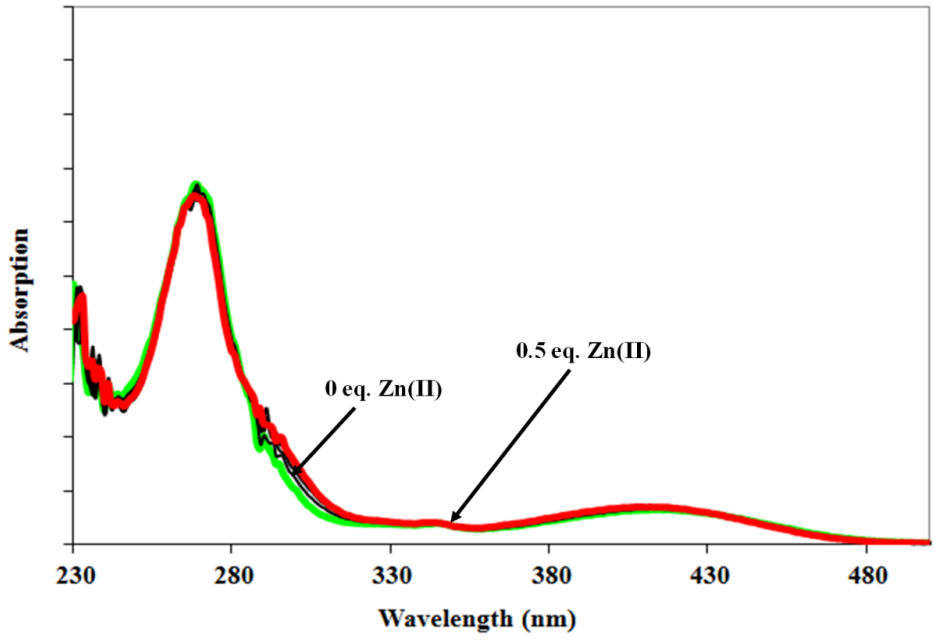

Figure 3.16. UV-Vis absorption zinc titration for 10^{-5} M 1-BPh$_2$ in THF from 0 to 0.5 molar eq. of Zn(II).

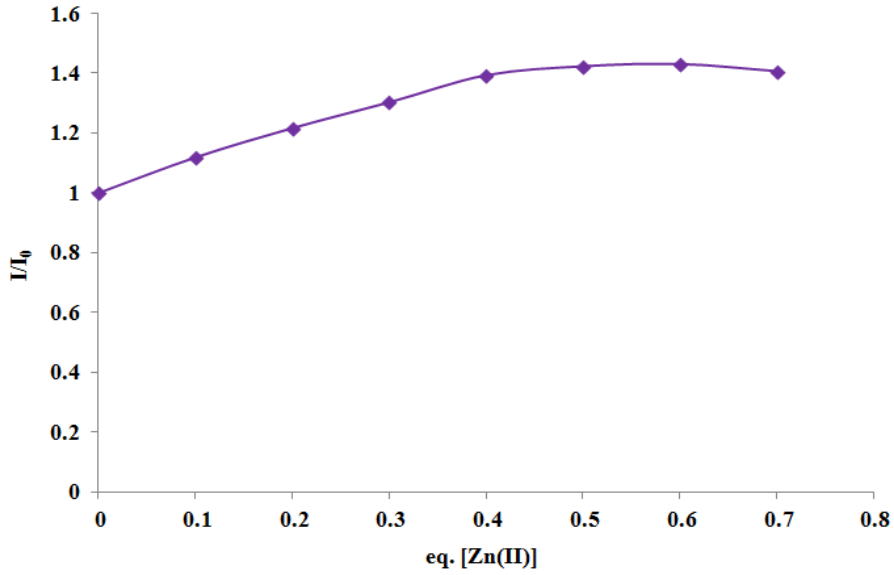

Figure 3.17. Stern-Volmer plot for the fluorescence emission Zn(II) Titration of **1-BPh$_2$**.

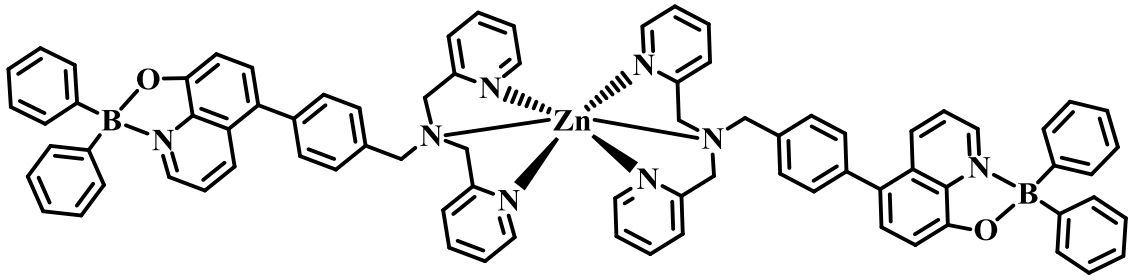

Scheme 3.5. Suggested binding model of Zn(II) ions to ligand **1-BPh$_2$**.

The Zn(II) titration emission spectrum for **1-Alq$_3$** (or 1-(OH)$_3$Al), shown in Figure 3.18, illustrates an emission at 525nm. As Zn(II) is added to the ligand solution, the emission peak undergoes substantial quenching with no significant wavelength shift. UV-Vis aborpstion Zn(II) titration spectra, shown in Figure 3.19, illustrated no change to the original data as Zn(II) increments were added to the sample.

A Stern-Volmer plot for the fluorescence **1-Alq$_3$** (Figure 3.20) Zn(II) titration indicates full saturation of the ligand solution occurs when 1.0 molar equivalence is achieved, producing a complex of 1:1 ligand to Zn(II), a ratio that does not match the previous measurements acquired for the Zn(II) titration of **1-BPh$_2$**. A proposed Zn(II) binding model for compound **1-Alq$_3$**, as deduced from the acquired titration data is projected to be of oligomeric nature. Due to the 1:1 complex to Zn(II) ratio observed for the binding model of **1-Alq$_3$**, it can be proposed that Zn(II) metal coordination numbers may be donated either by one singular **1-Alq$_3$** molecule or several different **1-Alq$_3$** molecules present. Having a singular **1-Alq$_3$** molecule donate all 6 coordination numbers for the octahedral Zn(II) ion seems unlikely due to the immense amount of flexibility required from the sensing complex for this binding scheme to exist. Having several complex molecules form a macrocycle with two Zn(II) ions permits for a lesser strain in binding scheme as well as keeps the 1:1 complex to Zn(II) ratio intact. It is therefore deduced that the **1-Alq$_3$**-Zn(II) is either of cyclic or oligomeric nature as shown in Scheme 3.6. This binding model may be further tested and confirmed by using either ESI (electrospray ioniation) or MALDI (matrix-assisted laser desorption/ionization) mass spectrometry measurements.

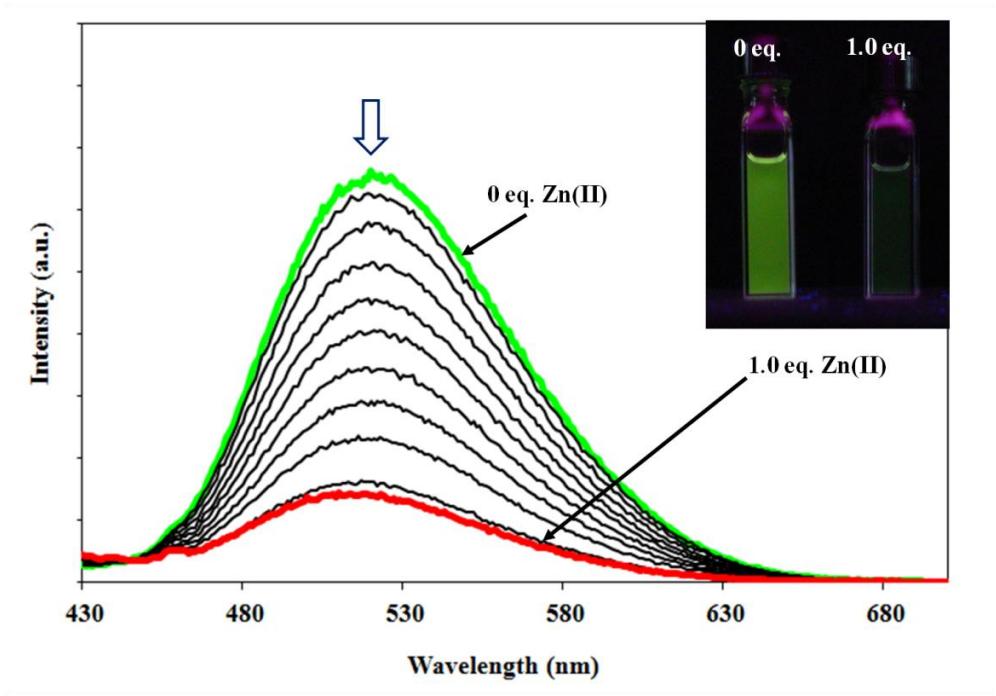

Figure 3.18. Fluorescence emission zinc titration for 10^{-5}M **1-Alq$_3$** in THF from 0 eq. to 30 eq. of Zn(II).

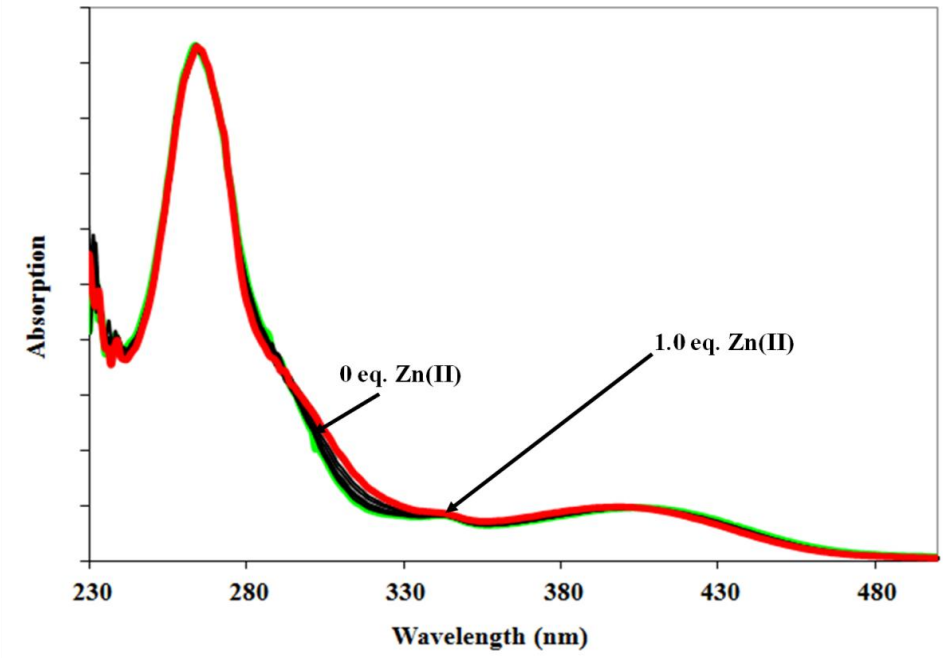

Figure 3.19. UV-Vis absorption zinc titration for 10^{-5} M **1-Alq$_3$** in THF from 0 to 1.0 molar eq. of Zn(II).

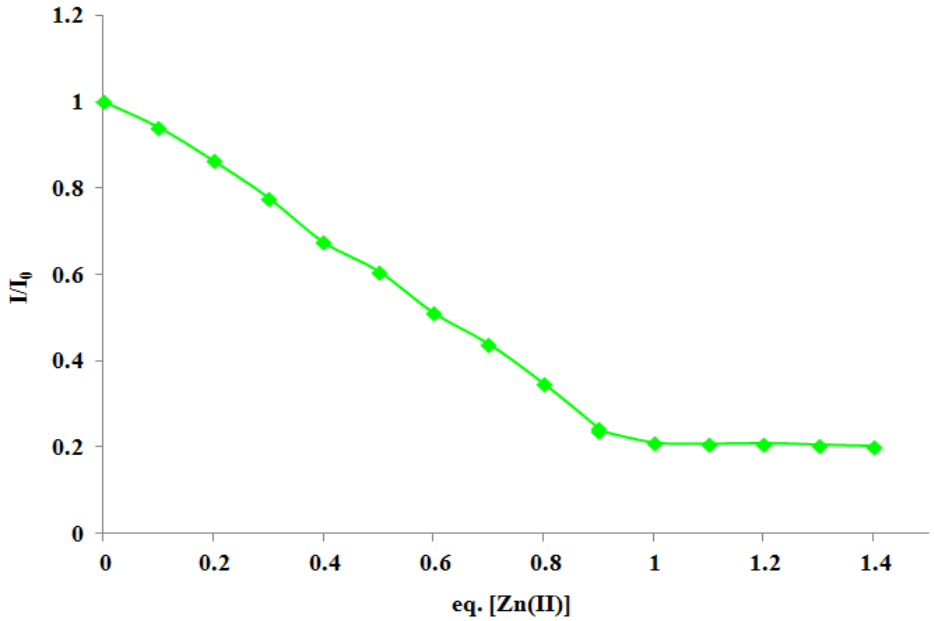

Figure 3.20. Stern-Volmer plot for the fluorescence emission Zn(II) Titration of **1-Alq$_3$**.

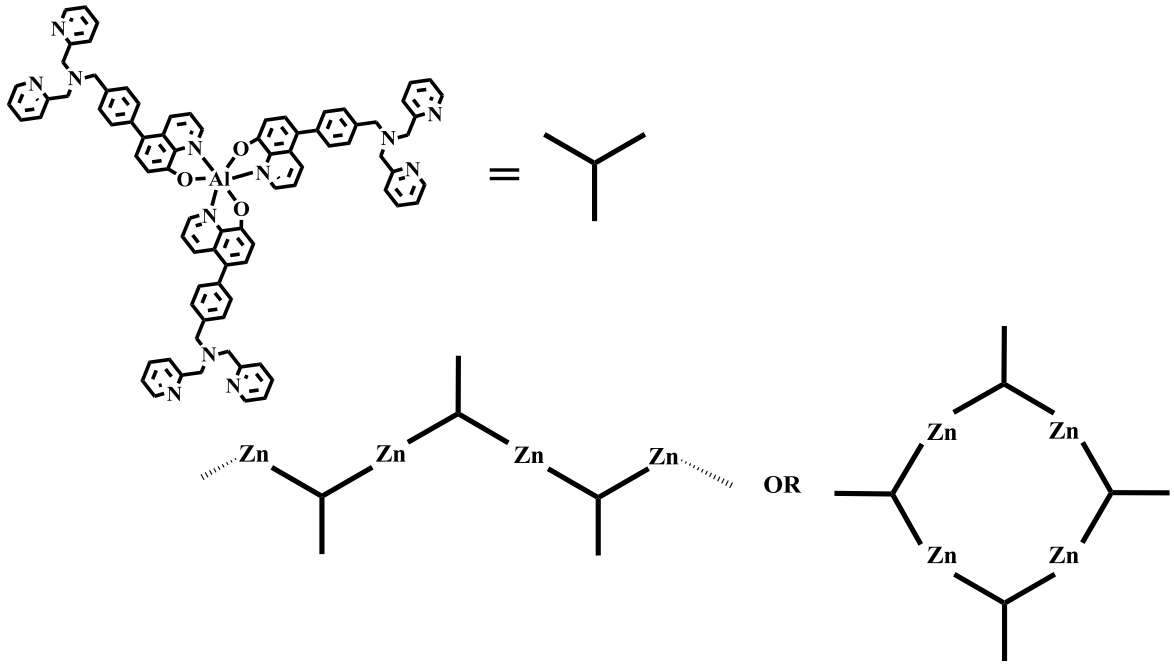

Scheme 3.6. Suggested binding models of Zn(II) ions to ligand **1-Alq$_3$**.

UV-Visible zinc titrations recorded for **1-MOM, 1-OH, 1-BPh_2** and **1-Alq_3** demonstrated a change in absorption intensity yet the wavelength at which absorption was measured remained unchanged. Indeed, no color changes occurred in visible light, and could only be seen under UV radiation. No further decisive information could be acquired from the UV-Vis titration spectra.

3.4 Conclusion

To conclude, four potential Zn(II) sensing compounds were successfully synthesized through a multi-step process with both a polypyridyl and 8-hydroxyquinoline site.

Characterization of all four compounds was achieved through ^{1}H NMR, ^{13}C NMR and high resolution mass spectrometry. Ligand interactions with Zn(II) were studied by recording fluorescence emission and UV-Visible absorption zinc titration. Further ligand luminescence characterization was also acquired through experimental quantum yield measurements as well as DFT molecular orbital calculations.

It has been determined that ligand **1-OH** can be used to detect both low and high concentrations of Zn(II). This is achieved by the emission of a blue light at 0 equivalents of Zn(II), green under UV radiation below 0.5 molar equivalents of Zn(II) and blue-green at higher concentrations of Zn(II).

1-MOM is a less preferred alternate to **1-OH,** as it can be used to detect Zn(II) with a lower emission wavelength spectrum. It achieves this by emitting blue wavelength radiation at 0 equivalents Zn(II), and undergoing a 'turn off' sensor action as Zn(II) concentration increases. At Zn(II) concentrations of 1.0 equivalents or more, a red-shift of the fluorescent emission towards a blue-green wavelength would be observed. Hence, this ligand can be used as a Zn(II) sensor, albeit in a less elegant manner than that of the **1-OH** ligand.

It would not be ideal to utilize ligands **1-BPh_2** and **1-Alq_3** as Zn(II) sensors due to their limitations in Zn(II) saturation, which only permits them to detect zinc up to 1.0 equivalents producing a very limited range of emission properties change in both cases.

Further studies into the effectiveness of the ligand could be accomplished by studying its affinity for Zn(II) as compared to other potential fluorophores. This would allow for the determination of binding selectivity of the ligand. The study of sensory ligand efficiency in the desired environment as well as in different solvents would also be preferred in order to better evaluate the full potential of the ligand.

3.5 References

[1] (a) C. E. Outten and T. V. O'Halloran, *Science.,* **2001**, *292*, 2488.; (b) C. Andreini, L. Banci, I. Bertini and A.J. Rosato, *Proteome Res.*, **2006**, *5*, 196.; (c) N. C. Lim, H. C. Freake and C. Brückner, *Chem. Eur. J.*, **2005**, 11, 38.; (d) W. N. Lipscomb and N. Strater, *Chem. Rev.*, **1996**, 96, 2375.

[2] (a) J. M. Berg and Y. Shi, *Science.*, **1996**, 271, 1081.; (b) P. Jiang and Z. Guo, Z. *Coord. Chem. Rev.*, **2004**, 248, 205.; (c) K. R. Gee, Z-L. Zhou, D. Ton-That, S. L. Sensi and J. H. Weiss, *Cell Calcium*., **2002**, 31 (5), 245.

[3] E. P. Huang, *Proc. Natl. Acad. Sci. USA*., **1997**, 94, 13386.

[4] (a) J-Y. Koh, S. W. Suh, B. J. Gwag, Y. Y. He, C. Y. Hsu and D. W. Choi, *Science*, **1996**, 272, 1013.; (b) A. I. Bush, W. H. Pettingell, G. Multhaup, M. D. Paradis, J. P. Vonsattel, J. F. Gusella, K. Beyreuther, C. L. Masters and R. E. Tanzi, *Science*, **1994**, 265, 1464.

[5] (a) M. P. Cuajungco and G. J. Lees, *Neurobiol. Dis.*, **1997**, 4, 137.; (b) Y. Zhou, H. N. Kim and J. Yoon, *Bioorg. Med. Chem. Lett.*, **2010,** 20, 125.

[6] E. Tomat and S. J. Lippard, *Curr. Opin. Chem. Biol.*, **2010**, 14, 223.

[7] P. D. Zalewski, I. J. Forbes and W. H. Betts, *Biochem. J*., **1993**, 296, 403.

[8] Z. Xu, J. Yoon and D. R. Spring, *Chem. Soc. Rev.*, **2010**, 39, 1996.

[9] C. Hu and U. Englert, *Cryst. Eng. Comm.*, **2001**, 23, 1.

[10] L. Regan and N. D. Clarke, *Biochemistry*, **1990**, 29, 10878.

[11] Y. Marcus, *Chem. Rev*., **1988**, 88, 1475.

[12] I. L. Alberts, K. Nadassy and S. J. Wodak, *Protein Sci.* **1998**, 7, 1700.

[13](a) G. K. Walkup and B. Imperiali, *J. Org. Chem.*,**1998**, 63, 6727.; (b) J. Kawakami, M. Ohta, Y. Yamauchi, and K. Ohzeki, *Anal. Sci.*, **2003**, 19, 1353.; (c) F. Wang, R. Peng and Y. Sha, *Molecules*., **2008**, 13, 922.

[14] (a) J. E. Kwon, S. Lee, Y. You, K-H. Baek, K. Ohkubo, J. Cho, S. Fukuzumi, I. Shin, S. Y. Park and W. Nam, *Inorg. Chem.*, **2012**, Article ASAP, DOI: 10.1021/ic300476e. (b) K. Hanaoka, Y. Muramatsu, Y. Urano, T. Terai, T. Nagano, *Chem. Eur. J.*, **2010**, 16, 568.

[15] (a) J. Ugolotti, S. Hellstrom, G. J. P. Britovsek, T. S. Jones, P. Hunt and A. J. P. White, *Dalton Trans.*, **2007**, 1425.; (b) S. L. Hellstrom, J. Ugolotti, G. J. P. Britovsek, T. S. Jones and A. J. P. White, *New J. Chem.*, **2008**, 32, 1379.; (c) Q. Wu, M. Esteghamatian, N-X. Hu, Z. D. Popovic, G. Enright, S. R. Breeze and S. Wang, *Angew. Chem. Int. Ed..*, **1999**, 38, 985.; (d) A. Hassan and S. Wang, *J. Chem. Soc. Chem. Commun.*, **1998**, 211.; (e) W. Liu, A. Hassan and S. Wang, *Organomettalics*, **1997**, 16, 4257.; (f) J. Ashenhurst, L. Brancaleon, A. Hassan, W. Liu, H. Schmider, S. Wang and Q. Wu, *Organomettalics*, **1998**, 17, 3186.

[16]Y. Cui, Q-D. Liu, D-R. Bai, W-L. Jia, Y. Tao and S. Wang, *Inorg. Chem.*, **2005**, 44, 601.

[17] V. V. N. Kishore, K. L. Narasimhan and N. Periasamy, *Phys. Chem. Chem. Phys.*, **2003**, 5, 1386.

[18] M. J. Frisch, et al. Gaussian 03, Revision C.02; Gaussian, Inc.: Wallingford, CT, 2004.

[19] L-O. Pålsson and A. P. Monkman, *Adv. Mater.*, **2002**, *14*, 757.

[20] Y. Cui and S. Wang, *J. Org. Chem.*, **2006**, 71, 6485.

[21] M. Amati and L. Francesco, *NATO Sci. Ser. II, Math. Phys. Chem.*, **2003**.

[22] V. A. Montes, R. Pohl, J. Shinar and P. Anzenbacher Jr., *Chem. Eur. J.*, **2006**, 12, 4523.

[23] W. L. Jia, D. R. Bai, T. McCormick, Q. D. Liu, M. Motala, R. Y. Wang, C. Seward, Y. Tao and S. Wang, *Chem. –Eur. J.*, **2004**, 10, 994.

[24] L. D. Pavia, M. G. Lampman and S. G. Kriz, *Introduction To Spectroscopy*, **2001**, Brooks/Cole: Washington.

[25] L-O. Pålsson and A. P. Monkman, *Adv. Mater.*, **2002**, 14, 757.

[26] (a) S. Kappaun, S. Rentenberger, A. Pogantsch, E. Zojer, K. Mereiter, G. Trimmel, R. Saf, K. C. Möller, F. Stelzer and C. Slugovc, *Chem. Matter*. **2006**, 18, 3539.; (b) Y. Cui, Q-D. Liu, D-R. Bai, W-L. Jia, Y. Tao and S. Wang, *Inorg. Chem.* **2005**, 44, 601.; (c) Y. Cui and S. Wang, *J. Org. Chem.* **2006**, 21, 6485.

[27] V. A. Montes, R. Pohl, J. Shinar and P. Anzenbacher Jr., *Chem. Eur. J.* **2006**, 12, 4523.

[28] S. Franzen, W. Ni and B. Wang, *J. Phys. Chem. B.*, **2003**, 107, 12942.

[29] A. Hazell, O. Mønsted, J. C. Rasmussen and H. Toftlund, *Acta. Cryst.*, **2006**, C64, m185.

Chapter 4

Summary and Future Work

4.1 Summary

In chapter 2 of the thesis, two triarylboron functionalized carboxylate ligands, one containing a duryl spacer and the second with a conjugated biphenyl linker, were synthesized and characterized using ^{1}H NMR, ^{13}C NMR, ^{11}B NMR, fluorescence emission and UV-Vis absorption spectroscopy. Both ligands were used to chelate to Tb(III) and Eu (III) metal ions separately to create four new lanthanide complexes. Ligand **1** was shown to efficiently sensitize both Tb(III) and Eu(III) luminescence, exhibiting bright green emission with high solid-state quantum yields. However, efficient sensitization of lanthanide luminescence with ligand **2** chelate was shown to only occur for complex **2Eu**, which displays bright pink luminescence with a high solid-state quantum yield. Complex **2Tb** showed no characteristic lanthanide luminescence peaks but exhibited only ligand-centered blue emission.

These observations were clarified and explained by studying the lowest excited energy state of both ligands and their relation to the lowest excited energy state of the lanthanide metal ions. It was observed that lowest triplet state of ligand **1** is above that of both the Tb(III) and Eu(III), providing the complex with efficient sensitization yielding bright lanthanide-centered luminescence. However, the triplet energy level of ligand **2** is only high enough for sensitizing Eu(III), but too low and close to that of Tb(III) to efficiently sensitize it.

Application potential for the new lanthanide complexes has been demonstrated by examining their luminescent responses toward F^-, CN^- and DPA. Several of the lanthanide

compounds have been found to be very promising as potential visual sensors for fluoride, cyanide and DPA in organic solution and the solid state as well.

In Chapter 3, the synthesis of four new compounds containing both a dipyridyl and an 8-hydroxyquinoline moiety with the aim to develop a new luminescent sensor for Zn(II) ion detection has been accomplished. All four compounds were characterized using ^{1}H NMR, ^{13}C NMR, HRMS and both fluorescence emission and UV-Vis absorption spectroscopy. Their use as luminescent sensors for Zn(II) in solution was assessed in a series of titrations spectra using both fluorescence emission and UV-Vis absorption data. While titration data acquired using UV-Vis spectroscopy did not yield any significant photophysical changes in any of the four compounds when exposed to Zn(II) ions, fluorescence emission spectra displayed significant and observable responses. Compounds **1-OH** and **1-MOM** exhibited fluorescence responses toward zinc(II) ions in a wide concentration range, from 0.1 eq. to 45 molar eq. and 30 eq., respectively, of a 10^{-5} M solution while complexes **1-BPh$_2$** and **1-Alq$_3$** demonstrated a lower maximum detection concentration by beginning their photophysical response at 0.1 eq. of a 10^{-5} M solution and completing it at 0.5 eq. and 1 eq. of Zn(II) ions added, respectively. Based on these studies, we concluded that though these compounds may be a good starting point towards the design of efficient and selective luminescent sensors for Zn(II), the simplification of the molecular structure and its number of analyte binding sites may aid in fine-tuning the molecule's photophysical characteristics.

4.2 Future Work

The impact of the Mes_2B moiety within the ligand chelate of a lanthanide complex on the lanthanide metal luminescence was demonstrated to be extremely beneficial yielding impressive quantum yields and emission colors. Further work varying either the linker between the boron moiety and the metal chelating group or the metal chelating group itself would provide us better insights to understand how to optimize the ligand-lanthanide interaction. In the interest of optimizing the complex's DPA sensing ability, replacing the lanthanide-chelating carboxylate moiety of the molecule with a multi-dentate ligand such as pyridine-2,6-dicarboxylic acid (**3**) or 2,2'-azanediyldiacetic acid (**4**) for stronger chelation to the Ln(III) metal (Figure 4.1) may be a good approach. Producing complexes utilizing other luminescent lanthanide metals such as Dy(III) should be explored in order to fully complete a lanthanide-based emissive color rainbow.

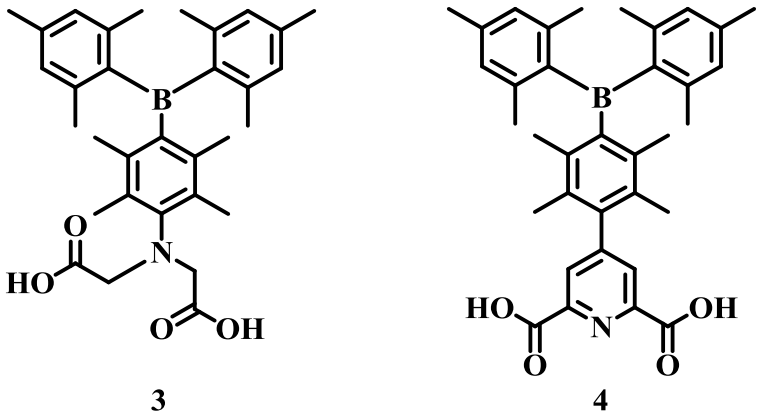

Figure 4.1. Proposed molecular structures for future lanthanide complex triarylboron-functionalized chelating ligands **3** and **4**.

Further work into the Zn(II) sensing molecule project should be focused on the detection selectivity of the sensing molecules for Zn(II) as opposed to other metals such as Ca^{2+} or Mg^{2+}.

This would allow for the determination of binding selectivity of the sensing compounds. Testing detection ability in other media such as different solvents or in the solid state should also be examined. Simplifying the molecular structure of the luminescent sensor by only including one Zn(II) binding moiety and replacing the hydroxyquinoline moiety with a non-chelating fluorophore would allow for a more basic photophysical response to Zn(II) contact. Modifying the nature of the fluorophore could additionally permit for the production of a compound with higher quantum yield, thus improving the ease of usage of the detection system.